Dipl.-Ing. Klaus Köck

Probability Based Transmission System Risk Assessment

DOCTORAL THESIS

to achieve the university degree of

Doktor der technischen Wissenschaften

submitted to

Graz University of Technology

Supervisor

Ao.Univ.-Prof. Dipl.-Ing. Dr.techn. Herwig Renner

Univ.-Prof. Dr.-Ing. Wolfgang Gawlik

Graz, August 2016

AFFIDAVIT

I declare that I have authored this thesis independently, that I have not used other than the declared sources/resources, and that I have explicitly indicated all material which has been quoted either literally or by content from the sources used. The text document uploaded to TUGRAZonline is identical to the present doctoral thesis.

Date

Signature

Acknowledgement

Writing a PhD thesis is a long and challenging task, which I wouldn't have been able to accomplish without the support and advice of my colleagues, friends and family.

First of all I want to thank Prof. Herwig Renner, who was my supervisor during my time at the institute. His door was always open for me and I enjoyed our discussions on professional as well as private topics. By sharing his theoretical knowledge and practical expertise with me, he made an important contribution to this thesis.

I would like to express my thanks to Prof. Gawlik for his valuable inputs and for reviewing my thesis.

Further, I would like to give special thanks to the head of the Institute for Electrical Power Systems Prof. Lothar Fickert, for contributing to my work by sharing his professional knowledge with me.

Many thanks to all of my colleagues for countless professional and personal discussions. Special thanks go to my long term office mates Josef and Thomas who got really good friends of mine during the time we shared together.

I also want to express my gratitude to my family, especially to my parents who made my studies possible and always supported me with parental advices.

Last but not least, I want to say thank you to my girlfriend Verena, who supported me emotionally and helped me to stay calm and enjoy life in a very challenging time period.

The research leading to parts of this thesis has been supported by the research project "Umbrella", which received funding from the European Union, 7th Framework Programme under grant agreement n° 282775-2.

Abbreviations and Acronyms

ACER ..... Agency for the Cooperation of Energy Regulators
$ACPTDF$ ..... AC-Power Transfer Distribution Factors
ARIMA..... Auto Regression Integrated Moving Average
ARMA ..... Auto Regression Moving Average
CDF ..... Cumulative Distribution Function
Coreso..... Coordination of Electricity System Operators
CTDS..... Common Tool for Data Exchange and Security Assessment
D-1 ..... Day-ahead
DACF ..... Day-Ahead Congestion Forecast
DC-PLF..... DC based parametric load flow
DSO ..... Distribution System Operator
EAC ..... exponentially accelerated cascading
EHV ..... Extra High Voltage
ENS..... Energy Not Served
ENTSO-E..... European Network of Transmission System Operators for Electricity
FACTS..... Flexible AC Transmission Systems
FCE ..... Forecast Error
FoO ..... Frequency of Occurrence
GW..... Gigawatt
HVDC..... High Voltage Direct Current
IDCF ..... Intraday Congestion Forecast
IEAR ..... interrupted energy assessment rate
ISO ..... Independent System Operator
LFCC ..... Load Flow Controlling Components
LODF ..... Line Outage Distribution Factor
LS ..... Lifting Scheme
MCS..... Monte-Carlo Simulation
MLE..... maximum likelihood estimator
MU ..... Monetary Unit
N-0 ..... Contingency free system state
N-1 ..... Single element contingency
N-k ..... k-element contingency
NERC ..... North American Electric Reliability Corporation
OH..... Operational Handbook
OPA..... Academic Simulation Model for Cascading Outages
OPF ..... Optimal Power Flow
PDF..... Probability Density Function
PST ..... Phase Shifting Transformer
PTDF..... Power Transfer Distribution Factor
RES ..... Renewable Energy Sources
RTSN ..... Real Time Snapshot
SARIMA ..... Seasonal Auto Regression Integrated Moving Average
SCADA ..... Supervisory Control and Data Acquisition

SSSC ..... Static Synchronous Series Compensators
STATCOM..... Static Synchronous Compensator
STLF..... Short Term Load Forecasting
SVC..... Static VAR Compensator
SVM ..... Support Vector Machines
RAS..... Remedial Action Schemes
TATL ..... Temporary Admissible Transmission Loading
TCSC..... Thyristor Controlled Series Compensation
TO ..... Transmission Owner
TSC..... TSO Security Cooperation
TSO ..... Transmission System Operator
UCTE ..... Union for the Coordination of the Transmission of Electricity
UPFC ..... Unified Load Flow Controllers

Variables

α, α_{PST} ..... Shift angle
α_0..... Load flow independent HVDC losses
α_1..... Linear load flow dependent HVDC losses
b..... Particular branch
B..... Set of branches
B_{branch} ..... Branch Susceptance vector
$\mathrm{B_{bus}}$ ..... Suceptance system matrix
β_0..... Load flow independent tripping probability of HVDC lines
β_1..... Load flow dependent tripping probability of HVDC lines
C..... Chance
C_{ft}..... Branch membership matrix
C_{loss} ..... Cost of active power losses
C_{MW} ..... Specific loss costs
$Corr(Z)$..... Correlation matrix
$\cos(\varphi)$ ..... Power factor
Δf ..... Change in frequency
ΔP..... Change in power infeed
$\Delta P_{G,g}$..... Post contingency change in active power infeed
$\frac{\partial P_{ij}}{\partial \varphi_i}$..... Partial derivative of the active load flow in respect to the voltage angle
$\frac{\partial P_{ij}}{\partial U_i}$..... Partial derivative of the active load flow in respect to the voltage magnitude
$\mathrm{\Delta P_{L,l}}$..... Post contingency change in active load demand
Δp_{lim}..... Limit for the change in relative load flow
ΔP_{lim} ..... Limit for the change in absolute load flow
ΔP_s ..... Forecast Balance Deviation
$\underline{\Delta U_b}$ ..... Branch voltage
$E[X]$..... Expectation value
F ..... Set of start nodes
fce..... Forecast error
fce_{norm}..... Normalized forecast error

f_n ..... Nominal system frequency
g ..... Particular generation unit
G ..... Set of generation units
H ..... Outage frequency
I ..... Set of branches in operation
$\underline{I_b}$ ..... Branch current
I_{base} ..... Common base for currents
Iqps ..... Inter Quantile Power Spread
J ..... Jacobean matrix
J_{red} ..... Reduced Jacobean matrix
λ ..... Network power value
L ..... Vertical Grid Load/Set of all loads
l_b ..... Line length
$\mathrm{L_P}$ ..... Load following a profile
L_R ..... Random part of the load
L_S ..... Special event dependent load pattern
$\mathrm{L_W}$ ..... Weather dependent load pattern
μ ..... Expectation value
$\hat{\mu}_{fce}$ ..... Estimate for the forecast error expectation value
n ..... Particular node
N ..... Set of power system nodes
ν ..... Scale parameter (t-location scale distribution)
n_b ..... Number of busses
n_l ..... Number of branches (lines, transformers, series equivalents,…)
O ..... Set of branches out of operation
p ..... Probability
P_{12PST} ..... Power flow through the PST
$\mathrm{P_B}$ ..... Branch load flow vector (Active Power)
P_{base} ..... Common base for active power
P_f ..... Parallel power source
$P_{G,p}$ ..... Nodal Infeed Forecast
$P_{G,r}$ ..... power plant schedules
$P_{HVDC,f}$ ..... Power injection at the start node of an HVDC line
$P_{HVDC,t}$ ..... Power injection at the end node of an HVDC line
P_{loss} ..... Active power losses assigned to node n
$P_{L,p}$ ..... Nodal Load Forecast
$P_{L,r}$ ..... extracted vertical grid load
$p_{malfunction}$ .... Probability of a malfunction of the protection device
P_{max} ..... Maximum in active power infeed
P_n ..... Vertical (residual) grid load at node n/ Nodal active power injection
P_n ..... Active power infeed set-point (Primary frequency control)
$P_{n,conv}$ ..... Conventional power plant infeed at node n
$P_{n,load}$ ..... Load connected to node n
$P_{N,p}$ ..... Nodal Forecast
$P_{N,r}$ ..... aggregated nodal power injection

$P_{n,RES}$ ..... RES infeed at node n
p_{res} ..... Residual probability
$P_{S,p}$ ..... control zone balance prognosis
p_{state} ..... State probability
p_s ..... System state probability
p_{sys} ..... Overall system state probability
p_{trip} ..... Branch tripping probability
$P_{trip\ hvdc,b}$ ..... Tripping probability of a HVDC Line b
Q_{base} ..... Common base for reactive power
R ..... Risk
ρ_{xy} ..... Correlation coefficient
s ..... Particular slack generator
S ..... Set of slack generators
S ..... Severity
σ ..... Standard deviation
Σ ..... Covariance matrix
S_{base} ..... Common base for apparent power
$\hat{\sigma}_{fce}$ ..... Estimate for the forecast error standard deviation
$S_{L,p}$ ..... Load Scaling Factor
S_N ..... Nominal value of apparent power
$s_{NG,p}$ ..... power plant sensitivity factors of the forecast day
$s_{NG,r}$ ..... power plant sensitivity factors of the reference day
σ_x^2 ..... Variance
T ..... Set of end nodes
Θ ..... Phase shift angle
$\underline{ü}$ ..... Complex turn ratio
$\underline{ü}_{p.u.}$ ..... Complex turn ratio in p.u.
U ..... Voltage
U ..... Uncertainty
$\underline{U_i}$ ..... Bus voltage
$\underline{U_j}$ ..... Bus voltage
U_n ..... Nominal voltage
$U_{max,b}$ ..... Maximum risk uncertainty for a particular branch b
$Var(X)$ ..... Variance
X_b ..... Reactance of branch b
X_{TCSC} ..... Reactance of a particular TCSC
X_{TCSC}^{min} ..... Lower limit in TCSC reactance
X_{TCSC}^{max} ..... Upper limit in TCSC reactance
$\underline{Y_b}$ ..... Branch admittance
$\underline{Y_B}$ ..... Branch admittance vector
Y_{bus} ..... System admittance matrix
$\underline{Z_b}$ ..... Branch impedance
Z_{base} ..... Common base for impedances

1 Summary

Due to the structural change the field of generation and transmission of electrical energy went through in the last decade as well as the high penetration of fluctuating renewable energies into the electrical power systems the need has risen for new system security assessment approaches accounting for the newly introduced uncertainties. On the one hand uncertainties come from renewable energy, but also the implementation of markets for electrical energy allowing intra-day trades added uncertainties. Classical methods have a deterministic nature, take point forecasts into account and screen the system for a more or less detailed list of contingencies. These security assessment methods give an easy to understand result – either there are any limits violated as a consequence of an active contingency or not.

The security assessment method proposed in this thesis is accounting for the stochastic nature of loads and infeeds by approximating historical nodal data with parametric probability distribution functions based on normal distributions. The implemented probabilistic load flow technique is able to take into account correlations of infeeds, loads, or both of them. This parametric approach allows a fast security assessment compared to conventional Monte-Carlo based approaches enabling the use of it in a daily security assessment process of TSOs. The core of the method is a state based recursive algorithm which links probability density functions of branch utilizations to likely system states originating out of a given system state. The output of the method is on the one hand an overall risk measure and on the other hand detailed measures for each first order contingency, which so can be ranked based on the risk they hold.

Analyses regarding the accuracy of the method were performed on a 118-bus test system. The proposed method was compared in a comprehensive case study to an AC-, a DC- and a simplified AC-Monte-Carlo Simulation.

The applicability of the proposed method for large scale transmission power systems was proven using a 1354-bus system. The study shows, that the performance of the security assessment method suits TSOs' needs.

2 Introduction

2.1 General

For the previous decade the way transmission power systems are organized, utilized and operated has changed fundamentally.

Organizationally, the field of generation and transportation of electrical energy went through a basic structural change. The three European Union's Energy Packages basically led to a separation of energy generation and energy transmission – the so called unbundling – to flatten the way for a Pan-European market for electrical energy. This market allows the providers of electrical energy in terms of power plant operators, brokers or agents to trade beyond the borders of their local transmission system on time horizons down to intra day market activities. Meanwhile different approaches of the implementation of unbundling exist. The widest spread of them are the ownership unbundling and the installation of an Independent System Operator (ISO). In the first option, the system operator is a completely independent company owning and operating the power system, which is the common option for central Europe, while for the second option the power system owner can be an active player in trading electrical energy, but the system has to be operated by an independent entity. Due to the fact, that electrical power systems form a natural monopoly regulatory instances for transmission system operators as well as ISOs are necessary [1].

The utilization of transmission systems in terms of physical load flows changed due to the reason, that the generation structure of electrical energy switched in the last years from fossil and nuclear power to renewable energy sources. On the example of Germany the phasing out of the nuclear energy after the incident of Fukushima in March 2011 led to a subsequent speed up of the energy revolution. The energy revolution's major goal is the shift from fossil and nuclear primary energy sources to a sustainable energy generation from renewable primary energy sources. The speed up of the energy revolution, led to a fast and extensive penetration of RES into the German power system. This turn from large scale thermal power plants, in terms of fossil and nuclear primary energy, to distributed energy generation in wind and photovoltaic farms led to a change in physical load flows. The power systems we have right now were designed to transport energy from generation nodes, were large scale power plants are located at, to load centers like cities, what is called a centralized generation structure. Due to the shift in primary energy sources the energy production changed to be more decentralized so the infeed of RES is distributed over multiple power system nodes as it is the case for large scale wind farms or in the subordinate system levels like it is the case for photovoltaics. Due to the fact, that the TSOs' power systems can't be adjusted to adapt the new physical load flow situation in time with the changeover from conventional power sources to RES TSOs are facing new challenges to maintain the system security, e.g. by the installation and operation of Load Flow Controlling Components (LFCC) like PSTs or FACTS as well as preventive or corrective redispatch actions. Both kinds of remedial measures are necessary due to the fact, that physical limits of equipment in terms of maximum ratings in power are not accounted for by the optimal market solution. The optimum found at the market can be either modified to meet the physical constraints by a costly redispatch arranged by the particular TSO or by modifying the set point of LFCCs.

The shift from need-based to supply-dependent primary energy sources also influenced the way power systems are operated. The volatile nature of RES introduced some new tasks to the daily work

load of TSOs like generation forecasting especially for wind and photovoltaics and new security assessment methods accounting for the volatility in market actions as well as the intermittent infeeds from RES.

Nowadays security assessment methods used by the TSOs are usually based on point forecasts, which are a composition of historic load patterns, power plant schedules for large generation units and weather based infeed forecasts for RES. All of these input parameters are uncertainty afflicted and show a more or less volatile nature introducing the need for power system security analysis methods accounting for the stochastic characteristics of the same.

The aim of this thesis is to develop a security assessment method which is capable of handling uncertainty afflicted input parameters and allows a comparison of different utilization cases and an identification of potentially vulnerabilities. This thesis is structured as follows. In Chapter 1 gives a short summary of the thesis. Chapter 2 holds a general overview about the motivation and the aim of the. Chapter 3 holds a comprehensive review of existing approaches. In Chapter 4 the proposed method is described in detail. Multiple analysis regarding the method are presented in Chapter 5. In Chapter 6 results are given for different exemplary power systems of different scales. A conclusion is given in Chapter 7.

2.2 On the Need for Risk-Based Power System Security Assessment

Due to the virtue of electrical energy for out society, maintaining the reliability of electrical power systems and the security of supply are the major goals of TSOs. Because of the exposed position of some parts of power systems like overhead lines or open air substations they are very vulnerable to attacks [2]. The increasing amount of digital appliances in remote monitor and control systems like the large scale penetration of smart metering devices in the low-voltage grid or the digitalization of substations in high- and medium-voltage grids depends on communication networks, which again potentially offer intruders new ways to gain anonymously access to the heart of a power system [3]. But not only attacks and manipulations can lead to a malfunction of a power system. Some historical events, which are the topic of subchapter 2.3, show, that the interconnected European power transmission system coordinated by the ENTSO-E can also be jeopardized by internal issues like line outages as consequences of an insufficient maintenance of transmission line routes, or misunderstandings in the common operation of cooperated power systems. In the worst case, such incidents can lead to a total blackout of the interconnected power system, what can have tremendous effects on the whole society as well as on the economy of affected countries. The success of the novel “Blackout” [4] as a work of popular literature and the fact, that the topic of power system security can be found in daily news papers show, that large scale outages are seen as a potential threat in the general public. Due to the meshed structure of the interconnected European power system an instant blackout of the same after losing one element is not very likely, but a single outage can trigger a cascade which finally ends up in a wide area outage or even in a blackout. A cascade is a series of chronologically phased branch outages as a result of subsequent overload caused protection device actions, which either can stop at a certain system state, where no further overloads are present, causing nearly no or a small number of lost nodes, or end up in a total blackout. To avoid potential system states leading to any kind of cascading events the N-1 criterion was introduced. It states, in its original form, a system as N-1-secure, if no overloads are present after each possible single-element first order contingency. Whether a system state of interest is N-1-secure or not can be determined by performing a complete contingency analysis.

The N-1 criterion based contingency analysis is well suited for deterministic point forecasts of power system data like nodal infeeds or the demand of loads, but the rising amount of uncertainties can't be considered. To be able to account for the stochastic nature of uncertainties coming from wind and photovoltaics forecasts as well as fluctuating load demand and market actions, a changeover from deterministic to a risk-based security assessment methods is necessary.

2.3 Historical Incidents

Due to the fact, that blackouts and major problems in interconnected power systems are rare events there are only a few incidents to mention in modern, well-maintained grids like the Italian blackout and the NY-blackout of 2003 and the system incident of 2006 of the ENTSO-E-area. Indeed there are power systems in a worldwide scope which do not show the reliability of European or North-American ones due to a lack in power generation units or weak designed resp. weak maintained power systems. This work is focusing on the probability and severity of incidents as well as the outage mechanics in modern, well-maintained state of the art power systems. In all three documented cases, cascading tripping led to severe network states and finally partially blackout.

2.3.1 System Disturbance on the 28th of September 2003

The incident of September 28, 2003 was triggered by a line outage due to line sag and led to a disconnection of the Italian power system from the European power system.

In the morning hours of September 28, 2003 a 380 kV line of the former UCTE power system connecting Mettlen in Switzerland and Lavorgo in Italy was outaged by the particular protection device due to tree flashovers. The Swiss and the Italian TSO unsuccessfully tried to reconnect the line to the power system. As an effect of the outage the loading situation of the line connecting Sils (CH) and Soazza (I) being a parallel path to the one outaged increased and was even overloaded. This line permits a short time overload for 15 minutes in terms of a TATL. Facing the fact, that the energy planned exchange power between Switzerland and Italy was exceeded and Italy imported too much power the Swiss-TSO asked the Italian-TSO to activate remedial measures to decrease the cross-border flows. At the same time while Italy decreased their imports the Swiss-TSO also activated remedial actions to prevent the line from tripping. The heavy overload of the line led again to an increased line sag resulting in tree flashovers and a protection device triggered tripping of the line about 20 minutes after the first incident. Subsequently after the first two line outages the load flow relocated to other lines resulting in multiple overloaded lines. According to the investigation report of this incident [5] the remaining lines online were didn't allow a stable power system operation ending up in voltage angle instabilities in Italy and nearly simultaneous cascading line trippings on the Italian border.

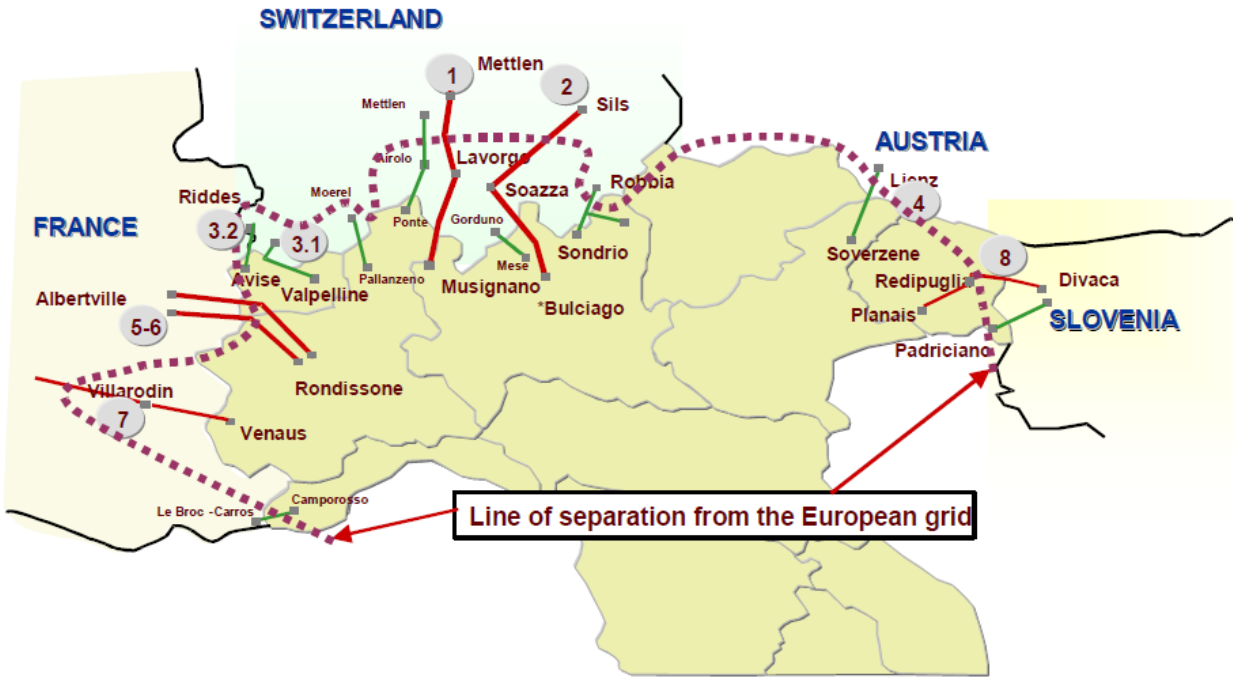

Figure 2-1. Post incident system state [5].

After the separation of the Italian power system from the Central European one, immediately a drop in frequency below 49 Hz was recorded in the Italian system. The power system was stabilized by the primary frequency control and load shedding procedures for two and a half minutes. Due to the unintentional tripping of several generation units after the stabilization of the power system it came to a rapid decrease of the frequency which could not be stopped by additional load shedding until the system frequency fell below 47.5 Hz where all participants of the grid were disconnected by under-frequency-relays ending in an Italian-wide blackout. The Central European part of the UCTE system showed a small positive frequency deviation which was limited by the function of the primary frequency control.

2.3.2 System Disturbance on the 4th of November 2006

On November 4, 2006 in the late night hours, an incident originating from the northern German power system happened, leading to about 15 million unsupplied households and a split of the synchronous area of the former UCTE power system into three sub networks. In the final report concerning the incident, the investigation committee gives an exhaustive report on the details of this disturbance [6] and its most important points are summarized in the following section.

The origin of the disturbance happened in the transmission system of E.ON Netz. A shipyard planned to transport a ship through the Ems River. To be able to pass the river the line of the transmission system connecting Conneforde and Diele has to be switched off. It was planned to transport the ship in the early morning hours of November 5, 2006 and the procedure was announced by the shipyard in the mid of September 2006. To be sure that the power system is not endangered by the outage of the line a security analysis was executed internally in E.ON Netz showing a secure system state. The power system was already weakened by some planned outages due to maintenance or construction work in the surrounding area of the line. Due to the fact, that the security analysis judged the system state as secure the permission to transport the ship was granted for November 5, 2006 at 01:00. The information was spread to the neighboring TSOs TenneT (NL) and RWE TSO (DE) which adopted the

change in topology into their security analysis tools. All the analysis of the system operators showed a highly loaded, but in a secure state corresponding the forecasted power-flow situation. To relieve the highly loaded power system the exchange program between the Netherlands and Germany was reduced for the planned time span.

The day before the incident the shipyard requested an advance of the outage by three hours. E.On Netz performed the obligatory security calculations for the requested date leading to the result, that the predicted system state is secure according to the N-1 criterion. This security analysis was performed only for the network area of E.ON Netz, but not for the neighboring TSOs due to the fact, that they were not informed about the advance in time. Due to the late announcement of the shipyard regarding the advance legal regimentations made an adaption of the exchange program between Germany and The Netherlands impossible, because the market rules forbid a change in exchange program from 08:00 on for the day ahead.

During the usual exchange procedure of forecast datasets between TSOs of the former UCTE, E.ON Netz provided on November 3, 2006 at 18:00 24 datasets concerning the next day. These files are collected and distributed to all system operators for a more comprehensive security analysis. However, this dataset didn't include the planned outage of the line. On November 4, 2006 E.ON Netz informed the two neighboring TSOs about the advance of the planned outage. To relax the system situation the TSOs on changing the set point of a shifting transformer. After this measure was taken TenneT and RWE TSO agreed to the switching action of the line. Before opening the circuit breakers of the line, a power-flow computation was performed by E.ON Netz showed no overloads and an empirical evaluation lead to the result, that the power system is N-1 secure. However, no N-1 contingency analysis was performed. At the same time RWE TSO executed power-flow computations and contingency analysis leading to the result, that their system is secure, but heavily loaded.

The two circuits of the Conneforde-Diele line were disconnected one after the other leading to a heavy loaded power-flow situation in the particular parts of the European power system. Subsequently the power-flow over the line Landesbergen-Wehrendorf, which connects the TSOs E.ON Netz and RWE TSO, increased. Due to significantly deviant flow limits in terms of alarm levels and protection device settings of this line between the two TSOs, RWE TSO – having the lower limits – received messages from the SCADA system notifying about flows, exceeding the alarm limit. RWE TSO requested E.ON Netz to take remedial measures to relax the power-flow situation on the particular line. As a consequence the stuff at E.ON Netz performed a switching action coupling the separated busbars in Landesbergen. This measure was expected to lower the line's power-flow and keep the system secure, but exactly the opposite happened. The line's power-flow increased and the overcurrent protection device of the line triggered an outage of it, what led to a cascading event through the whole European power system. Subsequent HVAC-line trippings occurred in the German, Austrian, Hungarian and Croatian parts of the power system leading to three separated grid areas. Due to the abrupt occurrence of imbalances in the separated areas action to stabilize the frequency were performed like an exhaustive use of primary frequency control as well as frequency dependent load shedding and so all the three separated areas stayed stable.

This incident mainly happened due to the lack in coordination of protection settings and the application of predefined remedial measures on a modified topology.

2.3.3 NY Blackout

On Thursday August 14, 2003 the central and north eastern part power system, and especially NYISO's grid area faced a major incident ending up in two islands, one in operation and one showing a blackout with an overall amount of lost load of approximately 23 GW of power according to the comprehensive investigation published in the NYISO's final report [7]. It took the involved Transmission Owners (TO) and their particular Independent System Operators (ISO) approximately one and a half day to restore the whole power system.

The incident originated from a severe system situation in the power systems of Indiana and Ohio western from New York at midday leading to a violation of the minimum values in voltage magnitude on multiple nodes in the particular extra-high voltage grid. During the early afternoon the utilization of the power system even increased. As initial event one generation unit in Ohio and consecutive three EHV lines tripped between Ohio and New York, but due to a fault in the monitoring system of the particular system operator it was not recognized. The cause for the line tripping were tree-flashovers as a consequence of the increased line sag due to the high utilization. The loss of this lines led to an increase in utilization of the regional high voltage power system which's lines were not able to take all the load flow ending up in a cascading event also affecting the extra-high voltage system. This cascading event caused an increase in the parallel EHV lines from the PJM area to the Ontario (IMO) area of about 100 MW. Afterwards overloaded circuits connecting the northern and southern part of Ohio tripped as well and a huge shift in power through PJM, NYISO, IMO and Michigan was the result to supply the northern part of Ohio. Additional subsequent outages in the power system area of Michigan effectively split the southern part of Michigan which was still connected to the northern part of Ohio and also connected to the system of Ontario. The load flows shifted to the transmission system of NYISO adding a transit of 3500 MW.

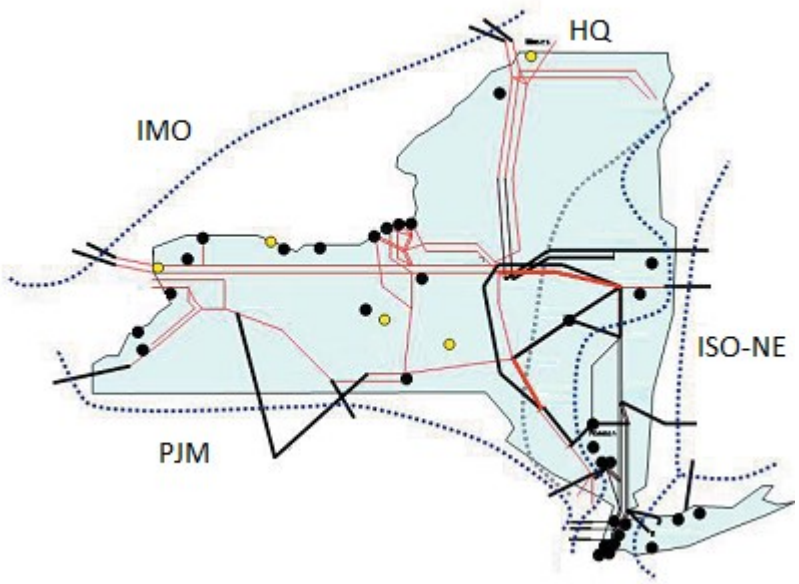

Figure 2-2. Post incident state of the NY-transmission system.

The high transit flows led to a tense situation at the tie lines between the PJM and NYISO are ending up in several tripping actions of lines connecting this two areas in one cascading event. Subsequently the tie lines between New-England and NYISO tripped leading to an immediate decrease in the NY, IMO, southern Michigan and northern Ohio island due to the lack in generation. In the separated New-England Island (Figure 2-2) the nominal frequency was recovered. The eastern part and the

western part of the NYISO system split up in two islands due to a “out-of-step” condition of the eastern part of the system. This eastern part split from the remaining bigger western island and showed a significant deficit in generation power leading to a nearly instantaneous blackout due to the low frequency and low voltage levels in the eastern NY island. After this total separation of the eastern NY power system, the IMO area and the NYISO area split resulting in a western NYISO and south eastern Ontario island showing a surplus in generation.

A re-closing of connection lines between the generation rich western NY island and the generation poor south west Ontario system led again to a power swing, a decay in frequency and so to the activation of load shedding schemes in the western NY area, ending in the tripping of the previously re-closed connection lines and about 3.5 GW of shed load in the western NY island. After the second tripping of those connection lines the frequency in the western NY island restored to a normal operation level.

The normal system configuration could be fully restored 33 hours and 30 minutes after the beginning of the incident.

3 State of Research and Research Questions

This subchapter gives an overview about the currently available scientific literature on forecasting methods, deterministic as well as risk-based security assessment methods and an example for a typical TSO practice on forecasting and security assessment.

3.1.1 Load Forecasting Methods

Since the very first attempts of interconnected grids, forecasting of the demand of load's connected to the particular transmission system has been an important topic to ensure the availability of power plants in terms of power plant schedules and also to anticipate congestions in power systems in terms of security assessment. Due to the virtue of this topic, numerous approaches on different focuses can be found in literature. An overview about the existing methods is given hereafter.

3.1.1.1 Univariate and Multivariate Models

Load prediction models can be categorized in univariate models, accounting for a single input variable (e.g. historic load data), or multivariate models, which are more sophisticated than univariate approaches and take a number of external parameters (e.g. weather data, time and date) into account. For the use in very short term load forecasting and short term load forecasting the influence of external factors is generally said to not have an effect on the accuracy of results and so univariate models perform according to the conclusions of naïve approach studies [8], [9] better e.g. for short term forecast horizons than complex weather accounting multivariate models which perform better on long forecasting horizons. Long term forecasting methods model multiple causes influencing the load behavior where the most affecting ones are the time in terms of seasonal characteristics like winter-summer, day-night, weekday-weekend, vacation and special days, the weather in terms of temperature, the degree of cloud covering, the wind speed and the humidity as well as the electricity price and the economic performance. Especially in regions, where electrical heating systems are widespread the influence of the wind on the load has to be considered because of its cooling effect underlying the effect of inertia [10]. Thermal inertia leads to a shift in time and so a cold or windy day does not directly cause an increase in energy demand because buildings have a thermal time constant. Every prediction result is always uncertainty afflicted, what is modelled as a term of randomness reflecting exceptional events like non-predictable natural and civil events.

3.1.1.2 Additive- and Multiplicative Models

Mathematical predictive methods can be separated into additive and multiplicative models [11].

$$\mathrm{L} = \mathrm{L_P} + \mathrm{L_W} + \mathrm{L_S} + \mathrm{L}_R \quad \textbf{(3-1)}$$

Eq. (3-1) shows an example for an additive implementation, where L denotes the total predicted load, L_P the load according to a standardized load profile, L_W the weather dependent part, L_S is a term for special events leading to a deviation of the usual load behavior and L_R is a random term.

$$\mathrm{L} = \mathrm{L_P} \cdot \mathrm{L}_W \cdot L_S \cdot L_R \quad \textbf{(3-2)}$$

In eq. (3-2) an example for a multiplicative approach is given. The acronyms are the same as for the additive model with the difference that they denote factors instead of summative terms. It can also be thought of additional factors like electricity pricing or a coefficient accounting for the increase of load over time to be integrated into the formula.

3.1.1.3 Long- and medium-term load forecasting approaches

To predict the energy demand long time (e.g. one year in advance), there exist basically two kind of approaches. End-use models and econometric models are used to predict load demand on long term horizon. End-use approaches are based on extensive knowledge on installed appliances. Customer's showing similar behaviors are categorized into groups to simplify the data handling. This approach is very sensitive regarding the quantity of information about the demand characteristics and their quality. Long term forecasting with end-use models is requires nearly no historical data, but on the other hand a lot of information about customers and their appliances is needed. The second popular approach for long term load forecasting are econometric models, which are based on statistics and economic theory. Econometric models are based on an estimation of a function between the load behavior and the weather and/or other influences. To reduce the effort loads can be grouped in characteristic collectives. The advantage of this approach is, that there are no detailed information needed on the appliances of customers, but a disadvantage is the necessity of long term historical data. Approaches combining end-use- and econometric-models are said to increase the accuracy of forecasts, but they require a long term history of load data as well as detailed information about the end-user-load-structure [11].

3.1.1.4 Popular Approaches

One of the most intuitive prediction approaches is the linear regression. Due to its simplicity it is widely use especially for load prediction. It can be implemented in a univariate or multivariate way. For deterministic influences like special days, weather and other external influences can be accounted by introducing additional variables. Linear refers to the characteristic of the parameters but not the shape of response surface. It is usual to implement a linear trend using regression models, but this approach is not able to account for business events like recession and booming due to the monotony of the trends on the whole investigation interval. Also short term prediction regarding the weather can be approximated using linear regression.

Another method called the similar day approach makes use of historical data to estimate the future not by trying to extrapolate the measure of interest e.g. the energy demand but by looking for days with nearly the same characteristics in the historical data set. Properties for identification of the similar day are the weather, the day of the week and the date. Implementing a trend, the data from a similar day in the past can be up-scaled to the desired forecast date. The accuracy of this approach can be optimized by looking for more than only one similar day in the historical data and joining them creating a linear combination of them.

Fuzzy logic is able to describe human expressions in a logical way and allows to implement them in mathematical models. Especially when it comes to load forecasting methods based on fuzzy logic outperform linear models [12]. An approach based on fuzzy logic allows to described the active load demand as a function of time and date, temperature and the day- or week-ahead energy consumption. When it comes to extreme events, well developed fuzzy logic approaches reach a good accuracy and outperform most of the statistic theory based methods.

Neuronal networks are a common method for prediction tasks. Especially when it comes to load forecasting they are used for different lag times in various realizations. E.g. a 15 minute short term load forecasting method with a resolution of approximately one minute is proposed in [13] using multiple underlying neuronal networks controlled by an upper neural network, which dynamically controls the weights of each network. The work presented in [9] outlines the data pre-recession as

indispensable to enable neural networks to do their work properly. The paper deals with load prediction based on weather ensembles coming to the conclusion that the prediction accuracy of the forecast can be improved by the use of weather ensembles.

A combined approach of neuronal networks and chaos theory is presented in [14]. It is based on the setup of a multi-dimensional chaotic time series in phase space. Further the neural network structure is determined by trial and error in an network optimization process, where the initially randomly set neural network weighting factors are optimized by training the network with historical data.

Principal component analysis is based on the reduction of the dimension of a multivariate data set to a set of orthogonal variables. So the original original variables are linear combinations of the orthogonal set. This method is very similar to modelling every appliance of a aggregated load pattern with the difference, that the number of different models is minimized by the exploitation of similar pattern in them. In paper [15] an approach for a univariate model is given, using day-of-the-week dummies and a quadratic trend a regression based solution of this problem is presented. Cross validation in combination with the method of minimum least squares is used in the mentioned paper for optimization purposes. The results have to be converted back from the space of principal components to the space of the input data. Also weather data can be implemented, extending the model to a multivariate one.

A widely spread approach for load forecasting is the method of exponential smoothing. Basically there are numerous ways how exponential smoothing methods can be implemented [16]. The most simple one is the first order exponential smoothing which is basically a weighted mean sum of a predefined number of historical values. A first order approach can be extended to a second order exponential smoothing method by taking a trend into account. A linear trend basically goes increasing or decreasing over the number of time steps. Exponential smoothing methods are always trained using past values of the time series to predict. By e.g. evaluating the second-order exponential smoothing based on available test data the forecast error can be determined. To optimize the accuracy of the model usually the method parameters are trained formulating an optimization problem with the objective to minimize the forecast error.

The exponential smoothing is not limited to linear trends only but it can be extended to n^{th}-order exponential smoothing leading to a n^{th} polynomial behavior instead of the linear. A special implementation of exponential smoothing method is the Holt-Winters seasonal exponential smoothing, allowing to account for one or even multiple different seasonalities (day, week, month, year) [17].

A special implementation of exponential smoothing models is the intraday cycle approach, which is principally based on one cycle for every day in the lag time. So it is not possible to model any weekly seasonality. This problem can be solved by modelling various intra-day cycles for differently shaped load profiles per day type. In paper [18], different intra-day profiles were designed for Monday, Friday, Saturday and Sunday. The remaining days where modelled by one IC due to the similar profile of these days. The accuracy can be improved by including an autoregressive term to this approach.

The Auto Regression Integrated Moving Average (ARIMA) procedure is a popular method for building statistical models and models forecasting purposes which was developed by Box and Jenkins. The underlying method of the ARIMA model is the ARMA algorithm. It consists of an AR part which is the autoregressive one and a MA moving average part. The AR model aggregates values from the past

weighted by a factor and takes a shock into account as a normal distributed random function. ARIMA models can be extended to SARIMA (seasonal ARIMA) models taking one or multiple seasonalities in to account [17], [18], [19].

Wavelet theory approaches are categorized under the hybrid models. In a first step the input data are transformed into different resolution spaces, then the sub-input data are processed by selected forecasting methods like ARIMA separately. The sub-results of the particular subsystems are combined by an inverse transformation. E.g. [20] this is done by a lifting scheme. In [20] the prediction on basis of this series is done by an ARIMA model, whose results are post-processed using an inverse lifting scheme proofing, that the LS-ARIMA-LS^{-1} method performs better than an ARIMA model for day-ahead (d-1) forecasts.

A second approach of hybrid models is the implementation of a trous algorithm [21]. First the input data is decomposed in different resolution levels followed by the calculation of the generated subsystems. The calculation results for the independent subsystems show different coefficients representing an approximation of the input data in the particular resolution level. Finally the subsystem's results are reconstructed forming the forecast values. This is done by combining the coefficients of the different base wavelets. The subsystems can be seen as independent chaotic time series. Studies show, that approaches implementing hybrid models perform well compared to naive methods for long term prediction tasks.

Expert systems are a heuristic approach, which require the expertise of a human being involved in the investigated process like a system operator and try to model their knowledge in a mathematical way. It must be possible to express the operator's knowledge in a way that programmers are able to implement it in software. In [11] expert system makes use of 11 different day profiles, weather data and load data of the previous five years. This developed method out-performed a conventional Box-Jenkins method in STLF. Another mentioned implementation in [11] of expert systems is a site independent set of rules, which was already tested on several different organizations in the US. The parameterization and rules where created without any site specific knowledge, but the forecast accuracy could be improved implementing site specific parameters. The investigation horizon of expert systems is limited by the horizon of the implemented expert rules.

The technique of support vector machines (SVM) is closely related to the method of neural networks, where non-linear functions are searched to model complex dependencies of variables. In SVM the non-linear functions are converted by a so called kernel into a more dimensional space, where it is possible to express them in linear equations and boundaries. The challenge to find a proper architecture for a neural network is replaced using SVM by the need of the optimal matching kernel. Some SVM approaches were already implemented resulting in a better performance compared to an autoregressive method [11] on a short term forecasting horizon.

In [9] a method for predicting the forecast error variance is proposed based on forecasting methods using weather ensemble predictions. Three methods have been investigated for comparison namely a naive approach, an exponential smoothing method and a neural network. Exponential smoothing turned out to perform best for short lags and the rescaled variance methods for long lags. Generally most of the literature concerning prediction is about forecasting and only some few publications are about modelling the forecasting uncertainty. When it comes to method comparisons the forecast error is a widely used measure to visualize the method accuracy.

3.1.2 Security Assessment Approaches

The aim of the security assessment in general is the evaluation of a system state with the focus to identify events, harming the supply of load ending up in a blackout in the worst case. Large blackouts originate in general out of complex chains of outages and events so called cascading events. A cascade can consist of many single line outages that are both, dependent or independent from foregone events. Tripping of lines and transformers with possible islanding, loss of generation, load shedding, as well as automatic and manual redispatch might take place during a cascade. Often a cascade is triggered by load flow independent events like earth faults caused by falling trees, direct and indirect lightning strokes. As a consequence, tripping due to overcurrent relays, undervoltage relays, or earth faults due to increased line sag can happen subsequently. These causes cover a part of the complex blackout mechanics. In addition to element outage cascades, wide area outages and blackouts can also be triggered by voltage collapse due to lack of reactive power [22], or due to voltage oscillations and transient instability [23]. Also the loss of system observability or controllability can lead to cascading outages e.g. when problems with the SCADA system occur and a system operator is not able to control the grid anymore due to the lack of information about it [24]. Most of the TSOs perform a deterministic security assessment to minimize occurrence probability of a blackout [25]. Usually lines with more than only one circuit are taken into account in form of a list of common mode failures according to the expert knowledge. The main statement of this criterion is, that the operated grid can withstand the occurrence of each listed contingency. The N-1 criterion is defined as necessary for a secure grid operation. Also the need for a set of remedial actions to be able to recover the N-1 compliance is mentioned. A violation of this rule is accepted during switching sequences, when consequences are restricted to a particular TSO's grid area and during remedial actions recovering the N-1 compliance. Several problems are arising with the use of the deterministic criterion. Although the N-1 criterion is simple to understand, it gives no information about the actual dispatch's risk. Hence, different N-1 secure system states cannot be compared in terms of the risk they hold. Neither the probability of the outage is known or its risk. Today's industry practice using the N-1 security criterion for security assessment is stated to be obsolete [24], because it was designed to coordinate a grid's security in a small-scale network and tie lines were designed for emergency reasons but not for trading and transit activities. Nowadays, the situation in energy transmission and energy trading has changed, but the security limits didn't evolve with the way the grid is used. With the number of considered line outages the probability for simultaneous element outages increases [26]. However, the effect of outages is not as threatening in a meshed grid as in conventional ones. Although the likelihood of a single element outage increases with more lines in a network, but the impact on the network customers associated with it decreases.

Due to the necessary consideration of multiple line outages, the N-1 criterion has to be rethought [27]. But an extension of this deterministic limitation in grid operation seems to be not feasible due to the fact that a k element outage contingency analysis leads to n^k calculations and is computationally exhaustive on a day-ahead basis. Ref. [28] sees the N-1 methodology to be useable in general but argues that outages harming only small loads should be tolerated to reduce the computation time. To keep the number of calculations at a feasible level, a tradeoff between accuracy and computation time has to be found. The method currently being used by the European TSOs is the calculation of all possible single line outages and by experts selected multiple line outages (N-2, N-3) enabling the consideration of the loss of multi-circuit overhead lines. According to [29], it is not reasonable to take preventive actions like it is usually done for the N-1 contingency cases for higher order cases, due to the fact that they happen very rarely compared to single element outages.

3.1.2.1 Probabilistic And Risk Based Security Assessment

In the previous subchapter it was outlined, that the N-1 criterion is not that well suited for nowadays power systems due to structural effects and the missing statement of N-1 contingencies about the severity of an event. Usually, for a reasonable dispatch of a power system a cascading event shows a very low probability but a high severity while outage events show a low severity and a comparably high probability. To combine events with high severity but low probability and events with high probability but with a low threatening potential in one measure the risk is the measure of choice, which is the product of probability and severity.

In literature various different severity measures are presented. In a technical view it can be defined in technical terms like “energy not served”, “lost load” as well as in technical threshold violations, or in economic terms like “outage costs”. The blackout size, the power shed, the energy not served, the number of customers disconnected, the duration and the number of lines tripped [27] are technical measures often used as a severity measure, but the also exist economical measures like the outage costs. This enables an economic analysis in terms of investment costs vs. the outage costs. The costs are calculated as a function of power not supplied and the outage duration following [30] and [31]. There are also other disciplines in which cascading events or similar procedures occur exist in [27] and risk based approaches are used for like in this case to determine the evolution of forest fires.

Due to the multiple complex outage mechanics it is not feasible to model all effects leading to blackouts [32]. It’s more common to model only the effects of interest or those having the highest impact. All methods assume trade-offs for the sake of simplicity or feasibility. Most of the methods do not analyze the full set of cascading causes but a subset of it. Another simplification is to focus on steady-state assumptions more than on dynamic investigations according to the review paper in [24].

An important topic in developing probabilistic security assessment methods is the visualization of the mostly complex information in a way which allows the operator to react fast on critical events. In [33] and [34] the simulation results coming from a probability risk assessment were visualized in form of a risk plot, along with the conventional N-1 limits as well as special selected N-k cases. To get to know this information [34] proposes the use of a Monte-Carlo simulation performing load flow calculations for a generated set of congested grid scenarios giving the amount of outaged load as well as the outage probability which enables the calculation of the risk. So the operating personnel has the operation relevant deterministic criterion as well as a risk indicator for the current system state giving more information than the simple statement “single outage secure” or “not-secure” without any additional information like limit margins.

3.1.2.1.1 Branching Process Based Methods

There is a lot of literature available on the topic of estimating the likelihood of a large scale outage, either based on real world data, or on outage simulations. Generally outages are said to follow an exponentially distribution in outages. New studies e.g. [35] show, that the probability of large events is not exponentially distributed like expected, but that they show a power-law distributed tail, which leads to the conclusion that the expected exponential distribution underestimates the occurrence of outages with a high value of lost load. So, a big outage in terms of energy and even a blackout is more likely than assumed. A sensitivity analysis performed in [36] leads to the conclusion that the discovered power-law tail is only present, when critical system states are investigated. System states operating far away from the limits show an exponentially distributed tail what is also mentioned by the authors of [31].

Many research papers [31], [37] and [38] make use of so called branching process models which allow the simulation of cascades with stage dependent propagation factors and different underlying offspring distribution functions like the negative binomial distribution, the Poisson distribution, or the exponential distribution.

The data used in [37] originate from the NERC's transmission availability data system, which is a list of time stamped outages occurred over a ten-year time period. These data are grouped into cascades and stages of cascades as part of the data preprocessing splitting the events into initial and higher level tripping. Both the initial as well as the offspring outages are assumed to follow a Poisson distribution. The propagation factor is calculated for each stage, and for simulations it is assumed that the first stages act as determined from data and the following stages show a propagation factor of the average value. The generating function of the branching process is a Poisson distribution. It is proposed to generate a system state with an initial outage who's cascading outage probability can be estimated through the recorded data. It is also assumed that the reference data set can be much smaller than the one used for this method.

In [22] outage data of an academic simulation model (OPA) as well as an output of the commercial software TRELSS is used to estimate the distribution of rare event cascading outages on the example of IEEE 300 and 118 bus networks. The OPA model uses a DC-load flow calculation method and also reflects the long-term dynamics of a grid by the line data evolving behavior. It is shown that the propagation factor defined as the Harris estimator increases by the load level. Two branching processes were investigated, the Galton-Watson branching process and the continuous state branching process. The Galton-Watson method shows a good match in estimating likely events, but the probability of rare events at the tail are underestimated. The continuous state branching process investigation led to a probability density function which is similar to the real value distribution, but is not very close to it. However, it could be improved by choosing a different offspring distribution (here the gamma distribution was used). It is assumed that the amount of calculated cascades for parameter estimation of the distribution can be lowered by a more precise knowledge of the distribution of the initial cascades. As a further result the Galton-Watson branching process was identified to be simpler to implement and more accurate.

Based on the rare number of cascading events in the past in [29], their probability density function is determined by introducing the likelihood of outage energy amounts in a discrete way. It proposes a new method for distribution fitting, the so-called EAC denoting the exponentially accelerated cascading. In [11] the maximum likelihood estimator (MLE) is used to find the best matching parameters of the investigated density functions. The results of each distribution fit in matching the input data were performed with a chi-squared test resulting in the better fit of the EAC model than a generalized Poisson distribution or negative binomial distribution. Also the numbers for the initial outage probability – the mean value for first element outages is found for the investigated data, as well as the propagation factor meaning the relation of next generation outage probability to the outage probability of the actual step.

In [34] a probabilistic model to predict the likelihood of cascading line outages following a primary line outage is given based on a logistic function with the post contingency line flow as well as the difference in line flow as input parameter. By the already mentioned logistic function, the outage probability is determined. To find the constant factors of the function, a calibration was performed

based on the outage data of three large- scale cascading events. The method consists of a load flow calculation for each step of the cascade leading to the knowledge before and after line outages.

3.1.2.1.2 Monte-Carlo and Ensemble Based Methods

The method presented in [36] focuses on the sensitivity analysis regarding the likelihood of hidden failures, spinning reserve capacity, and the control strategy. The method is based on the DC-load flow method for the sake of computation speed and takes into account hidden failures by implementing a load dependent outage probability function. It is assumed that cascade's outages do not likely happen at exactly the same time and so they are calculated step by step one outage at one step. The method is also capable of islanding by forking the calculation into sub-grids. The initially outaged line is selected randomly and then existing overloads are calculated. When no overloads are present hidden failure probabilities are determined. To keep the island steady-state-stable, load is shed until the equilibrium point. At the end of a cascade – so if a collapse is detected or there are no more lines above the limit and the hidden failure probability is below a certain limit - the total load lost, the line outage sequence and the path probability are logged. The whole procedure is for single cascade identification and repeated over an ensemble of lines. To ensure a balance between generation and load a DC-OPF is performed during the outage simulation. To keep the method realistic the DC-OPF is only enabled every three line outages to model TSO behavior. Due to the fact that large events are very rare numerous outage combinations have to be calculated to account for them. To identify these cases in a more computational economic way, rare event sampling is performed, which increases the likelihood of rare events to occur more frequently. The performed sensitivity analysis in this study led to the conclusion, that a low loading leads to low values in lost load while high loading close to the maximum rating causes a cascade in each possible case. Higher line loading also causes in relaxed system states the exponentially distributed tails to change into power-law distributed ones. Also, the spinning reserve amount has the same effect. A grid with a large amount of spinning reserve shows exponentially distributed tails while a grid with a small amount in rotating masses shows the power-law tail. When decreasing the hidden failure probability, power tails become steeper leading to lesser failures and a lower vulnerability but the power-law tail does not disappear.

The method presented in [35] shows the difference of taking cascading effects into account. TSO behavior like a manual re-dispatch is modeled by the implementation of a DC-OPF having line limits integrated in the objective to avoid line trips by overloads. This OPF is performed every third step of cascading events, modeling the reaction time of the system operator on congestions and critical line loadings. To enable the integration of load and generation units' frequency dependency on the one hand each generators droop and on the other hands each loads self-regulation factor was implemented. By this it is possible to calculate the remaining frequency deviation in terms of primary control as well as frequency dependent shedding mechanisms of loads at under-frequency and generation units at over-frequency. To also pay attention to security relay related line outages, either triggered by malfunction or by line overload, the basic outage probability depending on the line length is extended by an outage probability increasing with the amount of overload. As a hard limit for line flow 1.4 of the line limit was chosen. At this limit the line's outage probability is one. So the model integrating cascading outages is able to simulate two outage causes, the outage of overloaded lines and the outage of lines caused by protection system's hidden failures.

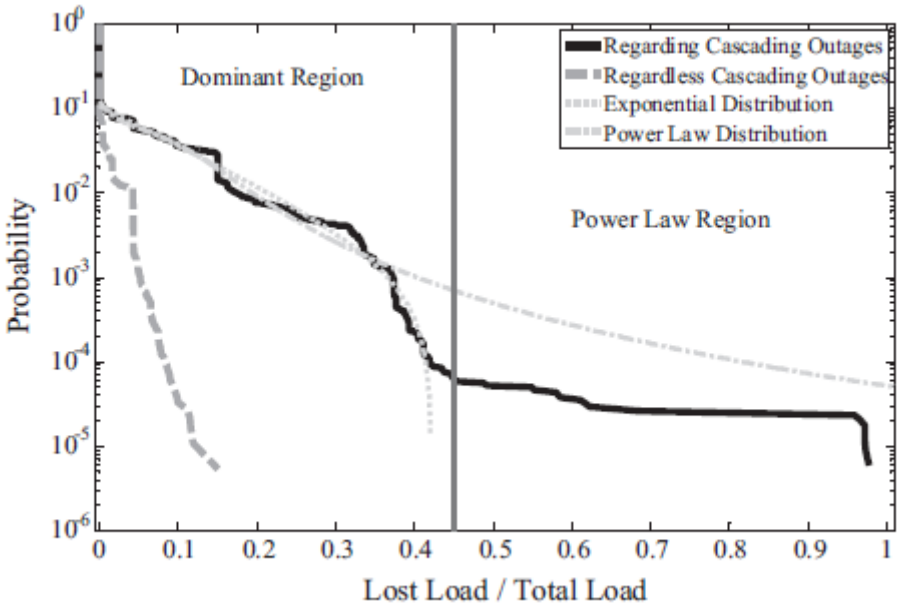

Figure 3-1. Visualization of the severity and the probability of outage events accounting and not accounting for cascading events [35].

Figure 3-1 shows the difference of taking into account only N-1 outages in contrast to taking into account possible cascades concluding that the consideration of only first order outages gives only a small part of the risk detected by the cascading method.

In [30] the difference in deterministic security formulation and probabilistic security criteria is shown. The N-1 security criterion doesn't reflect at all the risk of the actual system state, so there is an easy to understand yes or no decision in the form of an unacceptable risk or a secure system state. There is no information in the criterion about the clearance to any security limit. The implemented risk measure is outage costs which are determined out of the load lost and the outage duration. To be able to visualize N-1 secure coordinated system states in contour plots, a Monte-Carlo simulation was performed to find the N-1 related security limits.

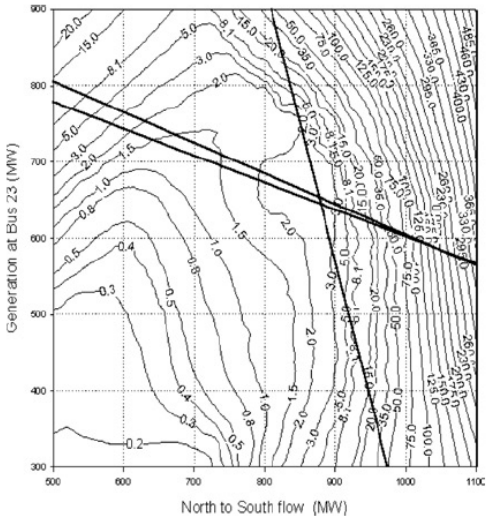

Figure 3-2. Contour plot with N-1 criterion limits [30].

Figure 3-2 shows those limits and visualizes the fact that N-1 secure states do not necessarily have equal risk. The upper centered boarder of N-1 security e.g. shows a risk of 1.5 while the lower right edge of the N-1 secure region shows nearly 20 times the risk.

The in [31] mentioned OPA model is a Monte-Carlo based system assessment tool allowing the simulation of an evolving grid. The outputs are the energy not supplied and each outage case's likelihood. The author of [31] states that a mitigation of likely outages of a small amount of load influences the occurrence of rare events. It is not easy to determine interdependencies of different remedial actions which can also worsen the problem directly or in form of evolving mechanisms. The success of the remedial action is directly linked to the system dynamics referring to a forest fire model [36]. Based on the assumptions that an operator can prevent the first 10 lines from tripping outages were enabled after a certain number of line overloads. The investigation shows that the outage costs of lesser than ten lines decreased to 40% while the costs of rare events increased to 110%. It was also shown, that a change in power system planning can affect the grids security over the long term. To express the impact of an outage the risk is formulated as the product of the outage probability and the outage value. The value of the outage is calculated as IEAR times the energy not served. The IEAR is the interrupted energy assessment rate. Another valid measure for the outage risk is mentioned to be the costs per customer times the customers so also the overall costs can be determined. In [31] the outage frequency is found to be power-law distributed following the available data from the OPA model.

The method presented in [28] utilizes the Markov process to model cascading outages. The outage probability is adopted at each step of the cascade to meet the changing facts during cascades. The method is Monte-Carlo based calculating all possible outages of the current stage followed by the enumeration of all possible states. These steps are continuously repeated until the load flow calculation converges no more or the termination conditions are fulfilled. The amount of lost load was not recorded during the cascade, but the probability density function showed an exponential tail for multi outage cascades.

In [23] the OPA model was modified to evolve either with the N-1 deterministic criterion or as a response on cascading outages. The first lines are upgraded if an N-1 calculation identifies a congestion, in contrast to the second criterion responding directly to cascading outages. The outage cascade is triggered by randomly tripping each line at an outage probability above 0.1%. The random variable is chosen to be standard-normal distributed. Also a redispatch by the use of an optimization is implemented to find the optimal system state. Load shedding is allowed, but a high cost factor in the objective leads to the avoidance of its utilization. The load grow is set to be 1.8% and is randomly distributed on the loads. The OPA model is top down to enable tractability and to keep simplicity. There are also some tradeoffs in the model like protection system failures, dynamics and human factors, which were not taken into account. The integration of cascading effects and the evolving grid leads to new possibilities in slow but complex dynamics in the grid. The N-1 criterion based evolution model shows a lower risk than the direct response on cascading outages, but the nominal transmission power capability of the lines is in the direct response somewhat like 15 times the nominal and in the N-1 case 150 times the nominal maximal power.

In [39] the authors show the impact of correlated uncertainties in terms of nodal infeeds in TSO networks based on a detailed AC-Monte-Carlo simulation accounting for outages due to under or over voltage events as well as overloads of branches.

3.1.2.1.3 Remedial Actions For Cascading Event Avoidance

Remedial actions can be categorized in preventive and corrective measures while the former are used to prevent the grid from reaching critical states while the latter are used to get the system back into a secure state.

3.1.2.1.3.1 Preventive Measures

Preventive actions can be the determination of a low risk system state by formulating a risk-based OPF or by switching operations to avoid outages and minimize the impact of outages on the system. Usually Remedial Action Schemes (RAS) are used, which are predefined procedures to mitigate congestions and remove problems in transmission grids [24]. On the one hand RAS can enhance the security of power systems, but when a malfunction in the procedure occurs due to stuck breaker RA-schemes can also causing cascading outages. If two RA-schemes overlap while both are requested, the possibility exists, that they influence each other in a way worsening the situation.

Generally, OPF based methods find the optimal solution for an optimization problem, minimizing an objective (e.g. generation cost) subject to various limits (e.g. transmission and generation capacity) [11], [26] and [40]. There are methods based on the optimization of the system state also with multiple objectives like the voltage profile, line loadings, and generation limits. The method proposed in [40] includes the system risk as part of the objective function, and determines the risk index as a sum of all sub risks. The risks are determined as the product of the estimated probability and the severity. The probability-estimate is calculated in dependence of the investigated line's length and the weather as well as the voltage level and geographical coordinates to determine an increased risk by lightning activities. The severity is estimated as a function of line load which reaches a maximum of 1 at nominal loading or a bus voltage below 0.9 p.u. Due to the computation effort in solving numerous AC-load flow problems only the first outages are calculated that way and the problems of the next cascade stages are solved by the sensitivities of the nearest foregone calculation. So the new system state's solution is found at trough the linearization at the parent's state. The benefit of such a Risk Based Multi Objective-optimization is, that in contrast to a DC-OPF it minimizes system stress not only on overloaded lines but also on the ones that are under nominal load. The results of the study where verified by a cascade simulation.

A method taking into account the uncertainty of nodal power injections in terms of RES infeeds is presented in [41]. An OPF is extended to account for uncertainty afflicted inputs while the method takes a maximum risk level as an input which leads to optimal dispatches showing a risk lower than the given limit. Due to the DC formulation of the OPF the method focuses on overload related outages.

3.1.2.1.3.2 Corrective Measures

An OPF can be used to find optimal corrective actions by redispatching the power infeed. Also the utilization of power from demand side management, i.e., load tripping, or the use of FACTS and tap-change transformers can be used to relax a critical grid situation. Implemented methods in [35], [36] use an OPF to simulate corrective TSO actions. Also for the reaction time of a TSO was accounted by limiting the corrective activities to each third outage only [36].

3.1.3 TSO Forecast Procedure

To guarantee a as secure as possible grid operation TSOs use forecasting procedures to assume the grid utilization of the future. Especially for the time horizon of operational planning exact predictions

of nodal loads and infeeds, or more general of nodal power injections, in the high and extra-high voltage grid are needed to enable a security analysis. Usually TSOs get aggregated schedules of balancing groups which don't hold any information about at which TSO node power is consumed and in which one it is fed in. TSOs also get planned schedules of large scale power plants connected to the TSO's power system directly or in an indirect way the underlying power systems of DSOs.

Facing the problem, that the vertical load is only observable in the form of an aggregated nodal load value for the TSO the vertical load can only be estimated. Based on available datasets from the past an expert chooses the - experience judged - best one as a basis for the prognosis process. From this reference day the TSO has the aggregated nodal power injection ($P_{N,r}$) available, as well as the latest forecast of the power plant schedules denoted by $P_{G,r}$, the power in generation on the reference time step r. Due to the fact, that usually only large scale power plants are directly connected to the transmission system, the TSO estimates sensitivity factors reflecting the participation of each particular power plant, connected to the DSO network, in the nodal power injection of the TSO's grid. By weighting the power plants' infeeds using these sensitivity factors, what is mathematically a matrix multiplication, the nodal infeeds of the reference time step can be determined. The desired data - the extracted vertical grid load $P_{L,r}$ of the reference day - is the difference between the realized nodal power injections' values and the nodal infeeds.

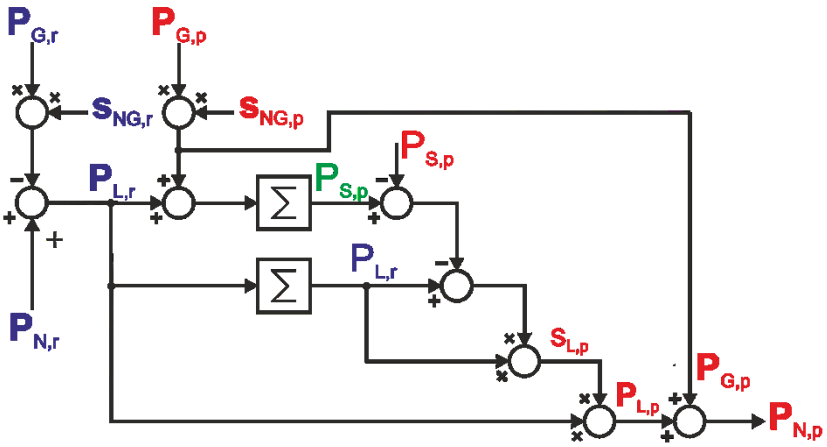

Figure 3-3. A common TSO forecast procedure.

Data available for the time step to forecast are power plant schedules $P_{G,r}$, power plant sensitivity factors $s_{NG,p}$ and the control zone balance prognosis $P_{S,p}$. By multiplying the prognosis infeed vector $P_{G,p}$ by the sensitivity matrix, according to the forecasted power system topology, the per TSO node infeed values $P_{G,p}$ can be determined. Due to the fact, that the forecasted value for the control zone power balance $P_{S,p}$ is given the deviation ΔP_s of the sum of power in generation and the previously extracted load data from the reference day from the actual forecast value can be calculated. This deviation. This deviation gives the absolute amount the extracted load has to be increased to meet the prognosis value. This is done by a linear scaling factor $S_{L,p}$ for the load data. Applying this scaling factor on the extracted reference time step's load data $P_{L,r}$ gives the nodal load forecast $P_{L,p}$. The sum of the nodal infeed forecast $P_{G,p}$ and the nodal load forecast $P_{L,p}$ give the nodal power forecast $P_{N,p}$. The overall formula is given in eq. (3-3), where $P_{L,r} = P_{N,r} - s_{NG,r} \cdot P_{G,r}$ is the extracted vertical grid load.

$$P_{N,p} = s_{nG,p} \cdot P_{G,p} + \left(1 - \frac{\sum P_{L,r} + s_{nG,p} \cdot P_{G,p}}{\sum P_{L,r}}\right) \cdot P_{L,r} \quad \textbf{(3-3)}$$

The here described TSO forecasting procedure doesn't explicitly account for decentralized infeeds in terms of renewable energy sources due to a comparable low penetration of them. TSOs with a significant amount of renewable energy sources like wind or photovoltaic handled them the same way as power plants in the example above. Regional forecasts for the particular primary energy source are used to estimate the infeeds into the power systems and distribution factors are used to account for their influence on the nodal power injection at the TSO's system.

3.1.3.1 Challenges in Data Mining

When it comes to modern approaches concerning the risk assessment of power systems the data need increases significantly by the necessary historical information either concerning the forecast error or measurements of nodal power injections. Due to the fact, that it's quite common, that the models for forecasting and the models for system monitoring at TSO site were developed independently from each other the nomenclature and also the depth of details widely diverge. This problem makes it almost impossible to extract the needed information of the forecast error. The only way to overcome this issue is to harmonize forecasting and monitoring models to allows a simple and straight forward calculation of the forecast error. Harmonized models would allow an easy identification of potentially avoidable errors in the forecasting process, without making use of estimating procedures, like it is actually the case introducing new effort and uncertainties which has to be accounted for in the framework of a risk assessment.

The aggregation of load and generation values, or more generally of different nodal power injections, on a nodal level introduces problems to security assessment procedures when the method is based on the identification of sources of uncertainties. A separation of the nodal power injection at a basis of at least load an generation units or better for loads and for each underlying generation facility would introduce the possibility to model uncertainties according to their particular source accounting for characteristics like minimum and maximum boundaries in terms of generation units or specific forecast error distributions for different technologies.

3.1.4 ENTSO-E

In Europe, the European Network of Transmission System Operators (ENTSO-E) is representing 41 TSOs from 34 countries and originates from the former UCTE. The ENTSO-E operational handbook holds rules which members of the ENTSO-E have to comply with. The operational security of TSOs' grids is processed in Policy 3 of the UCTE Operational Handbook [42] being in force at the moment. A new network code on operational security [25] specifying the process of the TSO security assessment in a more concrete and detailed way is finalized, published by ENTSO-E and also recommended by the Agency for the Cooperation of Energy Regulators (ACER).

According to the network code on operational security [25] each TSO has to define a contingency list consisting of internal and external contingencies which are potentially threatening the particular TSO's system. To identify active contingencies for a given system state beforehand each TSO shall perform security analysis on an operational planning and real time horizon. Remedial actions relieving the congestions identified by the contingency analysis are to be taken. If the effect of a contingency is limited locally and the TSO practices foresees it, the decisions can be made to avoid costly remedial actions. Each N-1 situation of the TSOs contingency lists has to be solved by remedial actions taken by the particular effected TSOs. After applying the actions, the former N-1 case gets the

N-0 case and so a contingency analysis has to be performed by the TSOs again to maintain the required system security.

Contingencies are classified in three types, namely ordinary, exceptional and out-of-range. In usual system operations only the set of ordinary contingencies needs to be assessed. Based on risk estimations of TSOs regarding the probability of exceptional and out-of-range contingencies due to a severe system state the particular contingencies are also taken into account. The particular TSO has to determine adequate remedial actions for the case of an exceptional or out-of-range situation. The simulations have to be performed on an up-to-date simulation model reflecting the actual topology of the grid. Changes in topology or generally the power system (e.g. restructuration or connection/disconnection of large scale generation units affecting the contingencies) have to be taken into account in the contingency analysis and so the lists of contingencies have to be adopted. The selection of contingencies of any category is up to the risk analysis of each TSO, but each of them should contribute on a harmonization of the decision making in nominating potential contingencies.

Summarized, TSOs have to be able to keep their particular system and the overall system in a secure operation state even in exceptional and out-of-range situations. This is ensured by contingency analysis in the time horizon of operational planning to real time operation. TSOs can solve contingencies by applying remedial measures predefined during system contingency analysis. Contingencies having only a regionally limited effect don't need to be resolved if it is the common practice of by the particular TSO. In terms of cooperation TSOs have to at least coordinate their contingency analysis with the TSOs in their observability area which are usually neighboring countries.

3.1.5 NERC

In the US, the North American Electric Reliability Corporation (NERC) is the reliability cooperation regarding transmission systems. It defines four categories reflecting system states and the effects given contingencies are allowed to have on the power system [43]. This studies are to performed on an annually basis as well as for an operation horizon of five years and a planning horizon of five to ten years The system states are categorized as follows:

- Category A: No Contingencies N-0
- Category B: Loss of a single element N-1
- Category C: Loss of multiple elements N-k
- Category D: Events resulting in cascading outages

The standard for operation planning foresees a at least a N-1 secure contingency planning [44] to be able to handle unscheduled changes in the power system.

3.1.6 System Security Cooperations

3.1.6.1 TSC – TSO Security Cooperation

The TSO Security Cooperation (TSC) consist of 27 TSOs in 24 countries and offers a platform where TSOs perform a joint security assessment for day-ahead operational planning called Common Tool for Data Exchange and Security Assessment (CTDS). The CTDS follows a decentralized approach with a centralized exchange center. The participating TSOs generate a forecast dataset individually on their own different forecast methods and upload it to the TSC, where all the datasets are merged and a security analysis is performed for all given time steps, which are usually on an hourly basis. The security assessment method is a N-1 contingency screening based on a AC-load flow algorithm. After

the merging and assessment procedure the system is reduced again to the particular areas of the TSOs and sent back to them. The TSOs then are obliged to find preventive measures to cope with given N-1 violations. Corrective measures can also be evaluated based on the dataset, but are not incorporated into the forecast dataset. After the integration of preventive measures, the modified forecast datasets are again uploaded to the TSC, where they are again merged, assessed, reduced and sent back. At the end of the TSC-process a daily telephone conference is organized, where remaining violations of the N-1 secure system state are processed and corrective measures are discussed as well as multilateral remedial actions for severe congestion cases are coordinated.

Figure 3-4. Participating TSOs in the Transmission System Operator Security Cooperation [45].

3.1.6.2 Coreso

Coordination of Electricity System Operators (Coreso) is a cooperation of TSOs in central Europe exchanging forecast datasets on different time horizons to provide the particular TSO information of the interconnected grid and so complementing their regional information. Coreso incorporates data aggregation and management, different functionalities on multiple time horizons and their visualization in a centralized tool.

On a two-day-ahead basis Coreso determines the cross-boarder-capacities and remedial actions in terms of phase-shifting-transformer set points for Central Western Europe. A development for optimization of cross-border-flows and an enhancement of the network security is actually in progress for Central Southern Europe.

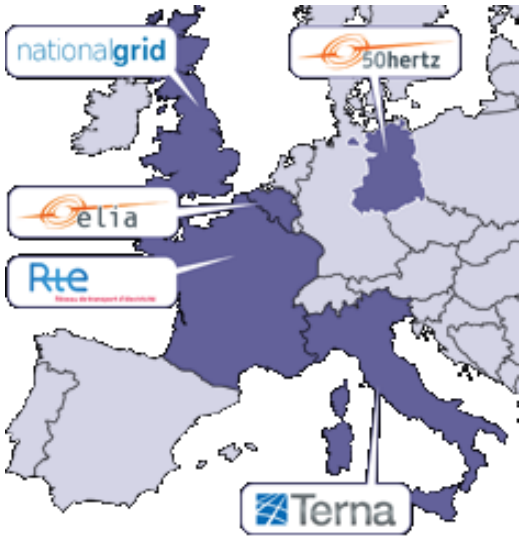

Figure 3-5. Participating TSOs in CORESO [46].

On a basis of day-ahead forecasts Coreso provides a security assessment platform in terms of contingency screening of N-1 and selected N-k events. This procedure consists of a merging of day-ahead (D-1) forecast data to a common grid model, the security assessment and a visualization of the results. The participating TSOs are able to apply remedial measures on their particular grid model and simulate the effects of these measures. A telephone conference and a report close the daily process.

The services performed on the Western European Grid intra-day cover forecast reviewing based on snapshot data and security assessment based on intraday congestion forecasts (IDCF) performed and delivered by TSOs as well as an analysis of the validity of remedial measures in terms of corrective actions recommended during the day-ahead congestion management.

3.1.7 Analysis of Real World Load Forecast Errors

In this subchapter forecast data for the time span of one year are analyzed in terms of statistical measures and compared for two European TSOs' power systems. This analysis is an essence of the work presented in [47].

3.1.7.1 Vertical Grid Load

One of the main challenges when forecasting transmission system loads in terms of active power is, that the actual load is observable for the TSO only in an aggregated manner. Underlying generation as renewable energy sources like wind farms and photovoltaics as well as conventional generation units like hydro or thermal power plants add up to the actual load in terms of end customers demanding power and so the load behavior itself can only be monitored directly by the TSO where no power plants are connected to. Additionally to the mentioned effects there is also the possibility of transit flows through distribution power systems if they are connected to two or more nodes of the transmission system and active power losses of the underlying power system. The particular infeeds and the actual load as well as the DSO transits and losses add up to the vertical grid load P_n according to eq. (3-4).

$$P_n = P_{n,RES} + P_{n,conv} + P_{n,load} + P_{transit} + P_{loss} \quad \textbf{(3-4)}$$

Due to the fact, that the actual load demand can only be directly or approximately observed at nodes, where no underlying conventional and renewable infeeds are present, suitable nodes were manually selected from a data basis of two European TSOs using expert knowledge. Basically, based on the knowledge of the power infeeds from conventional underlying generation as well as embedded RES, their participation information regarding transmission system node loads and the monitored vertical grid load at a particular transmission system node, the actual load could be approximated for all nodes, but due to a lack in information this extraction was not possible.

3.1.7.2 Available Data and Preprocessing

The forecast errors of load dominated transmission grid nodes of two different TSOs (referred as TSO1 and TSO2) were evaluated on the basis of hourly values available for each hour at minute 30. The determination of the forecast uncertainty was done by the subtraction of the monitored data from forecasted data.

3.1.7.3 Missing data handling

Due to measurement errors and measurement device failures there were time steps in the time series of the nodal power demand without any valid data. Nodal time series containing too much non valid data were removed from the data set. Any remaining time steps containing non valid data points were removed hereafter to enable the analysis of the data.

3.1.7.4 Normalization

To be able to comparison the data among each other, a suitable normalization was found. To avoid zero as a normalization reference as well as extreme values (maximum or minimum values) the mean as well as the minimum or maximum values were disregarded as a suitable reference. The 95%-5% inter-quantile of the monitored data ($iqps$ - Inter Quantile Power Spread) was found to be a good basis for normalization, so extreme values of the upper and lower 5% were neglected.

3.1.7.5 Analysis of Statistical Measures

In Figure 3-6 the mean and standard deviation of the active power forecast error are visualized for the nodes of TSO1. The data are plotted against the $iqps$ in active power. The standard deviation is

increasing with an increase of the power spread except for the violet and red marked nodes representing two exceptional nodes in the TSO's area feeding the capital city whereas the other nodes supply mainly a mix of urban and rural customer areas. The mean values seem to be non-related to the inter quantile power spread.

In Figure 3-7 the distribution parameters μ_{FCE} and σ_{FCE} for the grid area of TSO2 are visualized. The expectation values of the forecast error time series tend to zero and do not show a dependency based on the inter quantile power spread. The standard deviation of the data increases with the inter quantile power spread almost linearly.

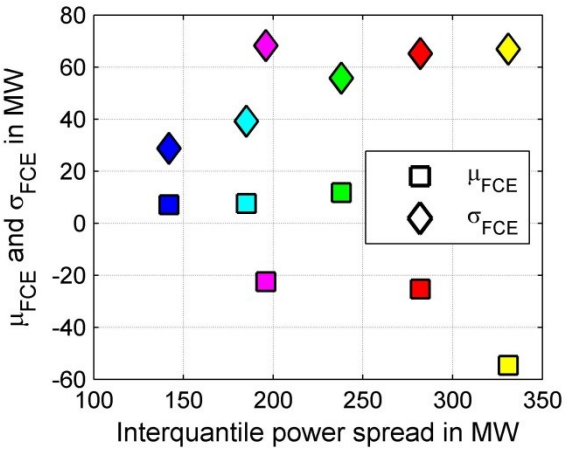

Figure 3-6. Distribution parameters (TSO1).

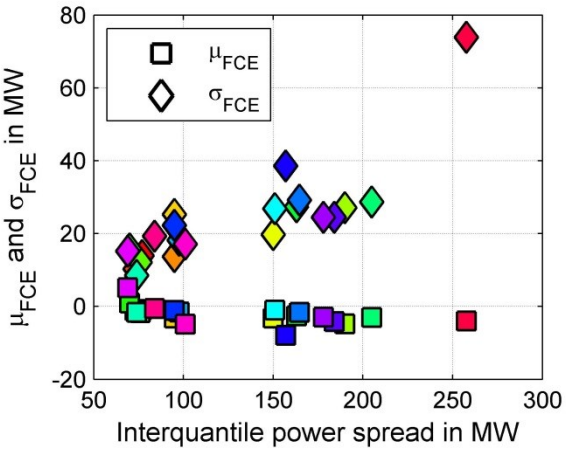

Figure 3-7. Distribution parameters (TSO2).

The normalized μ_{FCE} and σ_{FCE} values of the forecast error are presented in Figure 3-8 for both TSOs. The stochastic measures are given in Table 8-4 and Table 8-5 in Appendix B. The expectation value can be assumed to be zero for all nodes of TSO2 and increases with the $iqps$ value in the case of TSO1. The average normalized standard deviation of the forecast error is 26% in the case of TSO1 and 18% in the TSO2.

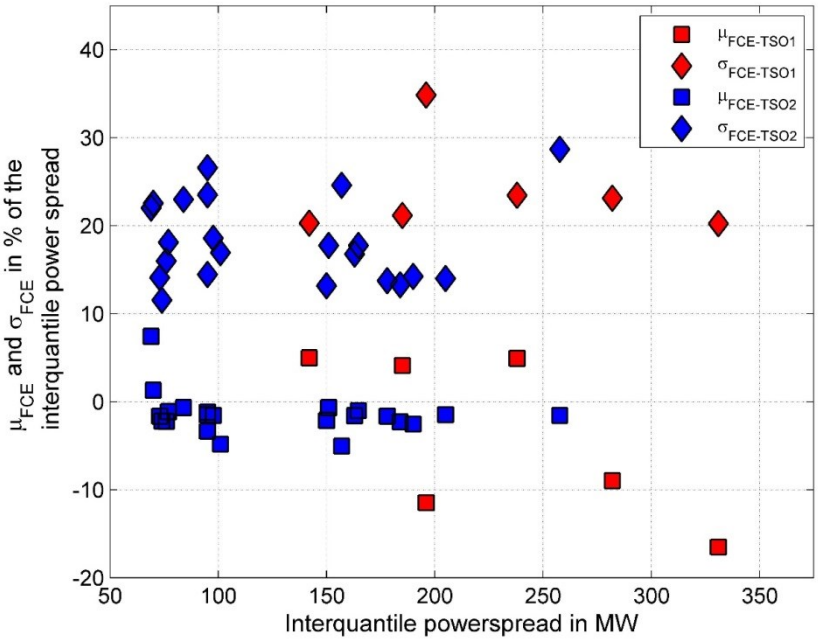

Figure 3-8. Weighted distribution parameters (TSO1-red, TSO2-blue).

3.1.7.6 Correlation of forecast errors between nodes

Besides the distribution parameters of the forecast errors for individual nodes also the correlation among them is important, when it comes to risk based security assessment. The corresponding correlations are analyzed below. The correlation coefficients of the forecast error for the grid area of TSO1 are visualized in Figure 3-9. Only the nodes 5 and 6 are slightly correlated.

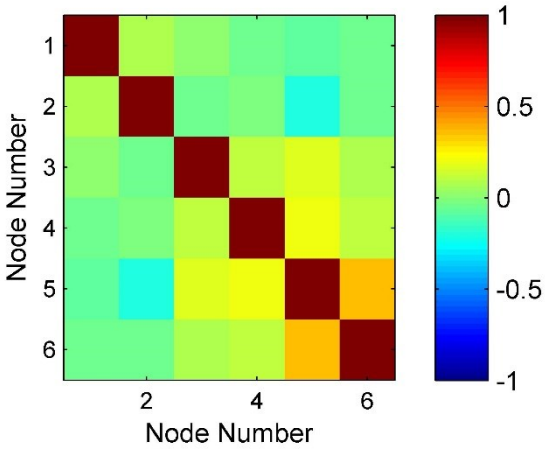

Figure 3-9. Nodal uncertainty correlation concerning the active power.

The visualization of the forecast error correlation coefficient is given in Figure 3-10 for the grid area of TSO2. The load nodes show a higher correlation value for more nodes than it is the case for the small power system of TSO1.

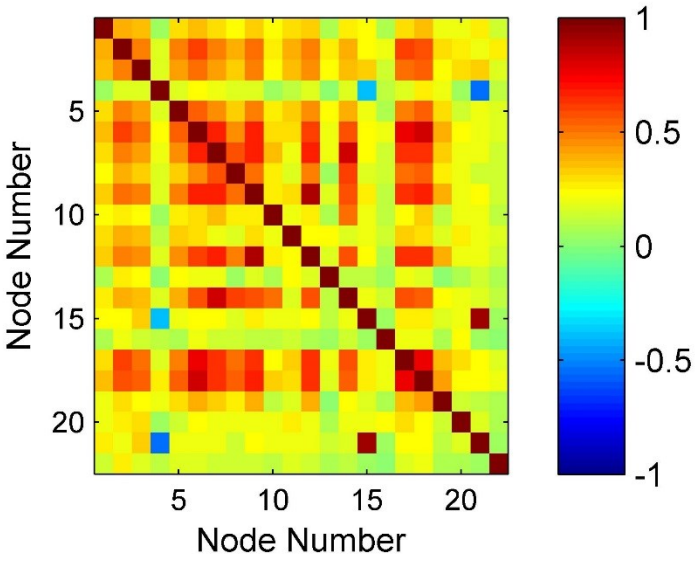

Figure 3-10. Nodal uncertainty correlation concerning the active power.

Concluding the statement is valid, that for both cases there are only a few nodes showing a negative correlation, what would mean, that the load of one node is reduced when the load increases at the particular negatively correlated node. In the grid of TSO1 only two nodes show a slight correlation, while nearly all loads of TSO2 are positively correlated. Negative correlation can be caused e.g. by switching actions and positive correlation can either be caused by similar load characteristics or a by an underlying DSO power system, which is connected to the transmission system at two or more loads.

3.2 Research Questions

Based on the new challenges in transmission system security risk assessment due to the still ongoing structural change in the field of generation and transmission of electrical energy and the survey of existing methods the following requirements for a new risk based approach were identified.

The method should be able to

- assesses and model forecast uncertainties.
- account for overload related outages.
- account for random outages.
- integrate significant parameters for tripping and system blackout, which are to be identified beforehand.
- handle a huge amount of system states.
- give an overall risk measure, which should be evaluated beforehand.
- give a range of uncertainty for the result.
- be applied on large scale power systems and deliver results in a limited time. Therefore different load flow methods should be compared regarding accuracy and computational burden.

4 Probability Guided Security Risk Assessment

4.1 Introduction and Specific Problem Definition

The new challenges rising from a Pan-European energy market and the rising penetration of renewable energy sources (RES) are, that they both bring uncertainty to the forecasting process. In former times, the operator of an integrated power system was able to dispatch the owned power plants to enable a secure grid operation. This means that the operator was able to react on a short time horizon to a load behavior in terms of active power demand which differs from the forecasted values. Today, high penalties in terms of redispatch costs are paid to the market players.

The actual security assessment methods used on a day-ahead time horizon by the members of the ENTSO-E is based on point forecasts and is not able to take uncertainties or trading actions into account. Depending on the particular TSO, up to 24 datasets are provided per day in the day-ahead congestion forecast process. At least four datasets for specified points in time have to be provided by every member TSO.

An enhanced method for the day-ahead contingency forecast process of TSOs should be able to handle the stochastic characteristics of power system loads and generation infeeds on the basis of historical data as well as the correlation of uncertainties It shall show a robust behavior, be applicable on large scale power systems in a limited simulation time and give a risk based measure as an output to allow a ranking of different system states and provide additional information to the classical contingency analysis.

4.2 Method Overview

The method presented in this thesis was designed to be applied on a typical time horizon of a day-ahead forecast horizon. It is able to handle forecast uncertainties like they arise from energy market activities, the large scale introduction of infeeds from renewable energies like wind and solar power. The forecast uncertainties are gained from historical datasets of the power system. To overcome the challenge in simulating all various scenarios which arise from all those historical data a parametric approach is used. The forecast uncertainty is simplified to be reflected by statistical measures as they are the expectation value and the variance of uncertainties. Due to the fact, that there are spatial correlations of forecast errors as well as correlations in time it is necessary to consider the correlation between them. The method of the parametric load flow allows to account for the effect of the uncertainties of infeeds and loads on the expected load flows respectively the variance of the power system's branches. To be able to compare the proposed parametric load flow to conventional Monte-Carlo based load flow methods different realizations of load flow methods are implemented and described in detail in chapter 4.3.1. All the probabilistic load flow implementations have in common, that their output are either stochastic measures, or density functions, reflecting the probability distribution of branch loading. To link the stochastic information about branch flows and the tripping probability of branches a heuristic function is used. This tripping heuristic accounts for protection relay intentional operation, unpredictable, load flow independent outages like avalanches or lightning strokes as well as load flow dependent outage causes like flashovers caused by line sag due to a heavy utilization and voltage related branch tripping. The output of this heuristic is one single cumulated measure per branch reflecting the probability of losing the particular branch.

The knowledge of estimates for the branch tripping probability enables the simulation and screening of numerous outage combinations. An overview about the different modules is given in Figure 4-1.

As an input data the method uses a forecast dataset, like it is already generated by TSOs for the day-ahead congestion management, historic data coming from periodically observations – the so called snapshots, statistical reliability data for each element of the power system and additional information concerning the primary frequency control. The input data is aggregated and referred to as input state.

The two major modules “Next Stage” and “Actual Stage” form the recursive loop which is essential for the screening of multiple system states. The module “Next Stage” evaluates an input system states regarding islanding, primary control actions, or frequency related immediate blackout, performs the probabilistic load flow computation, applies the tripping heuristic, determines the system state probability and filters tripping candidates. For each filtered branch to trip a new system state, based on the evaluated one, is generated and modified that way, that the filtered branch is tripped. This modified system state is then passed to the second major module “Actual Stage”.

The module “Actual Stage” mainly identifies system states based on the passed one in the same simulation stage. This means, that “Actual Stage” scans system states coming from simultaneous branch trippings. If a state exceeds the predefined limit in tripping probability the newly generated state is passed to the module “Next Stage”.

When there are no more system states exceeding the predefined limit in state probability the method returns to the module calling the current one. The simulation is finalized if there are no more system states exceeding the lower limit in system state.

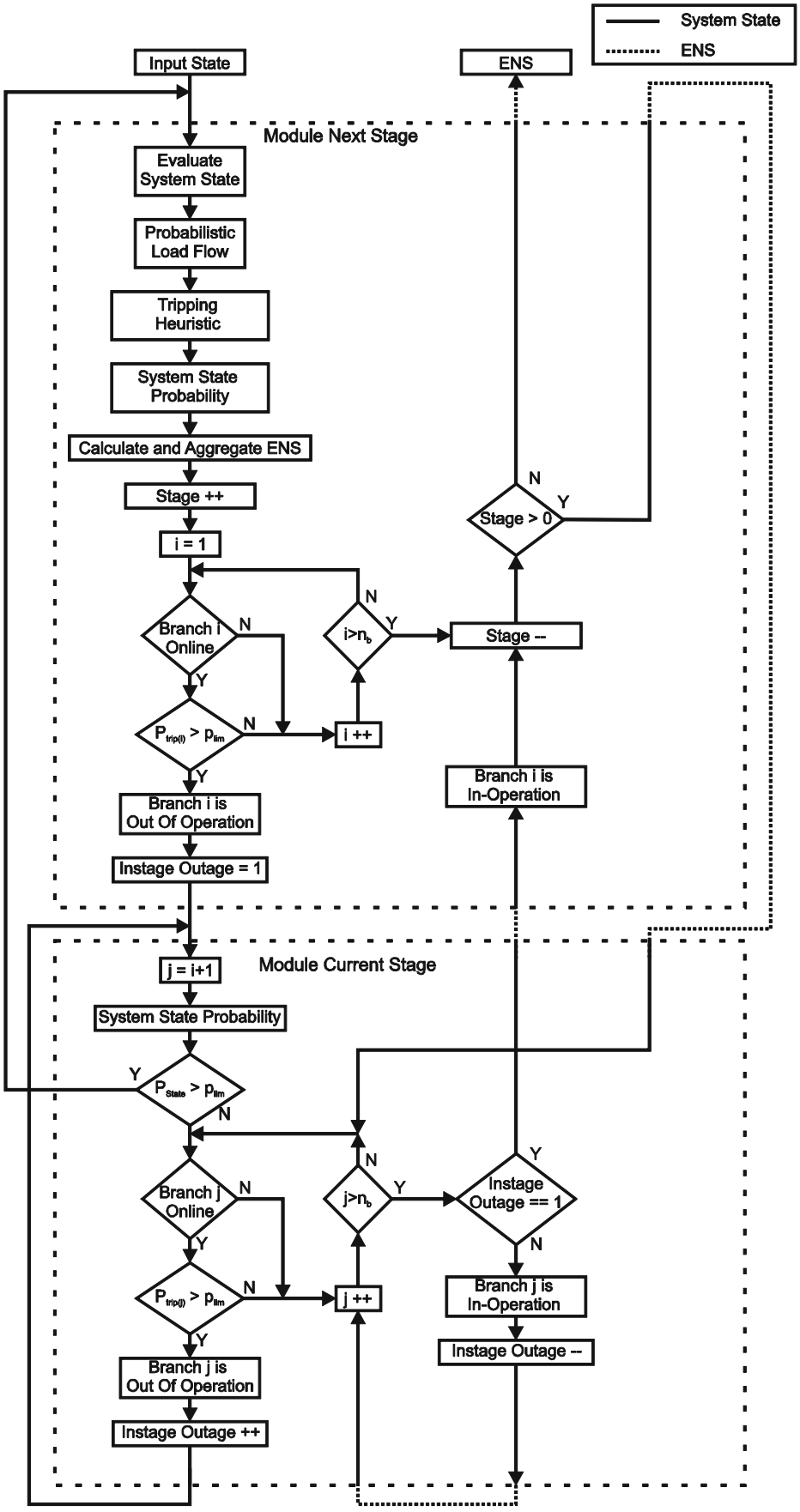

Figure 4-1. Method Flow Chart.

4.3 Probabilistic Load Flow

The probabilistic load flow was implemented in four different ways in this thesis to allow a comparison between the load flow methods. The implemented methods are three different Monte-Carlo simulation methods based on the AC-load flow, AC-PTDF and DC-PTDF and the DC-PTDF based parametric load flow (DC-PLF).

The proposed load flow method in this thesis is the parametric load flow which is able to handle uncertainty afflicted inputs in terms of nodal power injections (infeeds as well as load demands) and is a fast method due to the fact, that it is based on the iteration free DC-PTDFs.

4.3.1 Power System Modelling

The elements of a power system can be categorized in two groups which are shunt elements and series elements also named branches. Nodal elements represent loads and generation units as well as voltage controlling devices like SVCs and STATCOMs or shunt compensation devices. The terminology branch means lines, transformers, FACTS which connect two nodes like the TCSC series compensation units and HVDC-lines.

4.3.1.1 Conversion to per unit

It is common to convert the power system equation into per unit values. This simplifies the process of building the bus admittance matrix, because there is no need to introduce a reference voltage level and will lead the iterative solution process to a faster convergence or enable even convergence in limit conditions. There is only a need to provide normalization values in for power measures. Following eq. (4-1) apparent, active as well as reactive power values can be converted to per unit. They are normalized regarding S_{base}, P_{base} and Q_{base} which is the same predefined value showing the particular unit ($MVA, MW\ or\ Mvar$).

$$S_{p.u.} = \frac{S}{S_{base}} \qquad P_{p.u.} = \frac{P}{P_{base}} \qquad Q_{p.u.} = \frac{Q}{Q_{base}} \tag{4-1}$$

Voltage measures are converted into the per unit format by normalizing them to the particular node's nominal line voltage.

$$U_{p.u.} = \frac{U}{U_n} \tag{4-2}$$

All reference values can be determined out of the two given above. The reference for the per unit conversion of impedances, reactances and resistances can be determined as given in eq. (4-3).

$$Z_{base} = \frac{\left(\frac{U_n}{\sqrt{3}}\right)^2}{\frac{S_{base}}{3}} = \frac{U_n^2}{S_{base}} \tag{4-3}$$

Especially when it comes to the conversion of transformer resistances and reactances it is necessary to know for which node of the branch the given value is valid.

The normalization basis for current values is determined according eq. (4-4).

$$I_{base} = \frac{S_{base,ph}}{U_{base,ph}} = \frac{\frac{S_{base}}{3}}{\frac{U_n}{\sqrt{3}}} = \frac{S_{base}}{\sqrt{3} \cdot U_n} \tag{4-4}$$

The turns ratio can be converted into per unit following eq. (4-5).

$$\underline{\ddot{u}}_{p.u.} = \frac{\underline{\ddot{u}}}{\frac{\underline{U}_{i,n}}{\underline{U}_{j,n}}} \tag{4-5}$$

The results of the load flow calculation can be transformed to absolute values by multiplying the per unit value with the particular normalization value as stated in eq. exemplarily for the nodal apparent power.

$$S_N = s_N \cdot S_{base} \tag{4-6}$$

It is common practice to omit the index $p.u.$ The subsequent quantities are $p.u.$ values.

4.3.1.2 Power System Equations

To describe a power system in a mathematically way it is common to use the admittance matrix. It enables to take all aforementioned (branches as well as nodal elements) elements into account. Branches can be modelled as an element connecting two nodes and define the topology of the system. The load flow of a branch element represented in Figure 4-2 by a series impedance Z_b can be expressed in a mathematical way as follows.

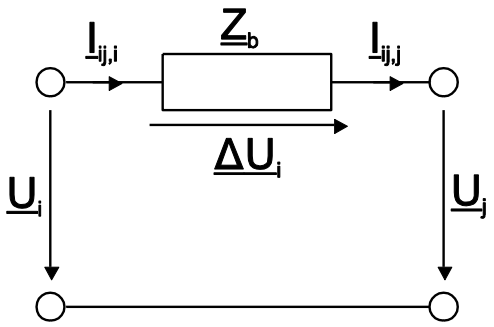

Figure 4-2. Branch Modelling.

By the knowledge of the nodal phase voltages U_i and U_j the branch current I_b can be calculated according to eq. (4-7).

$$\underline{I}_b = \frac{\Delta U_b}{\underline{Z}_b} = \frac{\underline{U}_i - \underline{U}_j}{\underline{Z}_b} = \underline{Y}_b \cdot \left(\underline{U}_i - \underline{U}_j\right) \tag{4-7}$$

In power systems nodes usually are connected by multiple branches.

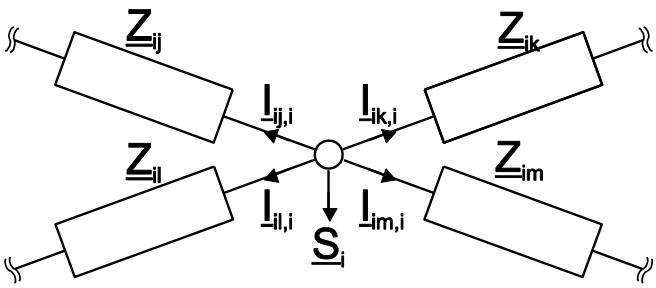

Figure 4-3. Meshed Grid Node i.

For this example eq. (4-8) is valid, assuming that nodal loads are defined as positive and it can be generalized according eq. (4-9).

$$I_{ij} + I_{ik} + I_{il} + I_i = 0 \quad \textbf{(4-8)}$$

$$I_n = \sum_{i \in N} I_{ni} \quad \textbf{(4-9)}$$

This generalized equation is valid for one node of a power system. To model this relation for all nodes the admittance matrix $\mathrm{Y_{bus}}$ is used. This matrix is calculated by using the branch membership matrix C_{ft} describing, where a branch begins, and where it ends. It has number of branches lines and number of busses columns and holds the value 1 at the particular column – reflecting the start node – where branch b begins and -1 where at the particular column where branch b's end is connected to. The system admittance matrix can now be calculated by a simple matrix multiplication according to eq. (4-10), where $\underline{Y_B}$ is a column vector holding all branch admittances.

$$\mathrm{Y_{bus}} = \mathrm{Cft^T} \cdot diag(Y_B) \cdot C_{ft} \quad \textbf{(4-10)}$$

4.3.1.3 Taking into account off nominal turn ratios and phase shifts

When it comes to transformers or series equivalents connecting two nodes with different nominal voltages the voltage ratio and the shift angle have to be taken into account.

The turns ratio of a transformer can be calculated by the quotient of the number of turns on the secondary side of the transformer and the primary side according to eq. (4-11).

$$\ddot{\mathrm{u}} = \frac{\mathrm{w_j}}{w_i} \quad \textbf{(4-11)}$$

Due to the fact that three phase transformers also can introduce a phase shift according to the way primary respectively secondary windings are connected among each other the complex turn ratio $\underline{\ddot{\mathrm{u}}}$ is defined as given in eq. (4-12), where $\Delta\psi$ is the angle which the secondary voltage $\underline{U_j}$ lags the primary voltage $\underline{U_i}$.

$$\underline{\ddot{\mathrm{u}}} = \frac{\mathrm{w_j}}{w_i} \cdot e^{-j \cdot \Delta\psi} \quad \textbf{(4-12)}$$

Due to the fact, that the voltage of the secondary node is given by the multiplication of the complex turn ratio $\underline{\ddot{\mathrm{u}}}$ and the voltage of the primary node eq. (4-13)holds.

$$\underline{\mathrm{U_j}} = \underline{\ddot{\mathrm{u}}} \cdot \underline{U_i} = \underline{U_i} \cdot \ddot{\mathrm{u}} \cdot e^{-j \cdot \Delta\psi} \quad \textbf{(4-13)}$$

The secondary winding's current is determined by multiplying the primary current with the reciprocal value of the turn ratio in terms of absolute values. Due to the fact that both, the current as well as the voltage experience a phase shift by $-\Delta\psi$ the calculation of the complex value of the secondary winding's current is performed by dividing the current of the primary winding by the conjugate complex turn ratio.

$$\underline{\mathrm{I_{ij,j}}} = \frac{\mathrm{I'_{ij,j}}}{\underline{\ddot{\mathrm{u}}^*}} = \underline{\mathrm{I'_{ij,j}}} \cdot \frac{1}{\ddot{\mathrm{u}}} \cdot e^{-j \cdot \Delta\psi} \quad \textbf{(4-14)}$$

The power system equations for two nodes i and j connected by a transformer or a series equivalent with different nominal voltages as shown in Figure 4-4 can be determined by taking the complex turn ratio into account.

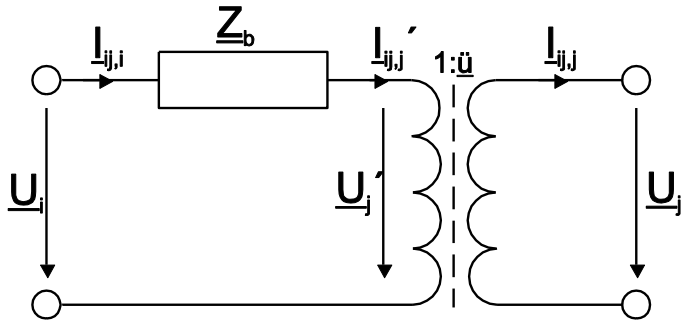

Figure 4-4. Branch Modelling.

In eq. (4-15) and (4-16) the current equations for branches with turns ratios and phase shifts are given.

$$\underline{\mathrm{I}}_{\mathrm{ij,i}} = \frac{\underline{U}_i - \underline{U}_j'}{\underline{Z}_b} = \frac{\underline{U}_i}{\underline{Z}_b} - \frac{1}{\underline{Z}_b} \cdot \frac{\underline{U}_j}{\underline{\ddot{u}}} \tag{4-15}$$

$$\underline{\mathrm{I}}_{\mathrm{ij,j}} = \frac{\underline{\mathrm{I}}'_{\mathrm{ij,j}}}{\underline{\ddot{u}}^*} = \frac{1}{\underline{\ddot{u}}^*} \cdot \left[\frac{\underline{U}_i - \underline{U}_j'}{\underline{Z}_b}\right] = \frac{\underline{U}_i}{\underline{\ddot{u}}^* \cdot \underline{Z}_b} - \frac{1}{\underline{Z}_b} \cdot \frac{\underline{U}_j}{\underline{\ddot{u}}^2} \tag{4-16}$$

For a power system consisting of numerous nodes and branches the following generalized expression is valid for modelling a branch element b, connecting the nodes i and j and showing a complex turns ratio $\underline{\ddot{u}}$. The branch's impedance is given for the nominal voltage of node i.

$$\underline{\mathrm{Y}}_{\mathrm{ii}} = \frac{1}{\underline{Z}_b} \tag{4-17}$$

$$\underline{\mathrm{Y}}_{\mathrm{ij}} = -\frac{1}{\underline{Z}_b \cdot \underline{\ddot{u}}} \tag{4-18}$$

$$\underline{\mathrm{Y}}_{\mathrm{ji}} = -\frac{1}{\underline{Z}_b \cdot \underline{\ddot{u}}^*} \tag{4-19}$$

$$\underline{\mathrm{Y}}_{\mathrm{jj}} = \frac{1}{\underline{Z}_b \cdot \underline{\ddot{u}}^2} \tag{4-20}$$

4.3.1.4 Taking into account parallel losses and capacitances

In the case of lines, transformers and series equivalents, it's quite common to model the particular voltage dependent losses respectively the parallel capacitance as shown in Figure 4-5.

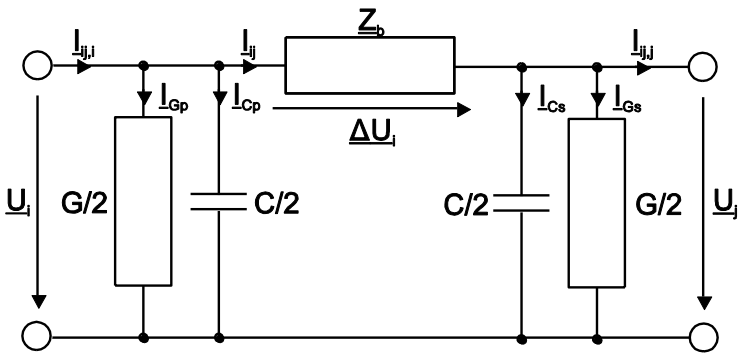

Figure 4-5. Modelling of Parallel Losses and Capacitances.

The parallel elements $G/2$ and $C/2$ are directly connected to the node i respectively j and they can be seen as an additional current injection in the particular node. This current injection is solely voltage dependent and can be calculated for the node i according to eq. (4-21) and (4-22) and analogous for node j accounting for turns rations if applicable.

$$\underline{I}_{Gi} = \underline{U}_i \cdot \frac{G}{2} \quad \textbf{(4-21)}$$

$$\underline{I}_{Ci} = \underline{U}_i \cdot \frac{j \cdot \omega \cdot C}{2} \quad \textbf{(4-22)}$$

Generalized the loss related current of branch b at the primary node i it is connected to can be expressed as given in eq. (4-23) for node i and analogous for the secondary node j. $\underline{Y}_{Lb}$ denotes the total parallel admittance of branch b reflecting losses.

$$\underline{I}_{Lb,i} = \underline{I}_{Gi} + \underline{I}_{Ci} = \underline{U}_i \cdot \frac{G + j \cdot \omega \cdot C}{2} = \underline{U}_i \cdot \frac{\underline{Y}_{Lb}}{2} \quad \textbf{(4-23)}$$

This current equation can be integrated into the bus admittance matrix following eq. (4-24) by adding the particular parallel admittance to the main diagonal of the bus matrix for node i and analougous for node j accounting for turns ratios if necessary.

$$\underline{Y}_{bus,ii} = \underline{Y}_{bus,ii} + \frac{\underline{Y}_{Lb}}{2} \quad \textbf{(4-24)}$$

4.3.1.5 From Current Flow to Load Flow

According to Ohm's law eq. (4-25)leads to the vector $\mathrm{I_N}$ of nodal current injections, where $\mathrm{U_N}$ is the vector of the nodal voltages.

$$\underline{\mathrm{I}}_{\mathrm{N}} = \underline{\mathrm{Y}}_{\mathrm{bus}} \cdot \underline{\mathrm{U}}_{\mathrm{N}} \quad \textbf{(4-25)}$$

When performing load flow computations, the given measure usually is a set of nodal power injections in terms of apparent power than nodal current injections. The nodal apparent power $\mathrm{S_N}$ can be calculated as the product of the diagonal matrix of the bus voltages and the conjugate of the nodal current vector $\mathrm{I_N}$.

$$\mathrm{S_N} = \mathrm{diag}\left(\underline{\mathrm{U}}_{\mathrm{N}}\right) \cdot \underline{\mathrm{I}}_{\mathrm{N}}^{*} = diag\left(\underline{\mathrm{U}}_{\mathrm{N}}\right) \cdot \underline{Y}_{bus}^{*} \cdot \underline{U}_{N}^{*} \quad \textbf{(4-26)}$$

Due to the circumstance that this equation system is not linear, it is not trivial to make the bus voltage vector U explicit. There are two ways to overcome this problem. Either, the application of an iterative solver or the simplification of the equation system. First, one leads to the common implementation of AC-load flow computation methods, the latter leads to the DC-load flow.

4.3.1.6 Load Flow Implementation of PFCCs

This section is about implementing PFCCs into the presented method. The selected PFCCs are HVDC lines, phase shifting transformers and as a FACTS device the TCSC. They all have the same effect on load flows in terms of steady state computation. They all have an effect on the active load flow, but they are modelled in different ways and so have a different influence on the risk of the power system.

4.3.1.6.1 HVDC lines

4.3.1.6.1.1 Integration of HVDC lines in the load flow calculation

HVDC lines are modelled in this work as active power injections. To account for the losses in active power they are modelled according to eq. (4-27) consisting of load flow independent losses reflected by α_0 and load flow dependent ones modelled by the parameter α_1 as proposed in [48].

$$P_{HVDC,t} = P_{HVDC,f} - \left|P_{HVDC,f}\right| \cdot \alpha_1 - \alpha_0. \quad \textbf{(4-27)}$$

The HVDC lines power injections are added to the systems nodal power vector P_N as given in eq. (4-28) resp.(4-29):

$$P_n = P_n + P_{HVDC,f} \forall n \in F, \quad \textbf{(4-28)}$$

$$P_n = P_n - P_{HVDC,t} \forall n \in T. \quad \textbf{(4-29)}$$

The parameterization of the dataset is exactly the same as defined in the MATPOWER format [49].

4.3.1.6.1.2 Outage probability modelling of HVDC lines

HVDC lines consist of power electronics and conventional lines, so the outage probability of HVDC lines differs significantly from HVAC lines. This is taken into account by formulating the "HVDC branch-loading to branch-tripping-probability function" consisting of an offset value reflecting the outage probability of the line (β_0 in eq. (4-30)) and a load dependent increasing part in tripping probability reflecting the power electronics part (β_1 in eq. (4-30)). Facing the fact that the utilization of HVDC lines is modelled here as deterministic values (the mean value is the set point of the HVDC and there is no variance in HVDC line loading) the outage probability is simply calculated by eq. (4-30).

$$\overline{P_{trip\ hvdc,b}} = \beta_0 + P_{hvdc,b} \cdot \beta_1. \quad \textbf{(4-30)}$$

4.3.1.6.2 Phase shifting transformers

Phase shifting transformers (PSTs) are used to control mainly the active load flow in a line they are connected to and as a consequence of meshed grids also the lines surrounding it. Due to the increased transits in the pan European transmission system numerous PSTs were installed to on control load flows and so to account for the security of the overall power system. PSTs have become an important degree of freedom in today's transmission system operation.

4.3.1.6.2.1 Variants of Shifting Transformers

There are different kinds of phase shifting transformers, namely symmetrical and asymmetrical shifting transformers [50]. Their voltage phasor diagrams are shown in Figure 4-6 resp. Figure 4-7. The main difference between these two kinds of shifting transformers is that the magnitude of the primary and secondary terminal voltage is not equal. So the symmetrical phase shifting transformer introduces solely a shift in voltage angle, but the asymmetrical one affects also the voltage magnitude. Assuming e.g., a perfect high voltage grid with reactive elements only the symmetrical shifting transformer would add an additional active load flow to the line it is connected to but the asymmetrical one would also cause a reactive one.

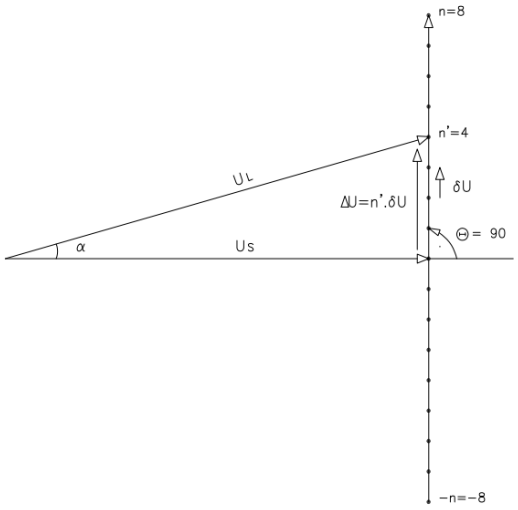

Figure 4-6. Asymmetrical shifting transformer with Θ = 90° [50].

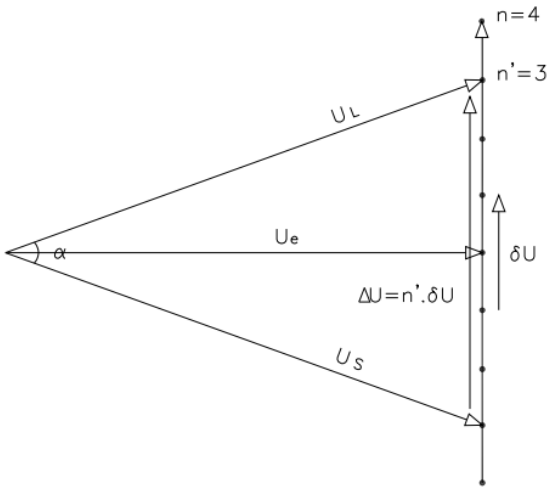

Figure 4-7. Symmetrical shifting transformer [50].

In the case of asymmetrical PSTs there are not exclusively those adding an additional voltage with a phase angle of 90° but also ones differing from 90°. The voltage phasors are visualized in Figure 4-8, showing the additional voltage with an angle $\theta \neq 90°$. For all variants the statement that the angle shift is influenced by the magnitude of the additional voltage is valid.

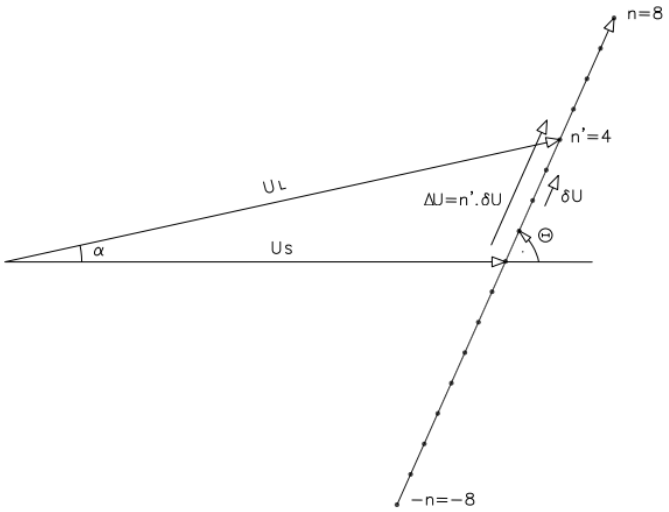

Figure 4-8. Asymmetrical shifting transformer with Θ ≠ 90° [50].

4.3.1.6.2.2 PST modelling

As already mentioned in the foregone section PSTs introduce an additional voltage angle spread and in some cases also influence the voltage magnitude. Due to the properties of the – in this method used – DC-load flow formulation it is not accounting for voltage levels so the only parameter of interest is the phase shift angle α of a particular PST.

The input data needed is stored according to the Matpower format given in [49]. The only input value needed is the shift angle α.

In Figure 4-9 the way how a PST in series to a line is modeled in the presented method is illustrated following to the work published in [51]. The first schematic shows a line modelled in DC-load flow simply by its reactance. In the second one a PST is placed in series to the line introducing an angle

shift of α_{PST}. Due to the DC-load flow formulation this voltage angle shift can be expressed as a parallel active power source. The set-point of the equivalent parallel power source P_f is given by eq. (4-31).

$$P_f = \frac{\alpha_{PST}}{X_{12}}. \quad \textbf{(4-31)}$$

Facing the fact that constant parallel power sources are hard to model it is replaced by nodal power injections on the beginning and the end of the line the PST is connected to which can be implemented in the equations of the DC-load flow by adding the injected power at the "from" node of the particular line and subtracting it at the "to" node of it.

$$P_n = P_n + P_f \forall n \in F, \quad \textbf{(4-32)}$$
$$P_n = P_n - P_f \forall n \in T. \quad \textbf{(4-33)}$$

In the "Simplification" subfigure in Figure 4-9 it is obvious, that the injected power adds up to the load flow of the PST so the real load flow can be calculated by subtracting the injected power from the particular branch's load flow.

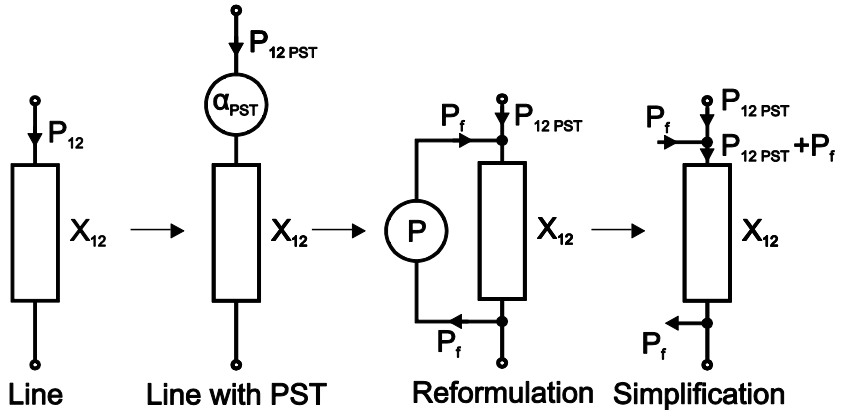

Figure 4-9. PST modelling [51].

The PST influenced load flow over the line can be determined according to eq. (4-34):

$$P_{12PST} = P_{12} - P_f. \quad \textbf{(4-34)}$$

4.3.1.6.3 FACTS

There are various types Flexible AC-Transmission Systems (FACTS) introducing controllability into transmission systems, either in terms of active or reactive load flows and in consequence in terms of voltage angles and magnitudes. [52] gives a detailed view on each of the FACTS devices. The most important FACTS elements in real world power system operation are static compensators like e.g., SVC and STATCOM. They are able to provide or demand reactive power in the node they are connected to and change their set-points very quickly. So they are ideal to locally compensate fluctuating demand in reactive power and account for the node voltage magnitude. In contrast to this the Thyristor Controlled Series Compensator (TCSC) introduces controllability in meshed grids by influencing the branch's impedance they are connected in series with. They generally consist of a thyristor controlled capacitor parallel to an inductor. Optionally there can be a fixed compensation by another capacitor in series. So a TCSC is able to change its reactance during power system operation and so influence the load flow of the line it is in series to and as a consequence parallel ones also. By lowering the reactance of the TCSC the load flow can be attracted, and by increasing the reactance it can be suppressed. FACTS-devices also to be mentioned are the Unified Load Flow

Controllers (UPFC) or the Static Synchronous Series Compensators (SSSCs) providing additional flexibility to the TSOs daily business.

Due to the limited relevance in pan European power systems in this work solely the TCSC FACTS element was selected for implementations, which can be modelled as a series reactance to the branch it is connected to according to the work done in [53]. The parameters of the TCSC element are a set-point X_{TCSC} and the maximum X_{TCSC}^{max} and minimum X_{TCSC}^{min} limits of the device which are used as constraints during an upstream optimization. During the cascading risk assessment, the set-point of the FACTs device is not changed but it's tested on plausibility by performing a check concerning the provided limits.

$$X_{TCSC}^{min} \leq X_{TCSC} \leq X_{TCSC}^{max}. \quad \textbf{(4-35)}$$

For each branch of the given power system a TCSC is connected to (B_{TCSC}) the branch reactance X_b is modified according to eq.(4-35).

$$X_b = X_b + X_{TCSC}\ \forall b \in B_{TCSC}. \quad \textbf{(4-36)}$$

4.3.1.6.4 Monte-Carlo Simulation based Methods

4.3.1.6.4.1 AC-Load Flow Method (Newton-Raphson)

There are multiple implementations known to solve the non-linear power system equations. The most popular of them are the Newton-Raphson or the Gauß-Seidl both having their advantages and drawbacks in terms of convergence and the number of iterations needed to gain a desired pre-defined accuracy.

4.3.1.6.4.2 DC-Load Flow Method

The DC-Load Flow method is based on the following assumptions leading to a linear equation system enabling an iteration free calculation.

1. Bus voltages are assumed to be 1 p.u.
2. Reactive power is neglected
3. The power system's branches are assumed to have a fully reactive characteristic
4. The system is lossless
5. Voltage angles are rather small

Assumption 3 mainly affects the system admittance matrix, which gets the system susceptance matrix as stated in eq. (4-37).

$$\mathrm{B_{bus}} = \mathrm{C_{ft}}^{\mathrm{T}} \cdot diag(B_{branch}) \cdot C_{ft} \quad \textbf{(4-37)}$$

$$\begin{aligned} \underline{\mathrm{S_n}} &= \mathrm{U_n^2} \cdot \underline{Y_{nn}^*} + \sum_{\substack{i=1 \\ i \neq n}}^{N} \underline{U_n} \cdot \underline{U_i^*} \cdot \underline{Y_{ni}^*} \\ &= U_n^2 \cdot Y_{nn} \cdot [\cos(-\psi_{nn}) + j \cdot \sin(-\psi_{nn})] + \\ &+ \sum_{\substack{i=1 \\ i \neq n}}^{N} U_n \cdot U_i \cdot Y_{ni} \cdot [\cos(\theta_n - \theta_i - \psi_{ni}) + j \cdot \sin(\theta_n - \theta_i - \psi_{ni})] \end{aligned} \quad \textbf{(4-38)}$$

Due to the fact, that the reactive power is neglected the term for the active power can be extracted according to eq. (4-39).

$$\mathrm{P_n} = U_\mathrm{n}^2 \cdot Y_{nn} \cdot \cos(-\psi_{nn}) + \\ + \sum_{\substack{i=1 \\ i \neq n}}^{N} U_n \cdot U_i \cdot Y_{ni} \cdot \cos(\theta_n - \theta_i - \psi_{ni}) \tag{4-39}$$

The assumptions that each voltage magnitude is 1 p.u. and the impedance of branches is reactive leads to eq. (4-40). Due to the assumption, that branches have an inductive characteristic the impedance of a branch could be expressed as $\underline{Z} = Z \cdot e^{j \cdot \chi} = j \cdot X = X \cdot e^{j \cdot 90°}$ and the admittance could be expressed as $\underline{Y} = Y \cdot e^{j \cdot \psi} = \frac{1}{\underline{Z}} = \frac{1}{Z} \cdot e^{-j \cdot \chi} = \frac{1}{X} \cdot e^{-j \cdot 90°}$

$$\mathrm{P_n} = \cos(90°) + \\ + \sum_{\substack{i=1 \\ i \neq n}}^{N} Y_{ni} \cdot \cos(\theta_n - \theta_i + 90) = -\sum_{\substack{i=1 \\ i \neq n}}^{N} Y_{ni} \cdot \sin(\theta_n - \theta_i) \tag{4-40}$$

If the voltage angle differences are rather small the value of the sinus function is approximately the function argument.

$$\mathrm{P_n} = -\sum_{\substack{i=1 \\ i \neq n}}^{N} Y_{ni} \cdot (\theta_n - \theta_i) = -\sum_{\substack{i=1 \\ i \neq n}}^{N} B_{ni} \cdot (\theta_n - \theta_i) \tag{4-41}$$

$$\mathrm{P_n} = -\mathrm{B_{bus}} \cdot \Theta_n \tag{4-42}$$

The bus susceptance matrix is singular so a reference bus has to be defined and the lines and columns related to it have to be omitted. This matrix is denoted by $\mathrm{B_{bus_{(\sim ref, \sim ref)}}}$.

$$\Theta_{N_{(\sim ref)}} = inv\left(B_{bus_{(\sim ref, \sim ref)}}\right) \cdot \mathrm{P_{n_{(\sim ref)}}} \tag{4-43}$$

4.3.1.6.5 DC-Based Parametric Load Flow (DC-PLF)

The probabilistic load flow is based on the assumption that the input variables are normally or close to normally distributed. This assumption allows to simplify load flow computations for uncertainty afflicted, which would usually require the use of Monte-Carlo simulation techniques, to determine the probability distribution of branch loadings in two calculation steps. Due to the fact that a normally distributed random variable can be fully described by the expectation value and the variance and the fact that the sum of normally distributed random variables again lead to a normally distributed variable. To be able to use this advantage in load flow calculations some simplifications have to be made. Due to the fact that the power system's branch loadings have to be directly expressible as a linear function of nodal powers the load flow equations need to be linearized. That directly leads to the use of power transfer distribution factors (PTDFs). They can either be computed based on the Jacobian matrix of an initial AC-load flow simulation or directly by the use of DC-load flow.

4.3.1.6.5.1 The Expectation Value

The expectation value of historical observations in the shape of a column vector X holding N observations where x_n is the n_{th}element oft he vector can be calculated according eq. (4-44). This value reflects the sum of the elements of X weighted by their probabilities of occurrence. Due to the fact that all observations in a time series have the same probability the expectation value is simply the mean value of a variables observations.

$$E[X] = \sum_{n=1}^{N} x_n \cdot p_n = \sum_{n=1}^{N} x_n \cdot \frac{1}{N} = \frac{\sum x_n}{N} = \overline{X} = \mu \qquad \textbf{(4-44)}$$

If the analyzed data is e.g. reflecting a forecast error an expectation value different from zero leads to the conclusion that the forecast method shows a systematic deviation.

4.3.1.6.5.2 Variance and Standard Deviation

The variance of the data in vector X can be calculated according eq. (4-45) and gives the expectation value of the squared deviation of the expectation value of the data in X. It is a measure for the spread of the data given in X. Often the standard deviation is used which is the square root of the variance.

$$Var(X) = E[(X-\mu)^2] = E[(X-E[X])^2] = E[X^2] - (E[X])^2 = \sigma_{xx} = \sigma_x^2 \qquad \textbf{(4-45)}$$

If the data in X reflects a forecast error a higher variance indicates a higher uncertainty.

4.3.1.6.5.3 Covariance and Correlation of Random Variables

Assuming Z to be a dataset of observations of multiple variables over time in form of a matrix with number of observations rows and number of variables columns the expectation value as well as the variance of each variable can be calculated separately. These two measures reflect only properties of the particular variable, but don't give any information about the interdependence of the variables among each other. To account for this interdependence of two or more random variables the covariance is used. The covariance reflects the variance of the joint variable of two variables.

The covariance can be calculated according eq. (4-46), where X and Y are variables of the observation set Z.

$$cov(X,Y) = E[(X-E[X]) \cdot (Y-E[Y])] = \sigma_{xy} \qquad \textbf{(4-46)}$$

The covariance is a measure which is quite common in statistics, but in data analysis often the correlation coefficient of variables is used more often, because of it's straight forward interpretability without the need of taking account of the variance of the particular variables and because it is bounded to lie between +1 and -1. It describes the relation of the joint variance of the two variables, relatively to the product of the standard deviation of each of them. E.g. perfect positive correlation reflects, that positive deviations of the mean values occur in the same observation points leading to a correlation coefficient of 1. On the other hand, if one variable has always it's highest values, when the other one shows it's lowest and vice versa the correlation coefficient would be -1.

By the knowledge of the covariance and the variances of the variables X and Y the correlation coefficient can be determined following eq. (4-47) for each combination of variables in Z.

$$\rho_{xy} = \frac{\sigma_{xy}}{\sigma_x \cdot \sigma_y} = \frac{cov_{xy}}{\sigma_x \cdot \sigma_y} \quad \textbf{(4-47)}$$

Assuming that the correlation coefficient and the variance per variable are given as input parameters the covariance matrix can be calculated according eq. (4-48).

$$\Sigma = \begin{bmatrix} \sigma_{xx} & \cdots & \sigma_{xy} \\ \vdots & \ddots & \vdots \\ \sigma_{yx} & \cdots & \sigma_{yy} \end{bmatrix} = \begin{bmatrix} \sigma_x & 0 & 0 \\ 0 & \ddots & 0 \\ 0 & 0 & \sigma_y \end{bmatrix} \cdot \begin{bmatrix} 1 & \cdots & \rho_{xy} \\ \vdots & \ddots & \vdots \\ \rho_{yx} & \cdots & 1 \end{bmatrix} \cdot \begin{bmatrix} \sigma_x & 0 & 0 \\ 0 & \ddots & 0 \\ 0 & 0 & \sigma_y \end{bmatrix} \quad \textbf{(4-48)}$$

If the correlation matrix is given the matrix of correlation coefficients can be calculated according to eq. (4-49), where $diag(\Sigma)$ denotes the matrix of main diagonal of the covariance matrix Σ.

$$Corr(Z) = \left(diag(\Sigma)\right)^{-\frac{1}{2}} \cdot \Sigma \cdot \left(diag(\Sigma)\right)^{-\frac{1}{2}} \quad \textbf{(4-49)}$$

4.3.1.6.5.4 Expectation Value of Branch Loadings

The foregone evaluated AC- as well as DC-PTDF matrices can be used to determine the expectation value of the branch loadings by performing a matrix multiplication. The vector $P_{N,\mu}$ holds the expectation values of the nodal power injections . This is valid for generators as well as loads when their particular nodal power injection is aggregated at the proper node.

$$\mathrm{P}_{\mathrm{B},\mu} = PTDF \cdot P_{N,\mu_{(\sim ref)}} \quad \textbf{(4-50)}$$

4.3.1.6.5.5 Variance of Branch Loadings

By the knowledge of the covariance matrix of the nodal power injections and the AC- respective DC-PTDF matrix the variance of all branch loadings can be determined, where $PTDF_{B,i}$ is the i[th] row of the PTDF matrix and $P_{N,\sigma(i)}$ is the standard deviation in nodal active power injection of node i.

$$\mathrm{P}_{B,\sigma(b)^2} = \sum_{i=1}^{n_b} \sum_{j=1}^{n_b} PTDF_{B,i} \cdot PTDF_{B,j} \cdot P_{N,\sigma(i)} \cdot P_{N,\sigma(j)} \quad \textbf{(4-51)}$$

The equivalent operation is given as a matrix operation in eq. (4-52), where $\mathrm{P}_{\mathrm{N},\Sigma}$ is the full covariance matrix of the nodal active power injections and 1_{nb} is a column vector of the size equal to number of busses.

$$\mathrm{P}_{\mathrm{B},\sigma^2} = \left(PTDF \circ \left(PTDF \cdot \mathrm{P}_{\mathrm{N},\Sigma)}\right)\right) \cdot 1_{nb} \quad \textbf{(4-52)}$$

4.3.1.6.5.6 AC-Power Transfer Distribution Factors

AC-Power Transfer Distribution Factors (AC-PTDFs) are a simplified approach to determine branch flows when performing a probabilistic load flow. Just one AC-load flow computation is needed to determine the Jacobian of the power system of interest in a given linearization point. The Jacobian consist of four different quadrants reflecting the linearized dependency between the change in active and reactive nodal powers and the nodal voltage magnitudes and angles according to eq. (4-51).

$$J = \begin{bmatrix} J_{11} & J_{12} \\ J_{21} & J_{22} \end{bmatrix} = \begin{bmatrix} \frac{\partial P_n}{\partial \theta_n} & \frac{\partial P_n}{\partial V_n} \\ \frac{\partial Q_n}{\partial \theta_n} & \frac{\partial Q_n}{\partial V_n} \end{bmatrix} \quad \textbf{(4-53)}$$

Facing the fact that the effect of a change in nodal power on the voltage angle and magnitude is needed the matrix has to be inverted. To be able to invert the system's Jacobian the reference node has to be omitted due to the fact, that the unreduced Jacobian matrix is singular.

$$J_{red} = \begin{bmatrix} J_{11_{(\sim ref,\sim ref)}} & J_{12_{(\sim ref,\sim ref)}} \\ J_{21_{(\sim ref,\sim ref)}} & J_{22_{(\sim ref,\sim ref)}} \end{bmatrix} \tag{4-54}$$

The inverted Jacobian (eq. (4-55)) matrix gives the gradients of active and reactive power with respect to the voltage angle and magnitude.

$$S_{red} = inv(J_{red}) = \begin{bmatrix} S_{11_{red}} & S_{12_{red}} \\ S_{21_{red}} & S_{22_{red}} \end{bmatrix} \tag{4-55}$$

In general, the apparent load flow of a branch from node i to node j can be calculated following eq. (4-56).

$$\begin{aligned} \underline{S_{ij,i}} &= \underline{U_i} \cdot \underline{I_{ij}^*} = \underline{U_i} \cdot \frac{\left(\underline{U_i} - \underline{U_j}\right)^*}{\underline{Z_{ij}^*}} = \underline{U_i} \cdot \left(\underline{U_i} - \underline{U_j}\right)^* \cdot \underline{Y_{ij}^*} = U_i^2 \cdot \underline{Y_{ij}^*} - \underline{U_i} \cdot \underline{U_j^*} \cdot \underline{Y_{ij}^*} \\ &= U_i^2 \cdot Y_{ij} \cdot e^{-j \cdot \psi_{ij}} - U_i \cdot U_j \cdot Y_{ij} \cdot e^{j \cdot (\varphi_i - \varphi_j - \psi_{ij})} \\ &= U_i^2 \cdot Y_{ij} \cdot \left(\cos(-\psi_{ij}) + j \cdot \sin(-\psi_{ij})\right) \\ &- U_i \cdot U_j \cdot Y_{ij} \cdot \left(\cos(\varphi_i - \varphi_j - \psi_{ij}) + j \cdot \sin(\varphi_i - \varphi_j - \psi_{ij})\right) \\ &= U_i^2 \cdot Y_{ij} \cdot \cos(-\psi_{ij}) - U_i \cdot U_j \cdot Y_{ij} \cdot \cos(\varphi_i - \varphi_j - \psi_{ij}) \\ &+ j \cdot \left(U_i^2 \cdot Y_{ij} \cdot \sin(-\psi_{ij}) - U_i \cdot U_j \cdot Y_{ij} \cdot \sin(\varphi_i - \varphi_j - \psi_{ij})\right) \end{aligned} \tag{4-56}$$

For the active load flow from node i to node j eq. (4-57) is valid.

$$P_{ij,i} = U_i^2 \cdot Y_{ij} \cdot \cos(-\psi_{ij}) - U_i \cdot U_j \cdot Y_{ij} \cdot \cos(\varphi_i - \varphi_j - \psi_{ij}) \tag{4-57}$$

$$\begin{aligned} \frac{\partial P_{ij}}{\partial \varphi_i} &= U_i \cdot U_j \cdot Y_{ij} \cdot \sin(\varphi_i - \varphi_j - \psi_{ij}) \\ &= imag\left(\underline{U_i} \cdot \underline{U_j^*} \cdot \underline{Y_{ij}^*}\right) \end{aligned} \tag{4-58}$$

$$\begin{aligned} \frac{\partial P_{ij}}{\partial \varphi_j} &= -U_i \cdot U_j \cdot Y_{ij} \cdot \sin(\varphi_i - \varphi_j - \psi_{ij}) \\ &= -imag\left(\underline{U_i} \cdot \underline{U_j^*} \cdot \underline{Y_{ij}^*}\right) \end{aligned} \tag{4-59}$$

$$\begin{aligned} \frac{\partial P_{ij}}{\partial U_i} &= 2 \cdot U_i \cdot Y_{ij} \cdot \cos(-\psi_{ij}) - U_j \cdot Y_{ij} \cdot \cos(\varphi_i - \varphi_j - \psi_{ij}) \\ &= real\left(2 \cdot \left|\underline{U_i}\right| \cdot \underline{Y_{ij}^*}\right) - real\left(\frac{\underline{U_i}}{\left|\underline{U_i}\right|} \cdot \underline{U_j^*} \cdot \underline{Y_{ij}^*}\right) \end{aligned} \tag{4-60}$$

$$\begin{aligned} \frac{\partial P_{ij}}{\partial U_j} &= -U_i \cdot Y_{ij} \cdot \cos(\varphi_i - \varphi_j - \psi_{ij}) \\ &= -real\left(\underline{U_i} \cdot \frac{\underline{U_j^*}}{\left|\underline{U_j}\right|} \cdot \underline{Y_{ij}^*}\right) \end{aligned} \tag{4-61}$$

These four partial derivatives can be calculated according to eq. (4-58) to (4-61) and each of the results is a column vector with the size of number of branches. To be able to perform the further mathematics in terms of matrix operations those vectors have to be reshaped following eq. (4-62) and (4-63).

$$\frac{\partial P_{ij}}{\partial \varphi} = C_f \cdot \frac{\partial P_{ij}}{\partial \varphi_i} + C_t \cdot \frac{\partial P_{ij}}{\partial \varphi_j} \quad \textbf{(4-62)}$$

$$\frac{\partial P_{ij}}{\partial U} = C_f \cdot \frac{\partial P_{ij}}{\partial U_i} + C_t \cdot \frac{\partial P_{ij}}{\partial U_j} \quad \textbf{(4-63)}$$

Due to the fact that the reference bus doesn't show a change in voltage magnitude or angle the rows related to it can again be omitted according to eq. (4-64) respective (4-65).

$$\frac{\partial P_{ij}}{\partial \varphi}_{red} = \frac{\partial P_{ij}}{\partial \varphi}_{(\sim ref, \sim ref)} \quad \textbf{(4-64)}$$

$$\frac{\partial P_{ij}}{\partial U}_{red} = \frac{\partial P_{ij}}{\partial U}_{(\sim ref, \sim ref)} \quad \textbf{(4-65)}$$

After reducing the network's reference bus one is able to determine the AC-PTDF matrix for the change in voltage angles as well as for the change in magnitude.

$$ACPTDF_{\varphi} = \frac{\partial P_{ij}}{\partial \varphi}_{red} \cdot S_{11_{red}} \quad \textbf{(4-66)}$$

$$ACPTDF_{U} = \frac{\partial P_{ij}}{\partial U}_{red} \cdot S_{12_{red}} \quad \textbf{(4-67)}$$

The sum of those two matrices is the actual AC-PTDF linking changes in nodal active powers to changes in active line flows.

$$ACPTDF = ACPTDF_{\varphi} + ACPTDF_{U} \quad \textbf{(4-68)}$$

4.3.1.6.5.7 DC-Power Transfer Distribution Factors

Based on the branch load flow equation given in eq. (4-69) and the assumptions made the line flow of a branch can be computed according to eq. (4-70).

$$\mathrm{P_{ij}} = B_{ij} \cdot \cos(90°) - \mathrm{B_{ij}} \cdot \cos(\theta_i - \theta_j + 90) = \mathrm{B_{ij}} \cdot \sin(\theta_i - \theta_j) \quad \textbf{(4-69)}$$

Assumption 5 again allows to approximate the value of the sinus function by it's argument.

$$\mathrm{P_{ij}} = \mathrm{B_{ij}} \cdot (\theta_i - \theta_j) \quad \textbf{(4-70)}$$

By using the C_{ft} matrix and the branch susceptance vector B_{branch} eq. (4-70) can be generalized for all branches in the system leading to eq. (4-71).

$$\mathrm{P_B} = \mathrm{diag}(B_{branch}) \cdot \mathrm{C_{ft}} \cdot \Theta \quad \textbf{(4-71)}$$

This matrix gives the effect of a change in the nodal voltage angle matrix on the active branch flows. Due to the fact, that in this study the voltage angle is neither an input nor an output parameter eq. (4-70) and (4-71) can be joined to the DC-PTDF matrix.

$$\mathrm{P_B} = \mathrm{diag}(B_{branch}) \cdot C_{ft_{(\sim ref)}} \cdot inv\left(B_{bus_{(\sim ref,\sim ref)}}\right) \cdot \mathrm{P_{n_{(\sim ref)}}} = DCPTDF \cdot P_{n_{(\sim ref)}} \quad \textbf{(4-72)}$$

This PTDF matrix allows to directly determine the branch load flow from the active nodal power injections.

4.3.1.6.5.8 Method Expandability

It can be thought of various expansions potentially enhancing the accuracy of results on different points of the method. Due to the fact that reactive load forecasting and the analysis of reactive load flows is not a topic of interest of the currently implemented forecasting and congestion frameworks of the TSOs the focus during the evaluation of the presented method was set on active power forecasts and flows. Given, that the forecast datasets quality concerning reactive power forecasting increases it could be thought of extending the load flow computation method by the implementation of a fast decoupled load flow [54] also taking into nodal reactive power injections and allowing a more accurate evaluation of branch flows.

To enable a fast risk analysis for a limited time horizon the Probabilistic Load Flow method was used instead of the in risk based security analysis popular Monte-Carlo simulation. This method causes the need for approximating historical forecast uncertainties with Gaussian distributions. To overcome the inherent limitations of this load flow implementation Gaussian mixture models [55] or Gram Charlier Expansions and as a special form Edgeworth Series [56] seem to lead to a significant enhancement of the method performance.

4.4 From Branch Loading to a Branch Outage Probability

To enable an outage simulation of the power system of interest the probability that a certain branch trips has to be quantified. A function that gives a link between the probability, that a branch is outaged, and the branch flow is presented in the publications [35] and [36]. These findings are based on the work published in [57] giving a link between the likelihood of a tripping of a branch and a system outage due to hidden failures in protection relays. In Figure 4-10 the function developed in [36] is presented. It describes the probability of a branch tripping as a function of the normalized branch flow, assuming that there are three ranges. The first one covers the branch flow from zero to the actual branch limit and it shows a probability p that a hidden failure will occur. The second range is from 100% to 140% of the branch limit value reflecting the over current protection relay limit. Here the probability of a hidden failure is assumed to rise linearly. The third range is above the over current protection device's set point leading to a definitive outage of the branch.

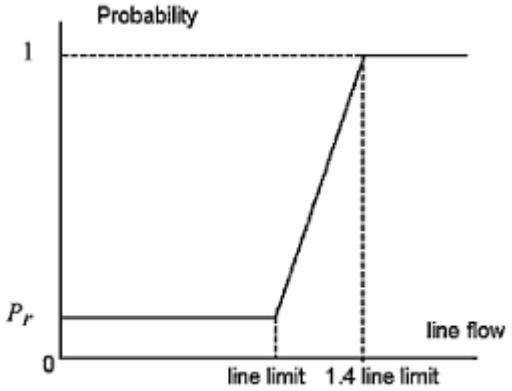

Figure 4-10. Relation between loading and outage probability [36].

Due to the lack in data concerning the probability of a hidden failure of a protection device this function was reworked to reflect the load flow dependent branch outage probability in a way, that it

can be parameterized using data which is available. The modified branch loading to tripping probability function is shown in Figure 4-11. The function consist of three different parts as follows.

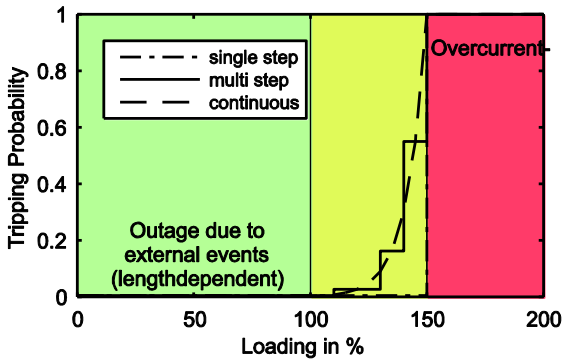

Figure 4-11. Branch tripping probability as a function of the branch loading.

The base tripping probability p_{trip} is reflecting branch tripping as a consequence of stochastic external causes like lightning strokes, falling trees, avalanches as well as internal causes like insulation failures and false protection relay tripping is highlighted in green and covers a loading range from 0% to 100% of the line limit I_{limit}. In the case of e.g. a tower line in a threatened area were the likelihood of an avalanche is high, detailed outage statistics of the particular TSO would reflect this increased tripping potential and enable an appropriate consideration of this circumstance during the simulation. However if those values are not available the work published in [58] gives an evaluation of branch outage statistics categorized by voltage levels and branch types like transformers, lines and cables as well as outage statistics for busbars and switching units. A sub category of this evaluation gives measures for independent outages of branch elements and reflects the outage frequency H which is the number of outages per year and kilometer. By evaluating the outage frequency for the duration of the investigated time horizon t_{inv} and the length of the branch of interest l_b the base tripping probability $p_{trip(I \leq I_{limit})}$ of a branch can be determined.

$$p_{trip(I \leq I_{limit})} = H \cdot l_b \cdot t_{inv} \quad \textbf{(4-73)}$$

The tripping probability for highly overloaded branches, where the loading I exceeds the protection device limit I_{prot} reflects, that branches are protected by over current protection relays, which prohibit a thermal damage of the element due to a heavy overload situation. The actual settings of the over current protection relays depend on the protection philosophy of the TSO. Usually the ratio between the over current protection setting and the long term thermal limit of the branch lies between 105% for conservative protection and 150% for TSOs making use of the thermal inertia of branches in terms of the TATL (temporary admissible transmission loadings) limits for corrective remedial actions as the report of the incident of 2006 shows. In eq. (4-73) it's assumed, that the overcurrent protection relay is working correctly every time the limit is exceeded by tripping the respective branch, but due to malfunction, it can happen in some rare cases, that the relay won't trip the branch. The occurrence probability of a malfunction of protection devices can be integrated into this function by reducing the value of the probability for a branch tripping in the red area by the according probability of a protection device malfunction ($p_{malfunction}$).

$$p_{trip(I > I_{prot})} = 1 - p_{malfunction} \quad \textbf{(4-74)}$$

For a branch loading between the thermal limit and the protection device limit $p_{trip(I_{trip}<I\leq I_{prot})}$ (yellow area) it is not that straight forward to formulate a dependency of the tripping probability from the utilization. On the one hand, the base tripping probability is still present due to the fact that external effects are not load flow dependent. So a lightning stroke, or an avalanche and other phenomenon which are hard to or even impossible to predict is as likely for a heavily loaded line as for a line which is not in operation. The second reason which is modelled here is the rising likelihood of a flashover due to line sag when the loading of overhead lines exceeds the thermal limit like it was the case for the Italian blackout in 2003 according to the final report [5].

There are many other causes leading to a branch tripping, but the detailed modelling of outage mechanics is not the goal of this thesis. Additional causes for protection device triggered branch trippings could be distance protection relay actions as a result of high loading situations characterized by comparably low bus voltages and high branch currents or voltage protection relay actions due to undervoltage, again as a result of a severe loading situation. Due to the fact, that different TSOs use different protection device technologies with different settings and have varying protection strategies, the function in this range might differ from one TSO to the other. For this work, an assumption for the parameterization of the heuristic function was made. It is out of this work's scope to assess an exact model of the tripping behavior in this range.

4.5 State Based Approach

The approach presented in this thesis is state based one. The opposite would be an event based approach, which would select branches to trip by their particular outage probability regardless the probability of the system to stay in a certain topological configuration, here referred as system state.

The probability to stay in the initial stage defined by the topology configuration given by the forecast dataset is identically to the probability, that none of the branches in operation would trip, here referred to as the counter tripping probability of a state. Let $p_{trip,b}$ be the tripping probability of branch b and B the set of all branches in the system, the probability $p_{state,1}$ to stay in the initial state 1 is given by eq. (4-75).

$$p_{state,1} = \prod_{b=1}^{B}\left(1 - p_{trip,b}\right) \tag{4-75}$$

In a more general way the probability of state i defined by a set of branches to outage O and a set of branches staying in operation I is given eq. (4-76) in a recursive formulation, where $p_{state,i-1}$ denotes the probability of the foregone simulation stage. In the case of the initial stage $p_{state,i-1}$ would be equal to one.

$$p_{state,i} = p_{state,i-1} \cdot \prod_{o=1}^{O} p_{trip,o} \cdot \prod_{a=1}^{I}\left(1 - p_{trip,i}\right) \tag{4-76}$$

4.5.1 System State Filtering

Due to the fact, that a pre-evaluation of all possible system state probabilities is computationally infeasible for medium and large scale power systems, an approach was implemented allowing a probability based filtering during the simulation. A simplified method flowchart is given in Figure 4-12. In the module "Next Stage" the actual branch tripping probabilities as well as the system state probability of the given system state are evaluated. A filter criterion based on a predefined minimum

value in state probability p_{lim} is used on the one hand to select tripping candidates and on the other hand to decide either if the actual system state is evaluated or not.

The module "Current Stage" takes the information branch tripping probability and system state probability from the module "Next Stage". If the module "Current Stage" detects a branch who's product of the tripping probability and the actual simulation step's probability exceeds the lower limit in state probability, the branch is set offline and the module "Current Stage" is executed in a recursive way. The actual simulation step's probability is determined by taking the product of the system state probability of the previous system state and the tripping probabilities of branches tripped since then. This procedure allows to abort a particular sub-simulation loop of the recursive algorithm when the actual simulation step's probability is below the predefined limit without the need of evaluating the particular resulting system stage.

If the module "Actual Stage" detects a system state exceeding the given lower limit in system state the module "Next Stage" is executed in a recursive way.

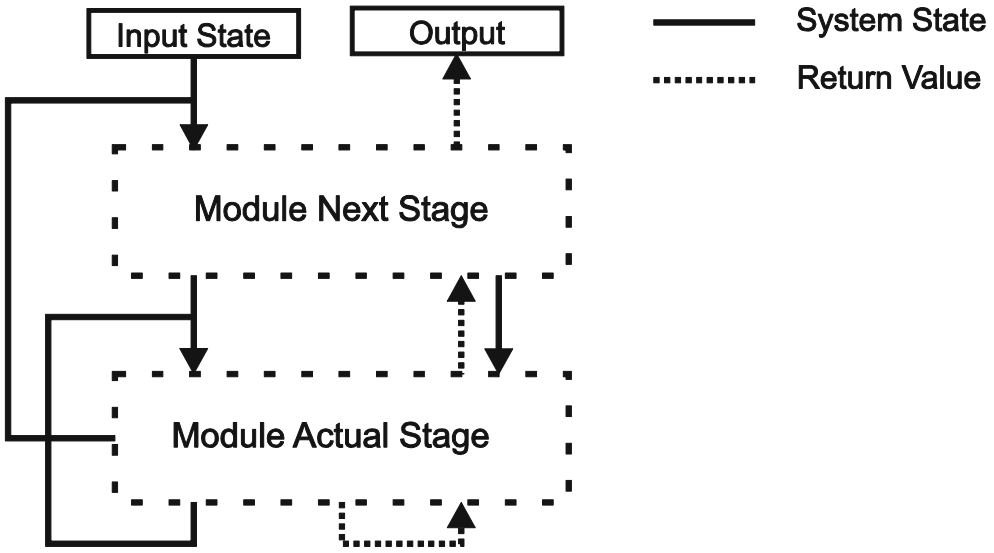

Figure 4-12. Recursive state approach.

This recursive loop is stopped, when there are no more system states or branches showing a system state probability or actual simulation step's probability exceeding the predefined lower limit p_{lim}. A simple example for this procedure is given in a graphical way in Figure 4-13. Given, that state A is the initial state in the actual simulation stage there is a state probability $p_{state,A}$ that the system remains in the same state. If this state probability exceeds the predefined limit p_{lim} this state is evaluated regarding the risk it holds. If, any branches' tripping probability exceed the predefined lower limit a outage simulation is performed for the particular branches. In the given example one of these sub-simulations leads to state B who's state probability exceeds the limit or to state C who's state probability is below the limit, but there is a candidate in terms of a branch to outage, in this case branch c, with a tripping probability $p_{trip,c}$ beyond the limit which leads to a system state D showing again a system state probability lying over the limit.

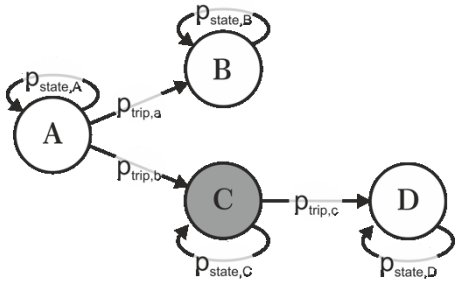

Figure 4-13. Skipping of unlikely system states.

To avoid the repetitive scan of identical system states starting from one initial case a masking method was used. E.g. an exemplary three branch network would lead to a complete system state graph as shown in Figure 4-14 for the initial state A. It can be thought of 16 possible tripping combinations of the exemplary power systems' branches a, b and c leading to new system states, where some combinations would lead to identical states due to the fact, that for simultaneous outages the order is irrelevant. In this example, there are six possible combinations, when accounting for the order, leading effectively to the same state where all branches are tripped. Also an outage combination of any two of the branches e.g. a and b would lead to the same state by two different ways to get there. Due to the fact that there is no need to account for the order of tripping events, because the branches selected here are simultaneous outages , a simple "branch to trip candidate" filtering process can be used to avoid this issue.

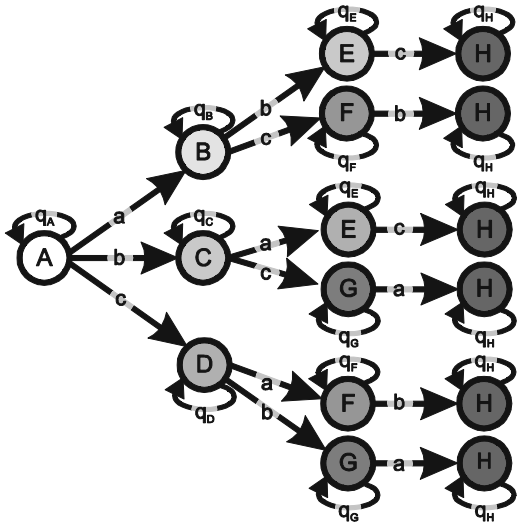

Figure 4-14. Nomination of intermediate states.

The filtering of branch outage candidates is realized by giving the branch trip candidates unique numerical values and selecting tripping candidates showing an index higher than the index of the forgone tripped branch of the same outage stage. This approach is visualized in Figure 4-15. For the given example this would mean, that after an outage of branch c with an equivalent numerical index of 3 no further outages in the current simulation stage would be allowed, whereas after tripping branch a from the stage's initial state A with a numeric equivalent of 1 branches b (numerical index 2) as well as c (numerical index 3) are allowed to be tripped, given, that the tripping probability exceeds the lower limit. Given the case, that starting from initial state A followed by a tripping of the branches a and b, while the tripping probability of branch c is not exceeding the predefined limit, State H would by filtered out and so not be reached by the simulation.

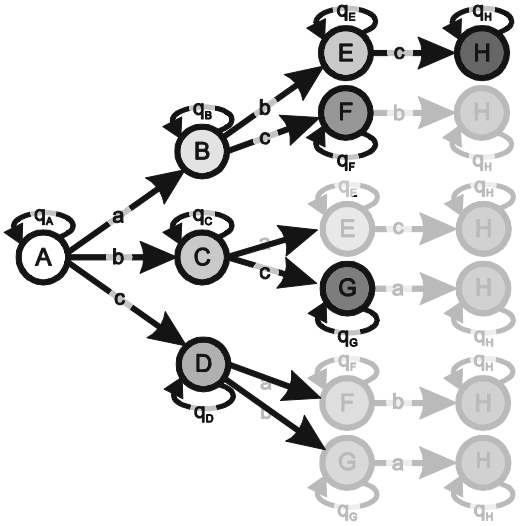

Figure 4-15. Potential system states after applying the proposed filtering method.

4.5.2 Other System State Filtering Strategies

Facing the circumstance, that the time available to perform a security analysis of a power system on the time horizon of operational planning is limited and ,anyhow a full screening of each and every contingency and also of combinations of contingencies is not feasible, a criterion has to be formulated, which filters system states of interest from those which are neglected.

4.5.2.1 Basic Filtering Strategies

The simplest way to limit simulation time is to stop after a pre-defined number of simulation steps, which are analogous to the number of system states discovered. This directly leads to the problem, that only the first contingencies would be scanned in detail and the other ones remain unvisited, because of the recursive characteristics of the presented method. This kind of filter criterion is simple to comprehend and to implement but does not lead to results of the desired quality concerning the uncertainty. In Figure 4-16 a generalized example is given for a simulation where the number of simulation steps is limited. The number or the variable in the circle reflects the actual simulation stage and the grayed out states are never reached by this approach. It can be seen, that a depth scan for the first outage candidates can be realized by using this criterion.

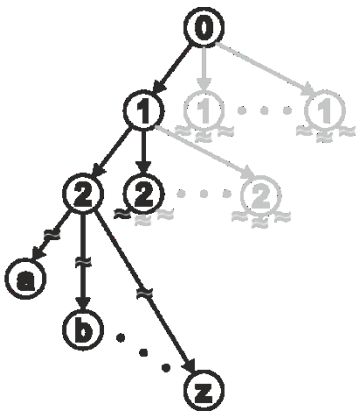

Figure 4-16. System stage visualization for a maximum simulation step limit.

A slightly more precise result can be reached by limiting the simulation steps after each single- and multi-element first order contingency. Facing the fact, that this filtering approach treats all first order

contingencies in the same way, without accounting for the potential risk the outages hold, numerous simulations are performed only marginally refining the result. A sub-simulation stops after a pre-defined number of post-first order contingency simulations leading to a depth scan of the first outage candidates for each post-contingency situation and their combinations, whilst the remaining ones are neglected even if they are holding a high potential risk. This approach ensures in contrast to the previously presented one that all fist order contingencies are guaranteed to be scanned. In Figure 4-17 system states – scanned states in black and neglected states in grey – are visualized showing, that this approach also leads to a depth search but in this implementation for each first order contingency.

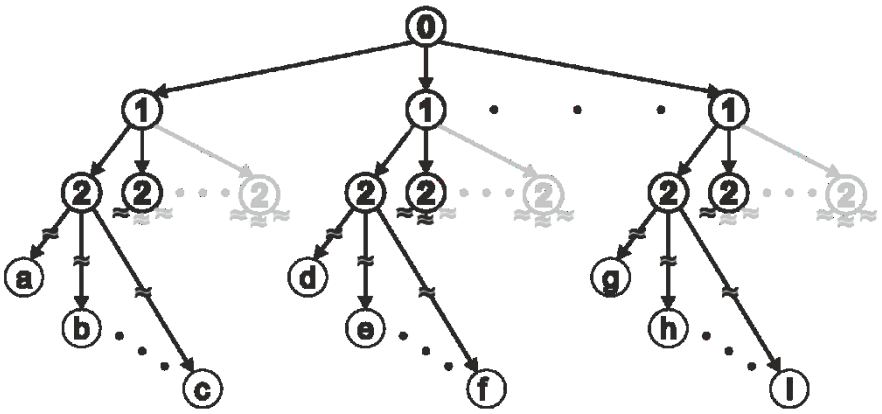

Figure 4-17. System stage visualization for a post first order contingency simulation step limit.

A similar approach to identify system states to be scanned during the simulation is to limit the depth of the scan performed during the security analysis. A pre-defined number reflecting the "maximum number of branches" is provided as an input for the proposed method. A sub-simulation is stopped each time a system state is visited, where this limit is reached. This approach is visualized in Figure 4-18, where it is obvious, that all sub-simulations stop when the stage a is reached. The usefulness of this state filtering method is limited to small values for the upper system stage limit a due to the fact, that the number of system states to scan follows a combinatory problem leading to a significant increase in computational effort.

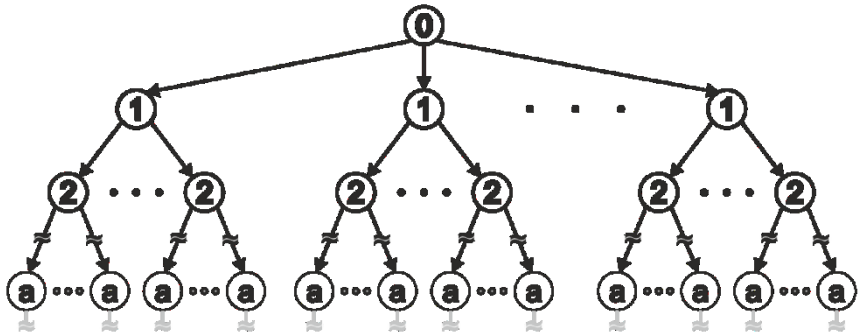

Figure 4-18. System stage visualization for a simulation stage limit a.

4.5.2.2 Load Flow Based Filtering

The presented method focuses on load flow related contingencies in high and extra high voltage power systems, so a categorization of system states to scan can be thought of by taking the change in load flow of a certain line after a contingency as a criterion. LODFs (Line Outage Distribution Factors)

in combination with the pre-contingency load flows of the system under investigation can be used to determine the influence of a tripping of one or more branches of a power system on the branches remaining in the system [59]. The post contingency load flow of branches which remain in the power system – denoted by the set of branches I – can be calculated according formula (4-77), where $LODF_{I,O}$ is the LODF matrix as given in eq. (4-78), reflecting the changes in load flows of a set of outaged branches O on the load flow of the set of branches remaining in operation I. P_o^0 is the pre-contingency load flow of the set of branches on outage O.

$$\Delta P_I^c = LODF_{I,o} \cdot P_o^0 \tag{4-77}$$

In eq. (4-78) $BRANCHPTDF$ is the PTDF matrix for branches reflecting the influence of a nodal power injection of 1 p.u. at the node, where the branch starts at and a demand of 1 p.u. at the end node of the particular branch on the power systems branches. C_{ft} is the branch membership function described in detail in chapter 4.3.1.1.

$$\begin{aligned} \mathrm{LODF}_{I,O} &= BRANCHPTDF_{I,O} \Big/ \left(E - BRANCHPTDF_{O,O}\right) \\ &= DCPTDF_I \cdot C_{ft_O}^T \Big/ \left(E - DCPTDF_O \cdot C_{ft_O}^T\right) \end{aligned} \tag{4-78}$$

A filter criterion can be implemented according to formula (4-79), where ΔP_{lim} is a predefined limit in absolute line flow change in MW.

$$|\Delta P_i^c| > \Delta P_{\mathrm{lim}} \; \forall \; i \in I \tag{4-79}$$

Another, more distinctive criterion formulation is given in eq.(4-80), where Δp_{lim} is the predefined minimum change in relative branch flow's absolute value.

$$\frac{|\Delta P_i^c|}{P_{n,i}} > \Delta p_{\mathrm{lim}} \; \forall \; i \in I \tag{4-80}$$

For both variants branches fulfilling the particular post-contingency filter criterion are selected for the subsequent outage simulation.

4.6 Stage Evaluation

If a system state is selected as a intermediate state by the filtering criterion the state is evaluated. This evaluation consist of an islanding detection, an estimation of primary frequency control actions, a criterion regarding large scale generation outages and a frequency estimation.

4.6.1 Islanding

To be able to detect a splitting of the power system under investigation in two or more islands, the following method was developed. In Figure 4-19 the flowchart for the approach is given, where f and t are vectors with the size equal to number of branches. The particular branch b starts at bus f(b) and ends at bus $t(b)$. The output of the method is the vector $NodeIsland$ with a size equal to the number of branches, holding a number reflecting the island, which the particular node is a member of.

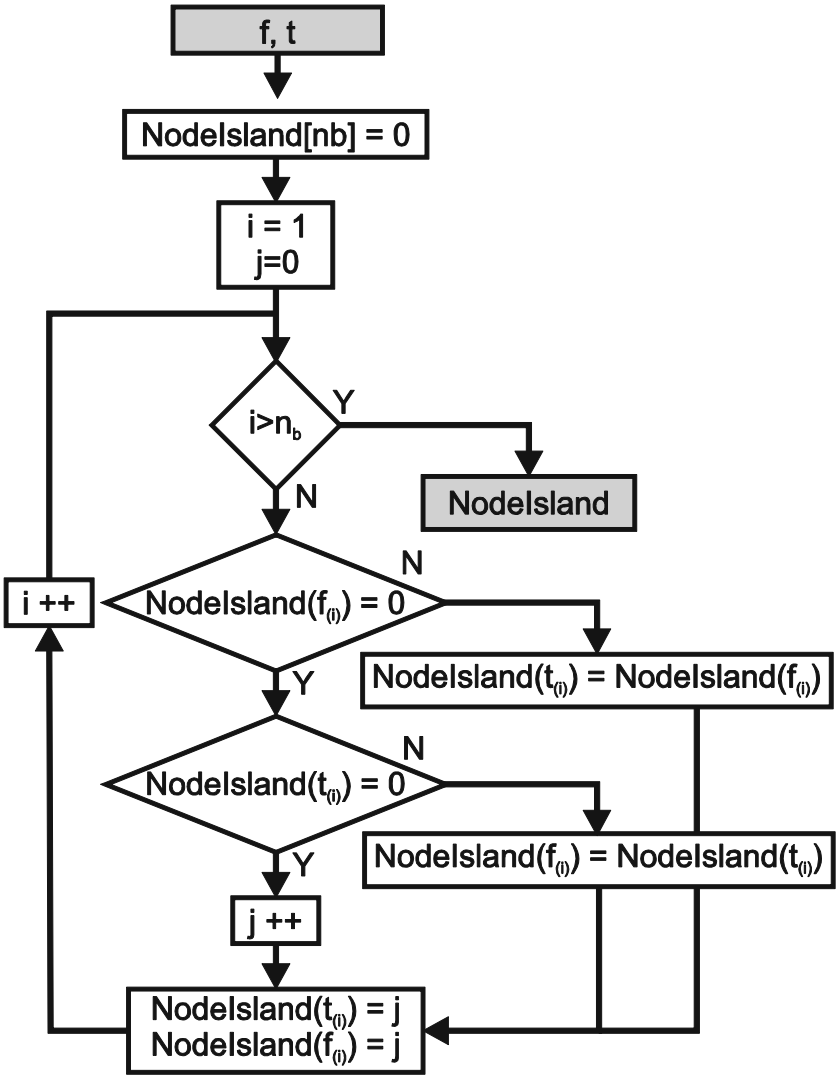

Figure 4-19. Islanding detection approach.

If a split of a power system into islands is detected a slack bus is added to the new island to ensure computational feasibility

4.6.2 Primary Frequency Control

The primary frequency control is an essential functionality of a interconnected power system consisting of multiple generation units. It accounts for the power balance, which is tightly coupled to the frequency. A loss of generation power in a system would lead without the presence of the primary frequency control and the self-regulation effect of the load to a blackout immediately. The self-regulation effect of the load describes the fact, that loads of transmission systems show a dependence of the frequency in terms of power consumption. This dependency is a positive one, which means that a decreasing system frequency causes a decrease in power consumption [60].

The primary control of generation units is characterized by the droop denoted by σ, which is defined according eq. (4-81), where ΔP is the change in power infeed and P_n is the set-point of the unit, Δf is the change in frequency and f_n is the nominal system frequency. A common range for the droop is 2%-6% and depends on the primary energy.

$$\sigma = -\frac{\frac{\Delta f}{f_n}}{\frac{\Delta P}{P_n}} = -\frac{\Delta f \cdot P_n}{\Delta P \cdot f_n} \quad \textbf{(4-81)}$$

In Figure 4-20 the power-frequency diagram is shown for two different droop values. The droop of configuration a is lower than the droop of b, so the full reserve denoted by P_{max} is allocated at a lower frequency deviation in the case a than in case b. The primary frequency control is not limited only to negative but also positive frequency deviation.

The following key facts give an overview about the primary frequency control.

- The primary frequency control is spread over all the inter-connected system
- Limited amount in power
- Stationary frequency deviation differs from the stationary
- Coordinated by the ENTSO-E
- Spread via contribution coefficients of control zones

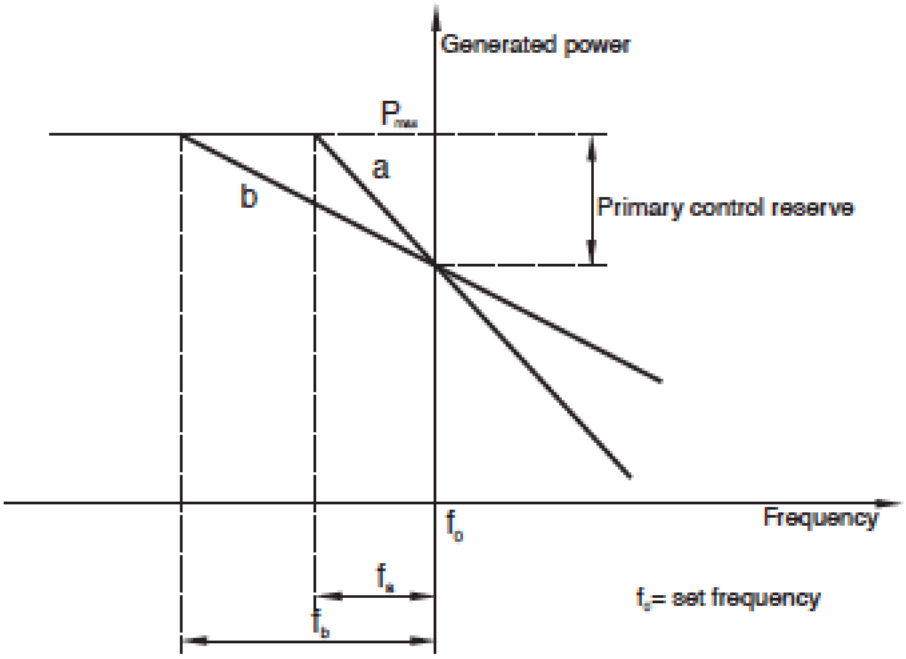

Figure 4-20. Definition of droop [60].

When it comes to power systems the primary control is usually not defined by giving the droop any more, but by the network power characteristics λ. According to eq. (4-82) its defined as the ratio of the change in power and the change in system frequency and is valid for static system states only.

$$\lambda = \frac{\Delta P}{\Delta f} \quad \textbf{(4-82)}$$

In Figure 4-21 three time courses of the frequency response on an incident are given. Case B1 and B2 show typical frequency responses after two different incidents, whereas case A reflects the worst case. So while the steady state frequency deviation is limited to $\pm 200\ mHz$ the dynamic frequency deviation exceeds this value. Case A is based on a reference outage of $3000\ MW$ leading to a stationary frequency deviation of $-200\ mHz$ and worst case to a dynamic deviation of $-800\ mHz$.

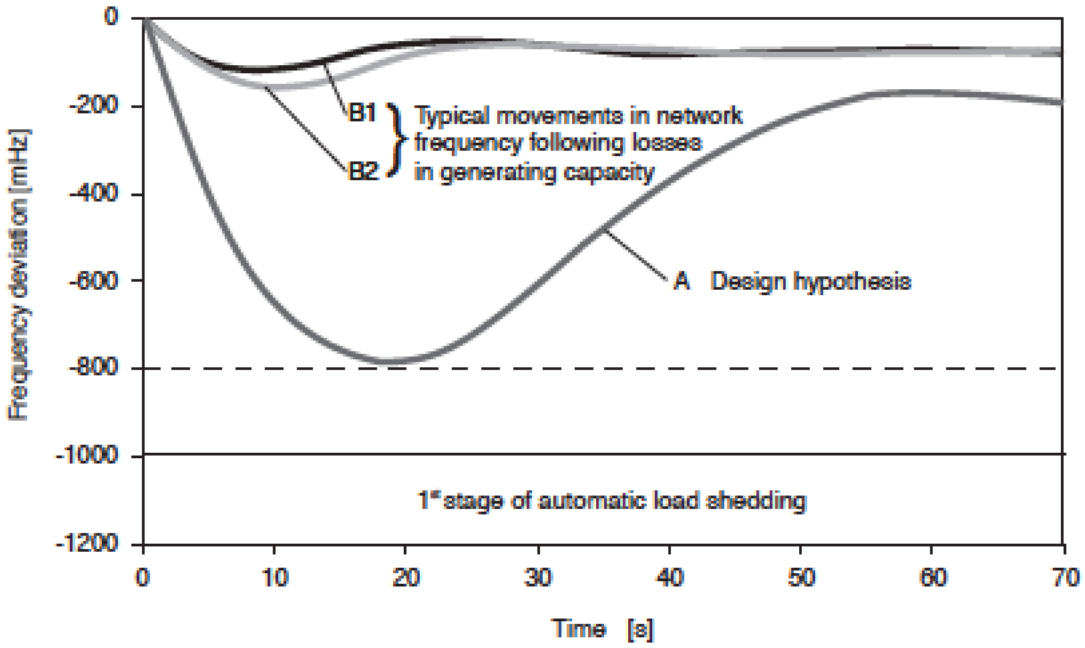

Figure 4-21. Frequency response after outages in the synchronous area [60].

The primary frequency control action and the stationary frequency response is modelled as the self-regulation effect of loads and the droops of power plants taking part in this control scheme. The droop σ is given in % and recalculated to MW/Hz according to formula (4-83) where P_N denotes the nominal power of a generation unit and f the frequency.

$$\lambda = \frac{\Delta P}{\Delta f} = -\frac{P_n}{\sigma \cdot f_n} \tag{4-83}$$

The self-regulation effect (λ_l) is assumed according to [12] to be 1%. So the overall grid frequency response on an imbalance in the system can be approximated by eq. (4-84).

$$\Delta f = \frac{\sum_{g=1}^{G} P_{G,g} - \sum_{l=1}^{L} P_{L,l}}{\sum_{g=1}^{G} \frac{P_{G,g}}{f \cdot \sigma_g} + \sum_{l=1}^{L} P_{L,l} \cdot \lambda_l} = \frac{\Delta P}{\frac{\Delta P_G}{\Delta f} + \frac{\Delta P_L}{\Delta f}} \tag{4-84}$$

The change in power as a response on the frequency deviation can be determined by simply multiplying the gradients of the generation units, or the loads self-regulation coefficient by the deviation in frequency according to eq. (4-85) and (4-86).

$$\Delta \mathrm{P_{L,l}} = \lambda_\mathrm{l} \cdot \Delta \mathrm{f} \;\; \forall \, \mathrm{l} \in \mathrm{L} \tag{4-85}$$

$$\Delta P_{G,g} = \frac{P_{G,g}}{f \cdot \sigma_g} \cdot \Delta f \;\; \forall \, g \in G \tag{4-86}$$

For the dynamic frequency response shown in Figure 4-21 is accounted by scaling the stationary frequency deviation by a predefined factor.

4.6.3 Lost Generation Criterion

To avoid computationally exhaustive evaluations of system states leading de facto to a blackout, a criterion was introduced, stating, that a loss of at least 10% of the overall generation power will end up in a blackout [61].

4.7 Output Measures

During the recursive simulation every detail of each scanned system state is stored and fed back to the initial simulation stage, so a comprehensive evaluation of sub-results concerning different measures of interest is possible. The most relevant output variables of the simulation's results set are presented in the following subchapters.

Data used in examples are generated on basis of the modified IEEE 118-bus network consisting of 186 branches and showing an overall load demand of 5090 MW.

4.7.1 State Probabilities

Due to the fact, that the main criterion if system states are accounted for or not is the state probability which reflects the likelihood of a particular set of line trips to emerge. For well-planned power systems the probability to leave the initial system state is rather low and the state probability of the initial system state is usually significantly exceeding 95% according to the numerous different simulations performed during the studies to this thesis.

A quite straight forward limitation in the overall system state probability p_{sys} is, that it has to be exactly one if the power system use case of interest was scanned completely. For an incomplete analysis like it is the case for this method, the overall state probability is bounded between zero and one. The overall system state probability is defined as given in eq.(4-87), where p_s is the occurrence probability of state s and S is the set of scanned system states during the recursive simulation. The overall system state probability is a measure for the completeness of the simulation. Due to the fact, that the system state probability is the main exit criterion for the simulation a lower limit leads to a higher number of states scanned and also to a higher value in the overall state probability.

$$p_{sys} = \sum_{s \in S} p_s \leq 1 \qquad \textbf{(4-87)}$$

In the case of an incomplete simulation there is a non-zero complementary probability p_{comp} according to formula (4-88), which is equivalent to the residual probability p_{res} reflecting the sum of state probabilities p_s of all system states not scanned denoted by N and is therefore a measure for the incompleteness of the simulation.

$$p_{res} = p_{comp} = 1 - p_{sys} = \sum_{s \in N} p_s \qquad \textbf{(4-88)}$$

As mentioned in section 4.5.1 , the exit criterion for the simulation process is the system state probability p_s of each state exceeding a given limit $p_{\lim}$. States not scanned (N) are fulfilling the inequality (4-89) and all scanned states' S eq. (4-90).

$$p_s \leq p_{lim} \; \forall \; s \in N \qquad \textbf{(4-89)}$$

$$p_s > p_{lim} \; \forall \; s \in S \qquad \textbf{(4-90)}$$

As a conclusion regarding probability measures as output values only the overall state probability is a reasonable candidate, because it reflects the amount of states scanned in a probabilistic view and gives an estimate for the completeness of the simulation.

4.7.2 Risk

In general, the risk R is defined as the product of the severity S and the occurrence probability p of a single event.

$$R = S \cdot p \tag{4-91}$$

The risk can be determined based on various severity measures like the "power not supplied" and its duration weighted equivalent "energy not supplied" or the "number of lost nodes". Even the "system frequency deviation" or the "primary frequency control activated power" could be used as a severity measure. Due to the fact, that it's a multiplicative quantity, low probability events showing a high severity and high probability events holding a low severity are judged equally. The given generally valid formula in eq. (4-91) can be refined to a system state based interpretation as given in eq. (4-92), where the index s denotes a particular system state.

$$R_s = S_s \cdot p_s \tag{4-92}$$

The risk value of one single system state doesn't hold a lot of information per se. It can be compared to the value of other system states, but it has to be seen in a wider view concerning the simulation. Additionally to the maximum state risk the information about the remaining uncertainty is needed to ensure a valid interpretation.

Determining the residual potential risk is not trivial due to a lack in available information about non-scanned system states. Therefore, the overall system risk of the screened power system's use case, which basically is the sum of all state risks, is determined. The lower limit of the overall risk is zero, meaning, that the power system under investigation holds absolutely no risk to fail, and the upper limit is the maximum value of the severity measure. For a power system with the amount of lost load as a severity measure the maximum system risk value could take the value of the overall power demand, which corresponds to a blackout with an occurrence probability of 100%. When it comes to well-planned power systems usually the probability of large disturbances is very low and the severity of likely events is quite low. Mathematically, the calculation of the overall risk R_{sys} is simply the sum of the risks R_s of all stages S scanned during the simulation as given in eq. (4-93).

$$R_{sys} = \sum_{s \in S} R_s \tag{4-93}$$

Due to the fact, that most power systems can't be scanned completely in a reasonable time span the simulation is incomplete, leading to an uncertainty afflicted result. The discovered risk during the simulation $\tilde{R}_{sys}$ and the residual risk, which is held in not scanned system states R_{res} give the actual risk value according to eq.(4-94). R_{res} can't be determined based on information available with a reasonable effort.

$$R_{sys} = \sum_{s \in S} R_s + R_{res} = \tilde{R}_{sys} + R_{res} \tag{4-94}$$

To decide about combinations which are scanned or not scanned, the state probability is the criterion of choice in this thesis, but in general it can be also thought of other filter criteria. The probability based criterion limits the computational effort and also controls the uncertainty affliction of the result. A lower limit in probability leads to a more detailed simulation. Because of the unknown number of outage combinations not scanned and the missing knowledge of the exact probabilities a direct computation of the residual risk is not possible based on the available information. To avoid giving a result in terms of one single number for a system risk without any

additional information about the quality of the statement a complementary approach was used to determine the uncertainty of the result. Based on the knowledge of each state's severity S_s and the maximum the severity S_{max} the complementary value can be determined. The complementary measure of "power not supplied" is the "power supplied". According to eq. (4-95) the chance value C_s of each state s is defined to be the product of the complementary severity value and the particular occurrence probability.

$$C_s = (S_{max} - S_s) \cdot p_s \quad \textbf{(4-95)}$$

Based on the state chance values, which can be evaluated straight forward from the data available as a result of the simulation the overall system chance can be calculated following eq.(4-96) for a complete simulation and eq.(4-97) for an incomplete one, where C_{sys} is the overall chance, and $\tilde{C}_{sys}$ is the aggregated chance of all scanned states and C_{res} is the chance all not scanned states hold, which is an information not being available based on the simulation results.

$$C_{sys} = \sum_{s \in S} C_s \quad \textbf{(4-96)}$$

$$C_{sys} = \sum_{s \in S} C_s + C_{res} = \tilde{C}_{sys} + C_{res} \quad \textbf{(4-97)}$$

In case of an incomplete simulation there is a resulting unknown component in terms of risk as well as in chance. Eq.(4-98) holds for a complete simulation, where both, the risk and the chance value are fully determined with no remaining uncertainty.

$$100\% \cdot S_{max} = R_{sys} + C_{sys} \quad \textbf{(4-98)}$$

Due to the fact, that the risk and the chance values are not fully determined there is some risk or chance undetermined – the residual uncertainty $R_{res} + C_{res}$ as given in eq.(4-99).

$$100\% \cdot S_{max} = \tilde{R}_{sys} + \tilde{C}_{sys} + R_{res} + C_{res} \quad \textbf{(4-99)}$$

Due to the complementarity of the risk and the chance measure a visualization based on these quantities is not a good choice, but the stage chances can be converted to a maximum risk value. This is done by applying eq.(4-100) where $R_{max,s}$ is the upper limit or also the worst case risk value at each simulation stage s.

$$R_{max,s} = S_{max} - \sum_{i=0}^{s} C_i \quad \textbf{(4-100)}$$

This can be explained stepwise for the initial stage for the following example. In the initial stage, without any computations neither a single risk value R_0 nor a chance value C_0 is known. So for the best case the risk is zero and for the worst case the risk is exactly the maximum severity measure according to eq. (4-100). Assuming the power system under investigation is well planned the probability to leave the initial stage due to branch outages would be very low and in contradiction the probability to stay in it is high. The severity is zero for the initial stage and as a consequence the risk R_0 is zero. The chance C_0 can be determined as given before and the maximum risk value decreases by C_0. For every additional simulation stage the minimum risk rises by R_s and the maximum risk decreases by C_s. It is obvious, that more simulation steps refine the result and lower the residual uncertainty.

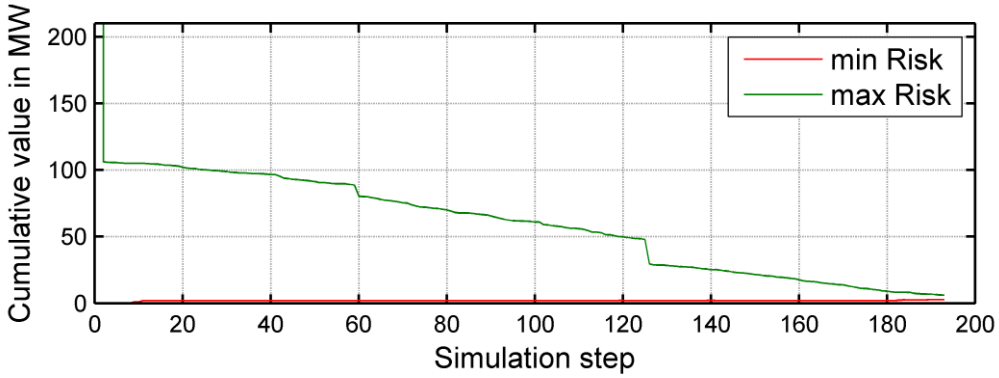

Figure 4-22. Cumulative risk and chance evaluation during the simulation.

The remaining potential risk is the difference between the maximum and the minimum risk value in Figure 4-22. A detailed illustration regarding this residual uncertainty is given in Figure 4-23.

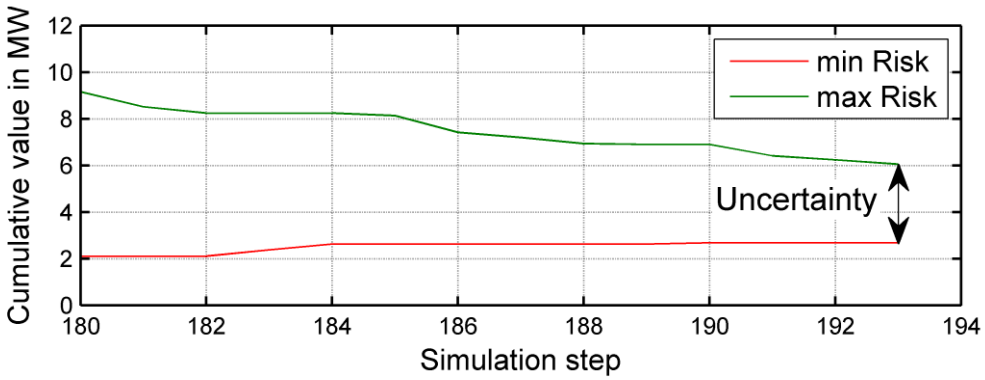

Figure 4-23. Cumulative risk and chance evaluation during the simulation (Detail).

For the purpose of comparing different power systems, or different use cases of one power system based on the risk, this kind of evaluation is meeting the needs, but when it comes to the detailed analysis of particular contingencies of one dispatch, or to the identification of threatened system elements this kind of evaluation doesn't provide any information.

4.7.3 Per State Results

As mentioned previously single state risk values are not very valuable without additional information about the simulation performed and the composition of each particular risk value in terms of state probability and severity. A visualization combining all relevant information is the severity-probability plot, which is usually extended by one or more iso-risk curves. In Figure 4-24 an example is illustrated showing risk values of simulated system states (red dots) and the according iso-risk curve of the maximum risk value. On the iso-risk curve the risk is the same for all probability-severity-combinations. It is limited by the maximum severity on the severity axis. This kind of presentation enables an analysis regarding the probability and severity of each particular state risk value. Additionally the lower limit in state probability p_{lim} – the simulation exit criterion – is visualized allowing a judgment about the quality of simulation results. If the lower limit in state probability lies on the left side of the iso-risk curve, reflecting the maximum risk value discovered there is no possibility that a not-simulated system state holds a higher risk than the discovered one. On the other hand, if the lower limit in state probability and the iso-risk curve show an intersection the simulation has to be refined to enhance the quality of the results due to the fact, that there could

exist a state showing a higher risk as discovered by the simulation in the set of not scanned system states.

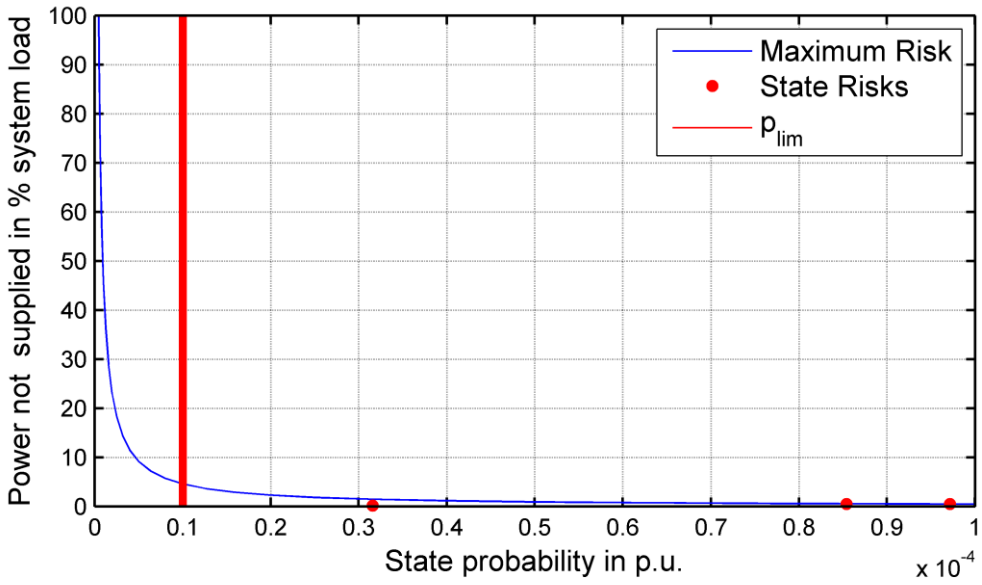

Figure 4-24. Iso-risk curve.

4.7.4 Per Branch Results

4.7.4.1 Aggregated Measures

To be able to rank and analyze contingencies the output data of the simulation is categorized in three groups, namely the contingency free state, post-first order contingency states and post multi-order-contingency states. The first one is simply reflecting how likely it is that the power system of interest stays in the initial state, the second states are grouped per first order contingency to reflect the risk the particular outage event holds and the third group holds all other system states which occur in succession to a multi-element first order contingency. By this classification mainly the above presented measures risk, chance and uncertainty are assigned to one of the groups “no contingency”, “single element first order contingency” and “multi element first order contingency” in terms of system states. An example is shown in Figure 4-24, the first order contingencies of the particular branches are given in the left plot while the right plot holds the aggregated share in risk, chance and uncertainty for all multi-element first order contingencies.

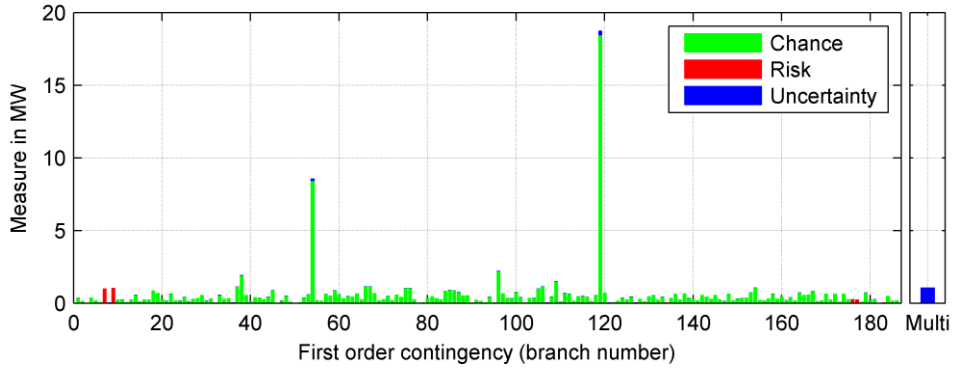

Figure 4-24. Risk, chance and uncertainty measure for every possible first order contingency. The results in the left plot are for single-element and those in the right is for all multi-element first order contingencies.

It is obvious, that this kind of presentation of results is mainly dominated by the chance measure due to the fact, that in general power systems are designed to have an adequate security margin and so the risk measure is comparably low. Usually the chance measure isn't in focus when it comes to risk assessment. To account for this Figure 4-25 holds the risk value and the uncertainty value, but not the chance measure, to allow the identification of contingencies holding a high uncertainty in the evaluated risk measure. Again the first 186 entries represent post-single-element and the 187th post-multi-element first order contingency system states.

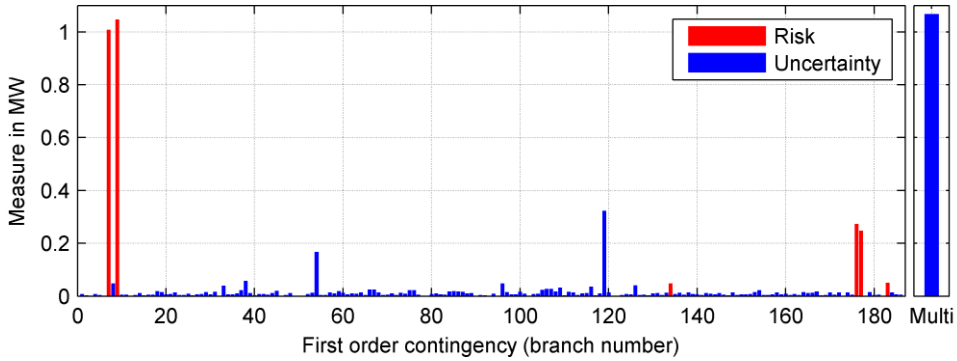

Figure 4-25. Contingency-wise aggregated risk and uncertainty measures.

The results shown in Figure 4-25 lead to the conclusion, that there are a few branches hiding high risk values while some other branches and also the aggregated multi-element contingency states show an even higher uncertainty value. To obtain better results the lower limit in state probability could be set to lower limits which also leads to an elongated simulation time.

4.7.5 Maximum Measures

Facing the fact, that the simulation is covering a tremendous amount of system states a power system could end up starting from a given initial state it can always only end up in one particular state. So an aggregated risk or chance measure is well suited as a performance indicator of the simulation and for a comparison of the overall system risk a power system's use case under investigation holds, but it doesn't really reflect the actual worst case situation. E.g. the overall system risk of a well-designed power system except for one single feeder showing a high loading possibly is similar to the one of a power system with structural deficits showing a moderate loading. This is due to the fact, that for the first case the high loaded branch shows a high outage probability and would lead to an amount of lost load of the load connected to the tap line. On the other hand for the latter case the outage probabilities of the branches would be quite low, but due to the structural deficits there would be numerous combinations leading to large area outages being equivalent to a high amount of lost load. Summarized the first case would show a low number of system states with a low amount of lost load and the latter one would show numerous states with comparable low outage probabilities but large amounts in lost load. These basically totally different cases could end up showing the same overall risk, but the maximum risk values would be quite different.

To determine the maximum values per single-element- and multi-element-first order contingency the result data of the simulation is categorized in post-single-element-first order contingencies per branch and in a category for all remaining post-multi-element first order contingencies. Based on the categorized results the particular maximum value is identified and used for the subsequent evaluation. The determination of the maximum risk per category is straight forward, whereas it is not trivial for the uncertainty. Based on the results of a simulation the maximal possible remaining risk, a

state which was not scanned during the simulation can hold, is limited. This limitation can be evaluated following eq. (4-101) by multiplying the maximal value concerning the severity measure S_{max} by the simulations lower limit in state probability p_{lim}.

$$R_{max} = p_{lim} \cdot S_{max} \quad \textbf{(4-101)}$$

On the other hand by the knowledge of the aggregated risk as well as the aggregated chance value per single-element first order contingency the maximum possible uncertainty per initial single branch outage can be determined. According to eq.(4-101) the maximum possible risk hidden behind the single-element first order contingency $R_{max,b}$ of branch b can be found by taking the product of the maximum severity and the particular first order contingency's occurrence probability. During the simulation, system states B were reached from this first order contingency state b and scanned for the particular risk R_s and chance C_s they hold. So the sum of this risks and chances reduces the remaining uncertainty $U_{max,b}$. Potentially, but not very likely the whole remaining uncertainty could be the risk value of one single system state. This is only valid, if the value does not exceed the maximum possible remaining risk R_{max} which is otherwise the maximum potential risk value of the particular category.

$$U_{max,b} = R_{max,b} - \sum_{s \in B} (R_s + C_s) = p_{state,b} \cdot S_{max} - \sum_{s \in B} (R_s + C_s) \quad \textbf{(4-102)}$$

Summarized the uncertainty per contingency is either given by the residual uncertainty of a contingency or the maximal possible remaining risk, depending which value is lower. If the maximum risk value exceeds the potential uncertainty in risk there is no possibility, that the system holds a higher, in the uncertainty hidden risk (after a first order contingency) than the one already found like it is the case for the branches 7 and 9 in Figure 4-26 and so the uncertainty affliction of the particular category is identically to zero. Additionally, the maximum possible remaining risk R_{max} as well as the potential remaining risk are illustrated

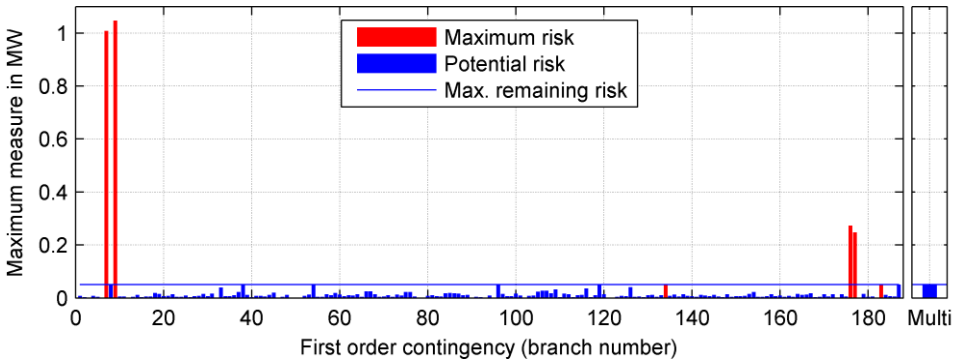

Figure 4-26. Contingency-wise maximum risk and uncertainty measures.

This kind of evaluation is useful for the ranking of n-1 contingencies in terms of the risk they hold. So, if there is a n-1 violation in a TSO's conventional deterministic system security analysis this type of output interpretation could be used in terms of decision support to judge about relaxations of n-1 constraints.

5 Analysis Regarding the Proposed Load Flow Method

5.1 Applicability of DC-Load Flow

The focus of the presented method is put on the application to transmission systems. According to the planning principles of TSOs the large distance transportation of reactive power has to be minimized to technically reasonable values. According to the planning directives of the German TSOs [62] the exchange of reactive power between control zones has to be as low as technically reasonable. Also the "Reactive Support and Control Whitepaper" of NERC [63] states, that the demand in reactive power of a transmission system's node has to be covered locally. All these requirements lead to presumption, that the DC-load flow method is able to perform well enough to use it in system security assessment approaches in transmission systems. To verify, that the deviation of results compared to AC load flow is in an acceptable range, the following analyses were performed. The first one is about the evaluation of deviations regarding a test system and artificially generated data and in the second one real world data is analyzed regarding usual power factors of power system branches.

5.1.1 Test System Based Analysis

In this subchapter the DC- and the AC-load flow computation methods are compared regarding the applicability on the IEEE 118 bus test system. A sensitivity analysis is performed for a change in active as well as in reactive power consumption of loads and as a direct consequence of power generation units. By modifying a dataset of 1000 artificially generated load flow utilization cases, sub datasets are produced. This is done by changing the active and reactive power consumption of loads. The active power consumption is varied in three steps from 1.0 p.u. to 2 p.u. and the power factor between 0.9 and 1.0 leading to 9 scenarios to investigate. The results of this analysis are visualized in Figure 5-1 in the form of a two dimensional histogram for branch loading and result deviation per scenario and in Figure 5-2 in the form of statistical measure plots respectively.

The top-left histogram given in Figure 5-1 shows, that most of the branches in the initial scenario are barely loaded and also show a low absolute deviation from -8% to +4% in branch loading, where 90% of the values show a deviation of -2.3% to 1.4%. With an increase in loads' active power demands (increase of the active power scaling factor p) also the deviations of the DC- to the AC- load flow results increase but stay in a range of 10% (-5.9% to +3.4%) around the actual value for 90% of all cases. The larger deviations in underestimation of the branch flow occurs for branches, showing a low to moderate loading, whereby the DC-method's deviation for high utilized branches, which are important for the presented method, are lesser and positive meaning a slight overestimation.

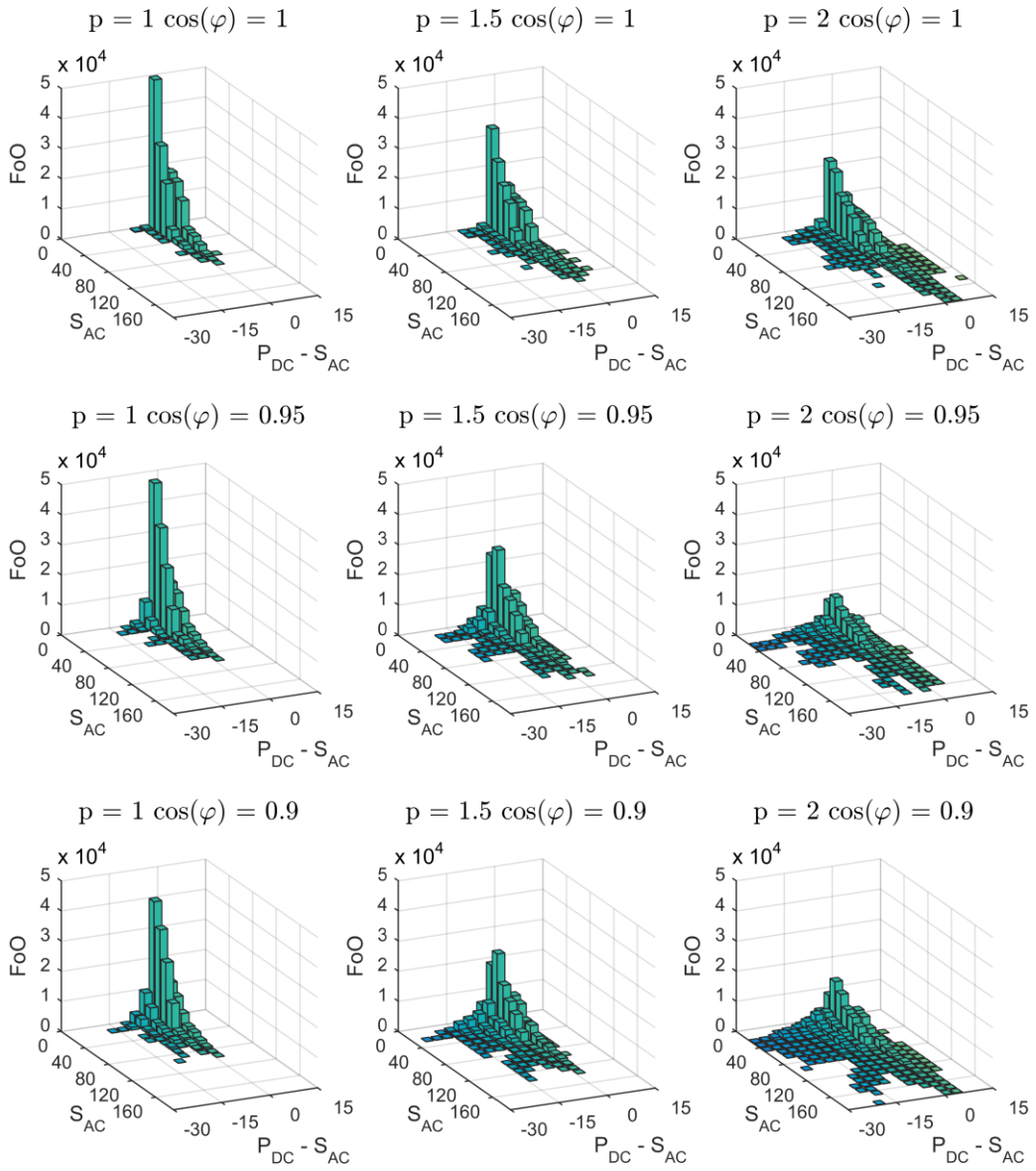

Figure 5-1. Two dimensional histograms regarding the frequency of occurrence of the branch loadings in % as a result of an AC-Monte-Carlo simulation and the deviation of the simplified DC-load flow pendent in % loading.

An increase in reactive power demand of loads is realized by generally decreasing the power factor $\cos\varphi$ for all loads in the test system leading to a deviation of the DC load flow method between -8.1% to 1.7% for a power factor of 0.95 lagging and from -10.1% to 1.4% for a power factor of 0.9 lagging for 90% of the result values in terms of branch flows.

In the bottom right histogram the results of the analysis of the test system with an increase in active load demand of 160% and a power factor of $\cos\varphi$=0.9 lagging are visualized. Branches showing a low and moderate utilization show the largest deviations of the load flow calculation results compared to the AC-Monte-Carlo simulation, whilst the accuracy increases for highly loaded branches. 90% of the deviation values are located between -18.4% and +4.3%, whereby positive deviations tend to occur for high branch utilizations and negative deviations for low and moderate loaded ones.

In the boxplot in Figure 5-2 common statistical measures of the evaluation regarding the deviation of DC- compared to AC-Monte-Carlo simulation results are given. The median value for the evaluation of the particular scenario is represented as a red line, the 5% to 95% interquantile as a blue box and extreme values as black whiskers.

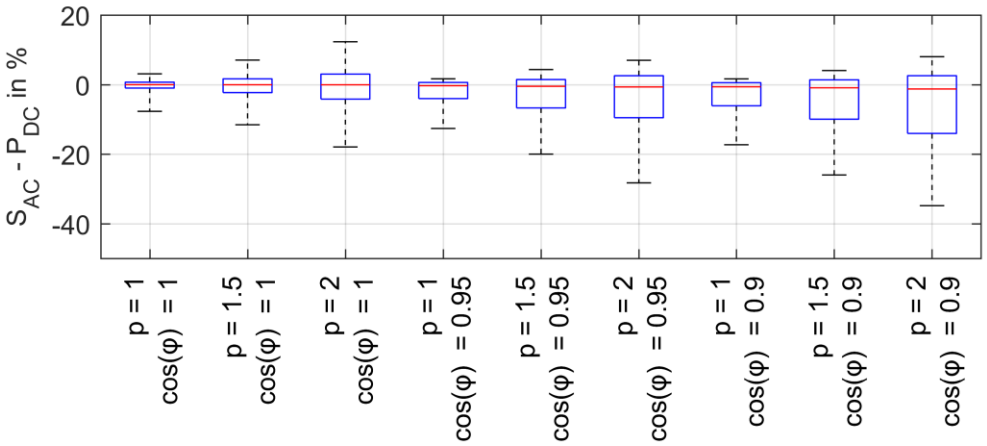

Figure 5-2. Statistical measures for different utilization scenarios with an X/R ratio of 10.

The visualization shows, that the accuracy of the DC-load flow method decreases with an increase in system loading (p) even for scenarios concerning the power factor, what is due to an increase in reactive power demand of the power system's lines with higher system utilization and an increased need of reactive power generation and transportation to maintain the nodal voltages in a flat profile in the benchmark method. Generally for all scenarios, the statements are valid, that negative deviations and positive deviations are nearly equally likely due to the fact, that the median values are close to zero, and as a second statement, that negative deviations show a higher magnitude than positive ones, which is due to neglecting reactive load flows in DC-based methods which always add up to the active load flow and so are a systematic source of deviation in load flow results, while the positive and the smaller negative deviations are due to simplifications regarding the interdependency of active and reactive power transportation leading to over- as well as underestimation of the actual utilization of a particular branch when using a DC-based load flow method.

To assess the sensitivity of the implemented DC load flow method, the same data was used to evaluate load flow results while neglecting the resistance of the branches. The according results are presented in Figure 5-3, again in the form of common statistical measures. Generally, it can be said, that the results of the DC load flow are closer to the benchmark due to the smaller 90% inter-quantile values in the latter study, while outliers still remain nearly equally for both evaluations. The mean value of the load flow deviation is identically either if the resistance of branches is taken into account or not. Unlike it's the case for the results when taking account for the resistance an increase in system utilization leads to an increase in underestimation of load flows in terms of the magnitude.

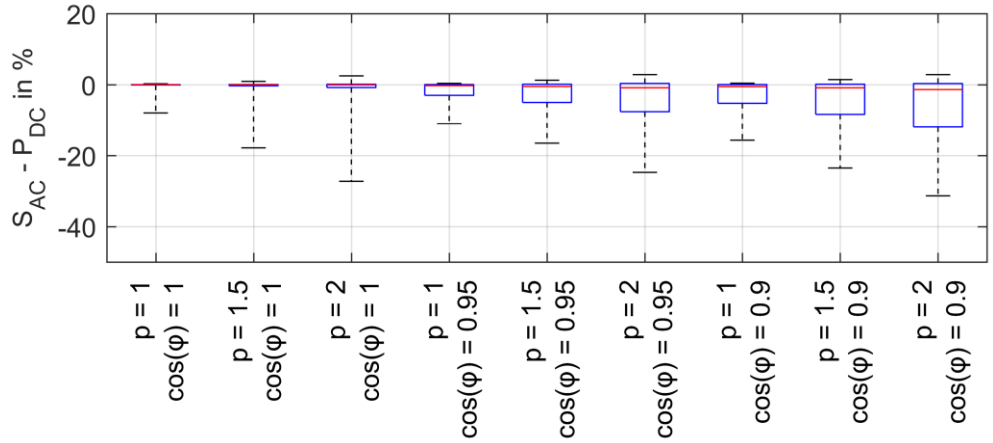

Figure 5-3. Statistical measures for different utilization scenarios with an R/X ratio of zero.

Analogous to the analysis regarding the accuracy and the applicability of the DC load flow for security assessment purposes AC-PTDFs were used to compare their performance in respect to the benchmark. The results of the comparison are given In Figure 5-4 in terms of statistical measures as mentioned in detail before.

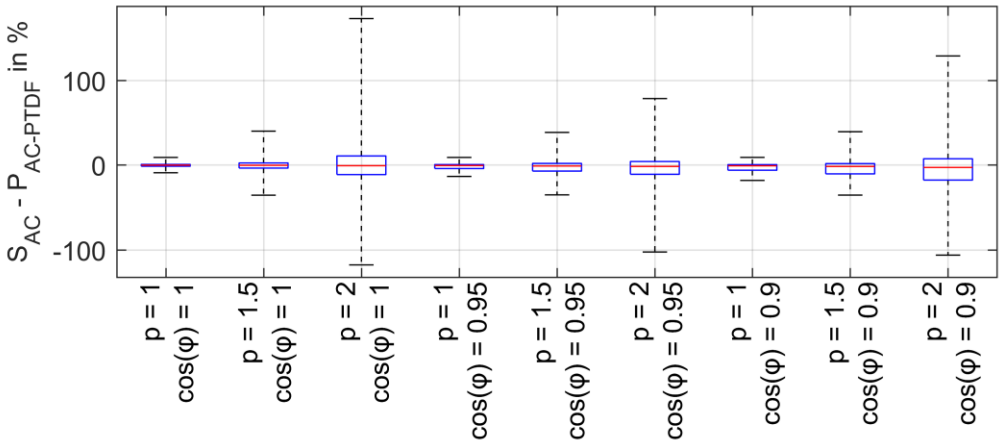

Figure 5-4. Statistical error measures for different utilization scenarios regarding the AC-PTDF MCS method. (X/R=10).

The results lead to the statement, that the AC-PTDF method is not well suited for the purpose of modelling high uncertainty ($\sigma_L = 0.2 \cdot \mu_L$) afflicted and is outperformed by the DC-PTDF MCS for this example. Studies performed in addition showed, that the AC-PTDF MCS approach outperforms the DC-PTDF MCS for uncertainties in loads beneath 5% ($\sigma_L = 0.05 \cdot \mu_L$).

5.1.2 Analysis of Measured Data

To verify the assumption, that in severe loading situations the reactive load flow can be neglected for the purpose of a fast security assessment, data of a real world power system was analyzed regarding active and reactive load flows and the particular deviation of branch utilization when accounting for active instead of apparent load flows. The investigated power system consists of 836 busses, 383 branches and data are available for one year. In Figure 5-5 the power factor and the normalized apparent power are visualized. The figure shows, that the power factor increases for higher values in branch utilization tending to a value of one.

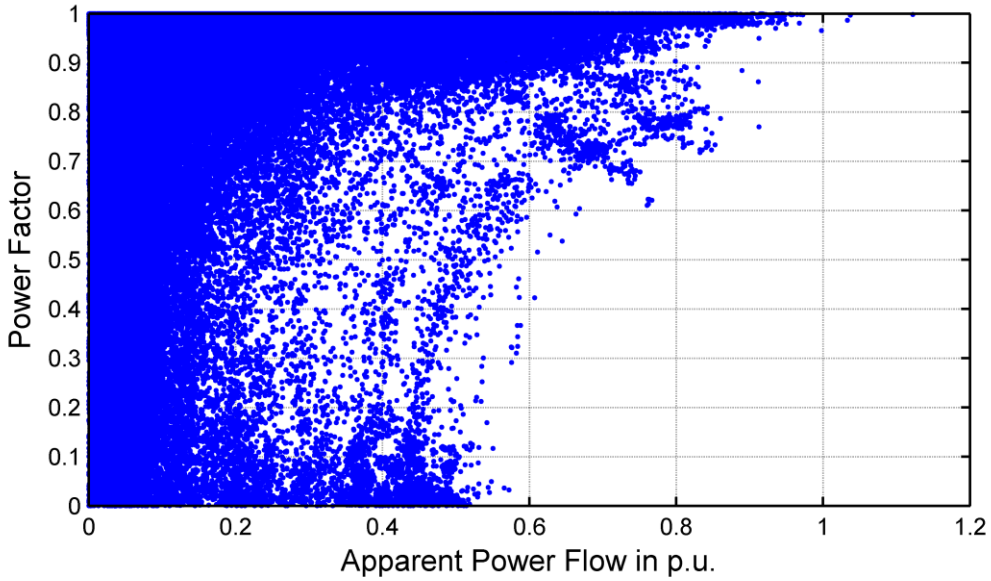

Figure 5-5. Branch flow power factor and and according apparent power in p.u.

Due to the fact that the scatter plot in Figure 5-5 doesn't hold any information about the population density, a bivariate histogram regarding branch utilization and branch flow power factor is given in Figure 5-6.

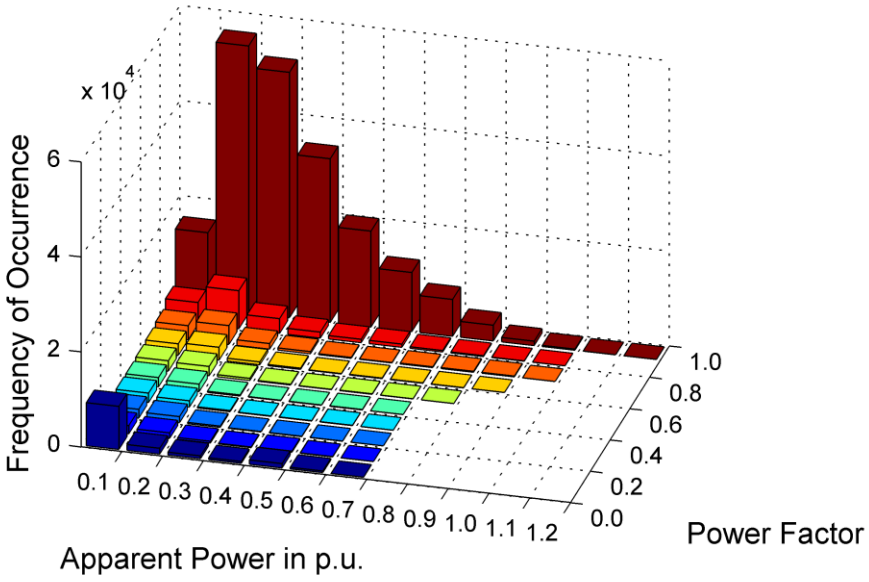

Figure 5-6. Histogram of observed branch load flows and the according power factors.

Based on this analysis the assumption, that the load flow of highly loaded branches is mainly dominated by the active load flow component is validated and thus the applicability of a DC-load flow based method is reasonable.

The conclusion can be drawn that high loadings correlate with an increase of the power factor.

5.2 Comparison of an AC-MCS, DC-MCS and DC-PLF Method

In this subchapter, different probabilistic load flow implementations in terms of simplification levels of load flow calculation are applied on exemplary use cases to determine the limits of the proposed method in terms of accuracy and to show the advantages and disadvantages of the presented method. As test power system a modified version of the IEEE 118-bus network according to the data as given in Appendix A was used. The modifications were necessary to ensure that the characteristics of the power system reflect those of a real world transmission system. Therefore the branch resistances were modified to show a X/R-ratio of 5 to 10 and their capacitances were set to zero. Reactive power compensation units, as well as switching transformers were neglected to exclude their influence in this part of the analysis.

Based on the results of the analysis presented in chapter 3.1.7, the uncertainty in power demand of transmission system nodes can be approximated by a Gaussian distribution with a mean value of zero and a standard deviation between 10% to 20% of the particular forecast value varying from node to node. Furthermore based on this assumption the distribution of the node's load can be represented by a Gaussian distribution with the mean value equal to the forecasted one and a standard deviation according to the standard deviation of the particular uncertainty distribution.

To be able to perform a comparison between Gaussian and non-Gaussian distributed uncertainties in active power generation different approaches were used described in detail in chapter 5.2.2 and 5.2.3 either based on weighted assignment of uncertainties to generation units for the Gaussian case and by a cost optimal dispatch using DC-OPF in the case of non-Gaussian ones.

5.2.1 Reactive Power Dispatch

To be able to compare AC-load flow solutions and DC-load flow solutions on a given basis of an active power dispatch of loads and generation units, reasonable assumptions have to be made in terms of reactive power infeed to account for an acceptable voltage profile. To achieve on the one hand a voltage profile between given limits and also as low as possible active power losses, which reflects the actual goals of a TSO when it comes to reactive power dispatching, an optimization problem is formulated. The objective function is given in eq. (5-1) and mainly holds the costs of active power losses (C_{loss}), which are covered by the slack generator and so are directly a function of the slack generator (P_{Slack}). The cost of the active power losses is modelled as a linear function of the active power losses with the factor C_{MW} giving the costs per MW. Due to the fact, that the costs of the losses are the only part of the objective function the particular value of the specific loss costs don't influence the result, as long as the sign is positive to achieve a minimization.

$$\min_{P_{Slack}} C_{loss(P_{Slack})} \quad \textbf{(5-1)}$$

$$C_{loss} = C_{MW} \cdot P_{Slack} \quad \textbf{(5-2)}$$

The optimization space is limited by the given dispatch P_D in active power of each generator not being a slack generator S, by the limits in reactive power infeed Q_{min} and Q_{max} of each generation

unit, by the particular node's voltage limit U_{min} and U_{max}, as well as by the branch limits S_{max}. The mathematical formulation of the additional constraints to a standard OPF is given in eq. (5-3) to (5-7).

$$P_g = P_{D,g} \;\forall\, g \in G \backslash S \quad \textbf{(5-3)}$$

$$Q_{min,g} \leq Q_g \leq Q_{max,g} \;\forall\, g \in G \quad \textbf{(5-4)}$$

$$P_{min,s} \leq P_s \leq P_{max,s} \forall\, s \in S \quad \textbf{(5-5)}$$

$$U_{min,n} \leq P_n \leq P_{max,n} \;\forall\, n \in N \quad \textbf{(5-6)}$$

$$|S_b| \leq S_{max,b} \;\forall\, b \in B \quad \textbf{(5-7)}$$

The result of solving this optimization problem for a given active power dispatch is an active and reactive power dispatch, which is at least N-0 secure, within the voltage limits and states a local optimum in terms of active power losses.

5.2.2 Gaussian Uncertainty Data

This subchapter gives a comparison between different load flow methods regarding the branch outage risk when the typically Gaussian uncertainty of the loads of the power system under investigation is covered by the generation units also with a Gaussian distributed uncertainty. This is realized with eq. (5-8) for determining the active power infeed of generation unit g and sample i. ΔP_i represents the uncertainty in load of the sample i and p_g is the participation of generation unit g in the overall generation of the forecast dispatch.

$$P_{g,i} = \left(\sum_{g \in G} P_g - \sum_{n \in N} P_{n,i} \right) \cdot \frac{P_g}{\sum_{g \in G} P_g} = \Delta P_i \cdot\; p_g \;\forall i \in I \quad \textbf{(5-8)}$$

Due to the assumption, that transmission system load uncertainties typically show a Gaussian distribution in uncertainty also the overall system load uncertainty shows a Gaussian uncertainty distribution since the sum of Gaussian distributed values again is Gaussian distributed [64]. By weighting the uncertainty to be balanced by the planned operation point of each generator, the overall uncertainty is simply a linear combination of each generators' uncertainty. As a consequence, the generation unit uncertainties also show a Gaussian distribution.

In the following figures the results of three different probabilistic load flow methods (as described in chapter 0) are given in terms of statistical measure plots as already described in detail in subchapter 5.1.1. The results of the DC-PLF method are given in Figure 5-7, of the DC-PTDF MCS in Figure 5-10 and the results of the ACPTF-MCS in Figure 5-11 for different power system utilization scenarios, where the system utilization factor p in terms of active load scaling and the power factor $\cos\varphi$ were altered per scenario.

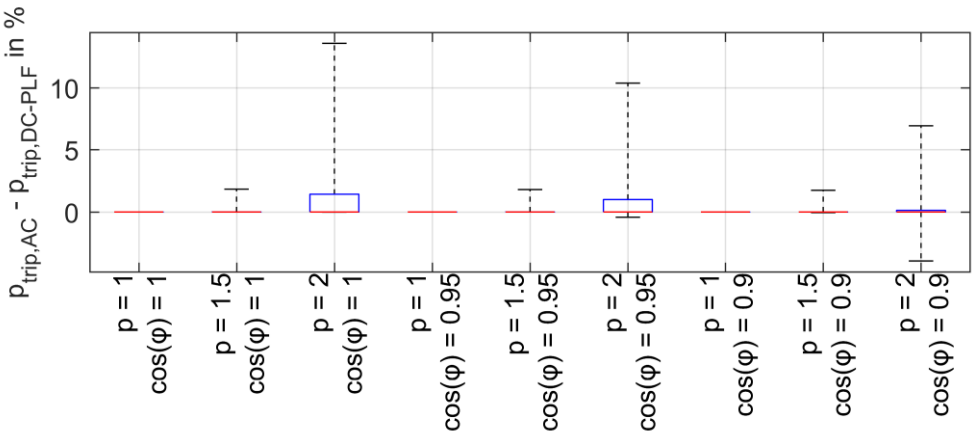

Figure 5-7. Statistical measures regarding branch tripping probability for the DC-PLF approach.

The plot in Figure 5-7 leads to the statement, that the accuracy of the DC-PLF method in terms of branch tripping probability decreases with increasing power system utilization. For a power factor of one the DC-PLF method tends to overestimate the outage probability, whereas a decrease in the load power factor leads to a more precise result for the high utilization case $p = 2.0$ in terms of the 90% interquantile, but also to an underestimation of the tripping probability for 5% of the branches. The actual branch tripping probabilities per load flow method implementation are given in Figure 5-8 for a high utilization and no reactive power demand scenario , where the blue bar gives the benchmark in terms of the AC-MCS solution. The AC-PTDF based MCS shows a poor performance compared to the benchmark and is outperformed for nearly all branches by the DC-PTDF method. The DC-PLF is tending to overestimate the outage probability in this example, what is due to the fact, that the branch loading to tripping probability function is implemented continuously for the MCS based methods and in the form of a stepwise approximation (Figure 4-11) for the DC-PLF.

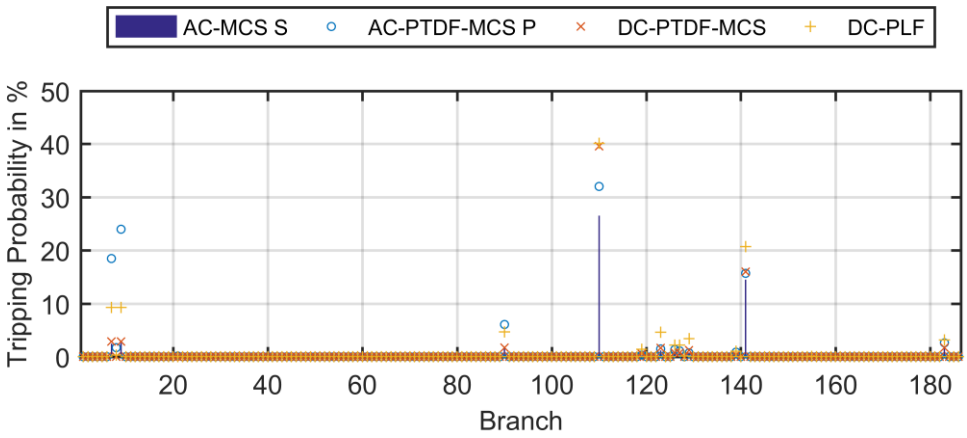

Figure 5-8. Branch tripping probabilities per branch and approach for the high utilization and no reactive demand scenario.

The branch outage probabilities for a high system load scenario showing a load power factor of $\cos\varphi = 0.9$ for all four approaches are given in Figure 5-9. Compared to the results for the scenario showing no reactive power demand in terms of loads the tripping probabilities increase to the additional load flow in terms of reactive power. Due to the fact, that the DC-based methods do not account for reactive power nodal injections of branch branch flows the results are the same for both scenarios. In the case of the AC-PTDF MCS approach the evaluated branch tripping probabilities

change with a different reactive power dispatch due to the fact, that the AC-PTDF matrix is generated based on the Jacobean matrix which is a result of an initial AC-load flow computation.

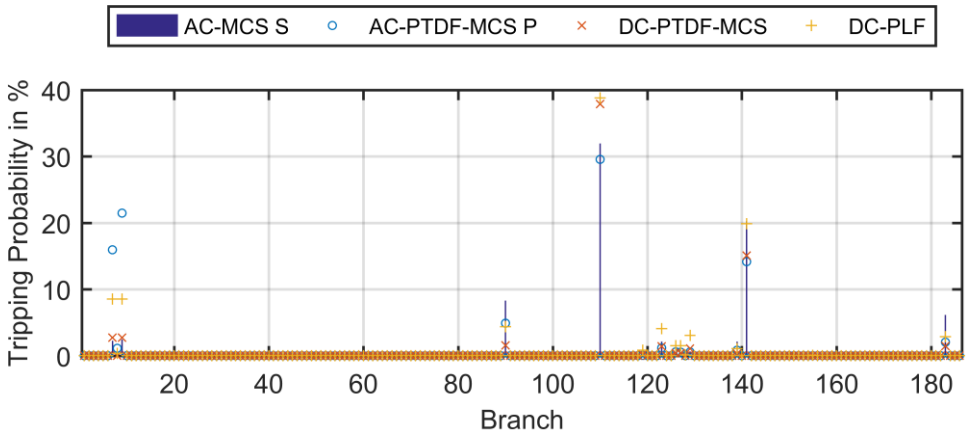

Figure 5-9. Branch tripping probabilities per branch and approach for the high utilization and high reactive demand scenario.

An evaluation of the performance of the DC-PTDF MCS is given in Figure 5-10. For the low utilization cases the performance is equal to the benchmark for all three reactive power scenarios. Compared to the DC-PLF approach the DC-PTDF MCS shows a better accuracy for the medium and high utilization test cases. However, the interquantile is zero for all scenarios so at least 90% of the branch tripping probabilities do not deviate from the benchmark.

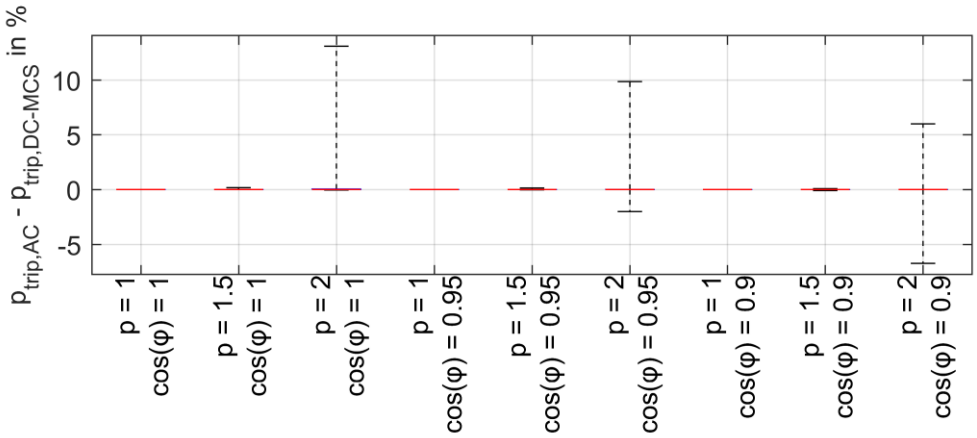

Figure 5-10. Statistical measures regarding branch tripping probability for the DC-MCS approach.

The statistical measures given in Figure 5-11 show, that the AC-PTDF MCS approach shows a good accuracy in terms of branch tripping probability compared to the benchmark for the low and the medium utilization cases regardless the reactive power consumption of loads, whereas it shows the poorest performance of the compared methods for the high utilization cases in terms of the maxima of absolute error.

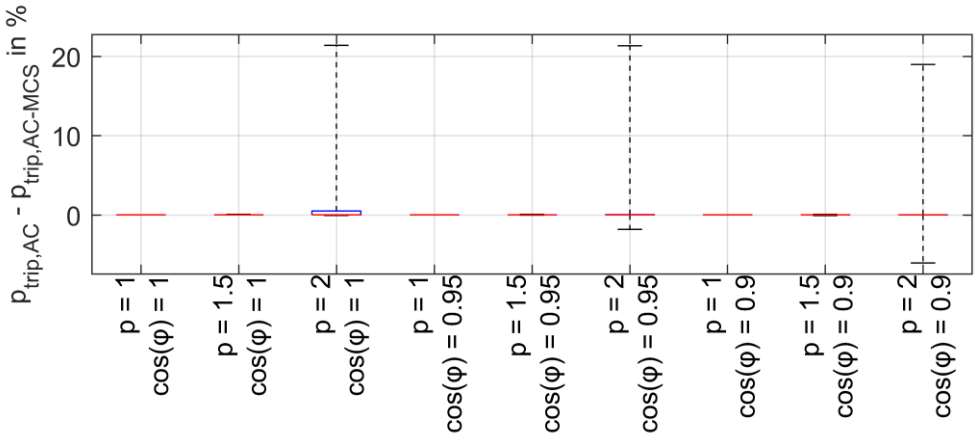

Figure 5-11. Statistical measures regarding branch tripping probability for the AC-MCS approach.

The conclusions which can be drawn from these evaluations are, that the AC-PTDF MCS approach is showing the worst performance of the compared methods regarding the determination of branch tripping probabilities for uncertainty afflicted loads covered in by generation units showing a Gaussian power distribution. Theoretically the output measures of the DC-PLF and DC-PTDF MCS methods should be identically, but do to the different implementations of the branch loading to tripping probability function the results deviate from each other. Especially high overloads near to the protection device limit are overestimated by the weighting function in the case of the DC-PLF approach. A remedy could be found by increasing the number of steps which would lead to an increase in computational effort and would elongate the methods runtime. For the performed studies the DC-PLF tends to overestimate the branch tripping probability, while the DC-PTDF MCS gives the best results of all compared approaches.

5.2.3 Non-Gaussian Uncertainty Data

This subchapter gives a comparison between different load flow methods regarding the accuracy in terms of branch loading as well as the branch outage risk when the typically Gaussian uncertainty of the loads of the power system under investigation is covered by generation units, showing a non-Gaussian distributed uncertainty. The non Gaussian distribution of the generation units is achieved by solving an optimization problem. The objective is the generation dispatch showing the lowest costs per sample and the solution space is constrained by generation unit active power limits and branch flow limits. If no contingencies are active for all samples in the synthetic load dataset one generation unit – the cheapest one – would cover the overall load of each sample and due to the fact, that the overall load is assumed show a Gaussian distribution this cheapest generator would also show a Gaussian distribution in active power infeed. The limitations in transfer capacity of branches and the operational limits of generation units cause, that not only the generation unit showing the lowest prices but also other ones cover the load. An exemplary dispatch distribution is given in the histograms depicted in Figure 5-12 for generation units, showing varying output power per sample.

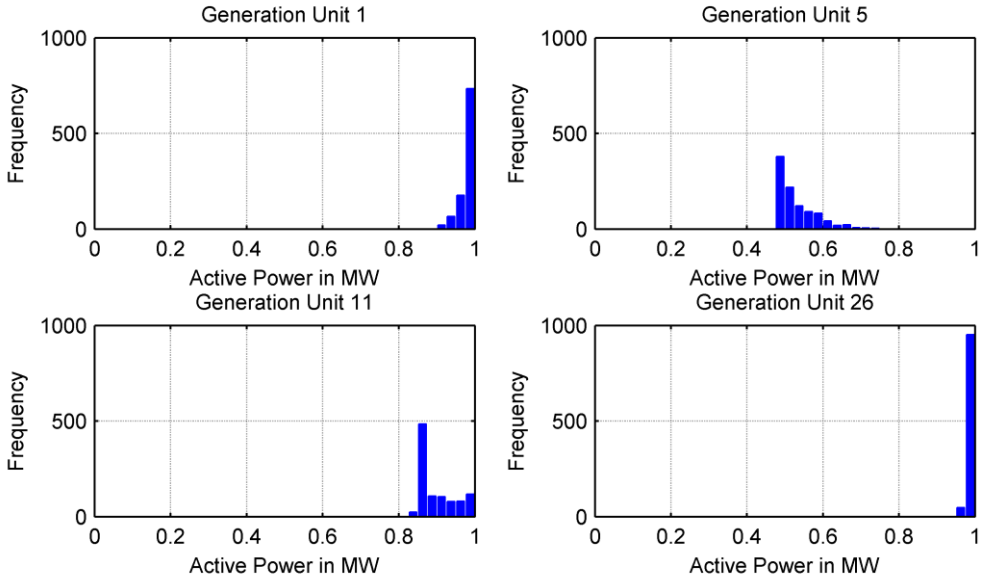

Figure 5-12. Active power histograms of uncertainty afflicted generation units in the test system.

The comparison regarding non-Gaussian generation unit active power infeed consists of an AC-, an AC-PTDF-, and a DC-PTDF-Monte-Carlo Simulation as well as a DC-PLF implementation. The AC-MCS solution is the benchmark for the analysis, which is performed for several test cases. Each test case is specified by a loading factor for linear load scaling, allowing the increase or decrease of the system's utilization, and the uncertainty in load given by a value for the standard deviation in percent of the actual scaled active power of each load in the system.

The following figures hold the results of the evaluations performed using non-Gaussian distributed power plant infeeds. In Figure 5-13 the results for the DC-MCS approach are visualized in terms of common statistical measures. For low and medium utilization scenarios the accuracy of the DC-PTDF MCS is equal to the performance of the benchmark method. For the high utilization scenarios the 90% of the evaluated branch tripping probabilities do not deviate from the benchmark solution. For the scenario without reactive power demand of the power system's loads 5% of the branch tripping probabilities are overestimated, whereas an increase in reactive power demand leads to an decrease in overestimation and an increase in the number of underestimations due to the fact, that for reactive load flows is not accounted for by the DC-PTDF MCS and so the branch utilization is systematically underestimated.

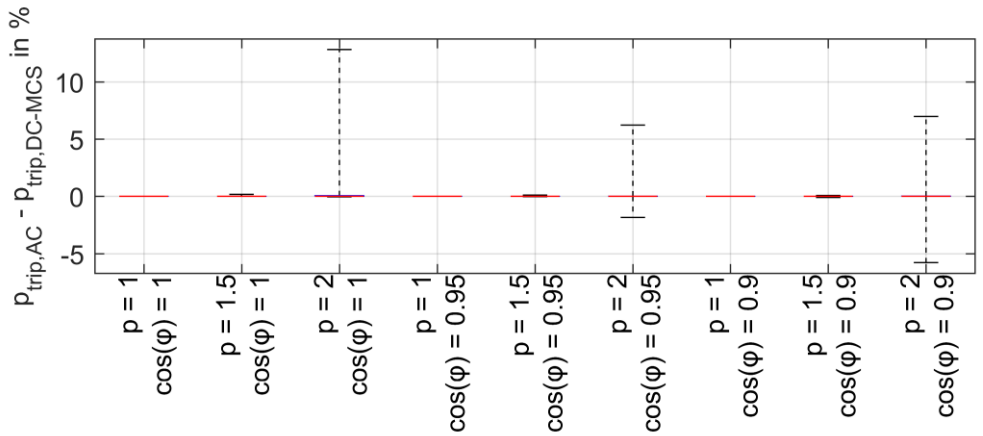

Figure 5-13. Statistical measures regarding branch tripping probability for the DC-PTDF MCS approach.

The evaluated branch outage probability values for all 186 branches of the underlying test system are visualized in Figure 5-14 for a high system utilization scenario without any demand of the loads in reactive power.

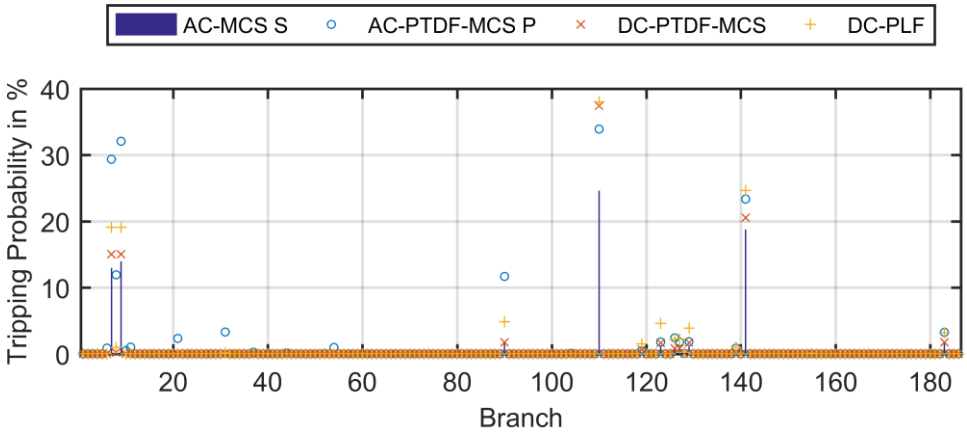

Figure 5-14. Branch tripping probabilities per branch and approach for the high utilization and no reactive demand scenario.

In Figure 5-14 the evaluated branch tripping probabilities are given for a high system utilization scenario with a demand of the loads in reactive power according to a power factor of $\cos\varphi = 0.9$.

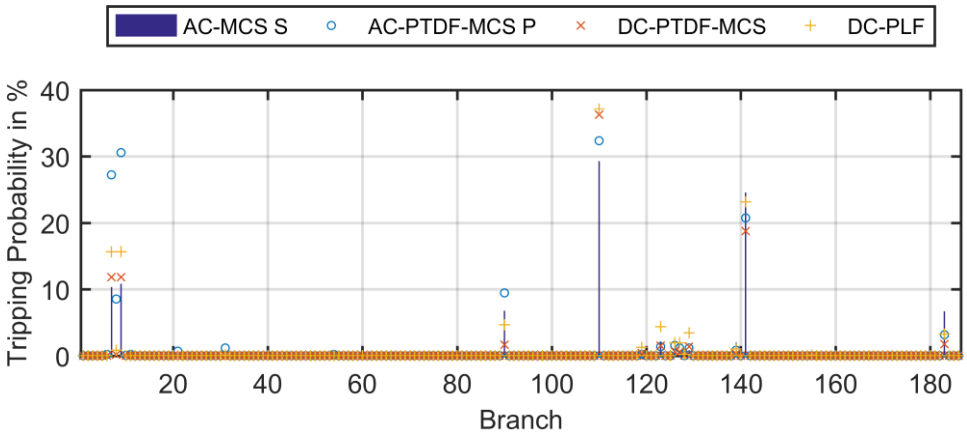

Figure 5-15. Branch tripping probabilities per branch and approach for the high utilization and high reactive demand scenario.

A comparison of Figure 5-14 and Figure 5-15 leads to the conclusion, that the AC-PTDF MCS is outperformed by the DC based methods for both test system scenarios and is tending to highly overestimate the actual benchmark. The DC-PLF approach shows, as it is the case for Gaussian uncertainty data a good accuracy for the low and medium-loaded scenarios, while it tends to overestimate the actual benchmark results for highly loaded scenarios. Comparing the statistical measures in Figure 5-13 for the DC-MCS and Figure 5-14 for the DC-PLF approach, the for Gaussian load data mentioned effect was also noticeable for non-Gaussian uncertainty data, that the accuracy in results is better for highly loaded system scenarios with reactive power demand of the load in terms of the 90% inter-quantile. This effect can be attributed to the discretization of the branch utilization to branch outage probability, due to the fact, that the effect can be observed for both, Gaussian and non-Gaussian uncertainty data.

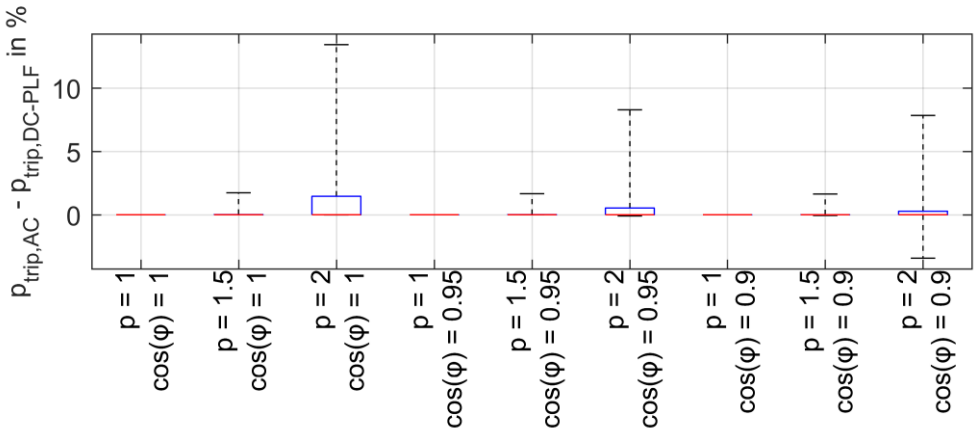

Figure 5-16. Statistical measures regarding branch tripping probability for the DC-PLF approach.

Comparing the statistical measures regarding branch tripping probability of the DC-PLF in Figure 5-16 for non-Gaussian and Figure 5-7 for Gaussian uncertainty data in terms of power plant dispatches the results are similar and deviate from each other in details. E.g. the maximum deviation of the medium utilization scenario showing a power factor of 9.95 takes a higher value for Gaussian uncertainty data than for non-Gaussian while the 90% inter-quantile of the high utilization and high reactive power demand scenario is higher for the non Gaussian uncertainty data.

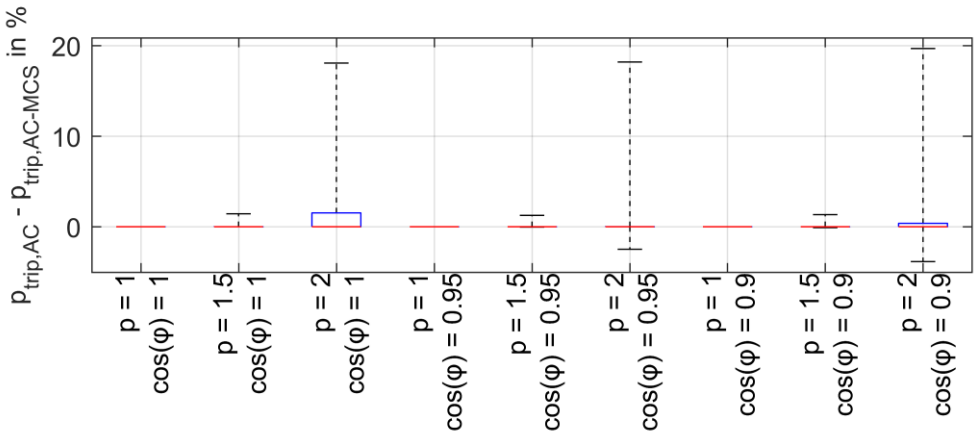

Figure 5-17. Statistical measures regarding branch tripping probability for the AC-PTDF MCS approach.

The AC-PTDF MCS shows a similar performance for the Gaussian and non-Gaussian uncertainty variants, but is clearly outperformed by the DC load flow based methods.

Concluding this subchapter leads to the statement, that the accuracy of the DC-PLF is comparable for both, Gaussian and non-Gaussian power plant uncertainty data. The AC-PTDF MCS is clearly outperformed by both DC-load flow based approaches for uncertainty data showing a standard deviation of 0.2 based on the actual scenarios active power setting. Additional reactive load flows lead - for the DC-load flow based methods – to an offset of the uncertainty, the uncertainty margin, the difference between the maximum and minimum value remain approximately similar.

6 System Case Studies

This subchapter holds risk based security evaluations of the IEEE 118-bus test system and the Pengase 1354-bus test system [65]. Investigations concerning the sensitivity of the result from different parameters were performed and the capabilities of the proposed method were presented.

The sensitivity analysis was performed for the below listed parameters:

- Effect of the approximation of the tripping heuristic
- Gaussian vs. non-Gaussian uncertainty data
- System Loading
- Uncertainty margin
- Correlation of uncertainties

6.1 Analysis Regarding the Tripping Heuristic

One of the central elements of the presented approach is the tripping heuristic described in detail in chapter 4.4. Due to the fact, that different implementations (continuous exponential function or step wise approximation as given in Figure 6-1) of this heuristic lead to different results in terms of risk measure this influence is the topic of interest in this subchapter.

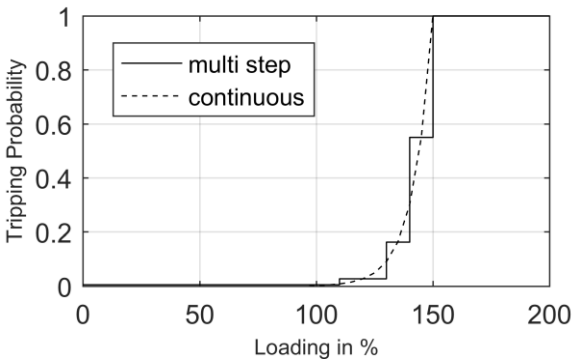

Figure 6-1. Different implementations of the branch loading to tripping function.

The risk measure for a dispatch is analyzed by the use of a DC-MCS implementation with the stepwise approach and one with the continuous exponential function. The simulations were performed for the modified IEEE 118-bus network with a Gaussian load uncertainty, showing a standard deviation of 20% of the particular load's active power consumption, and also a Gaussian uncertainty in terms of power plant infeeds.

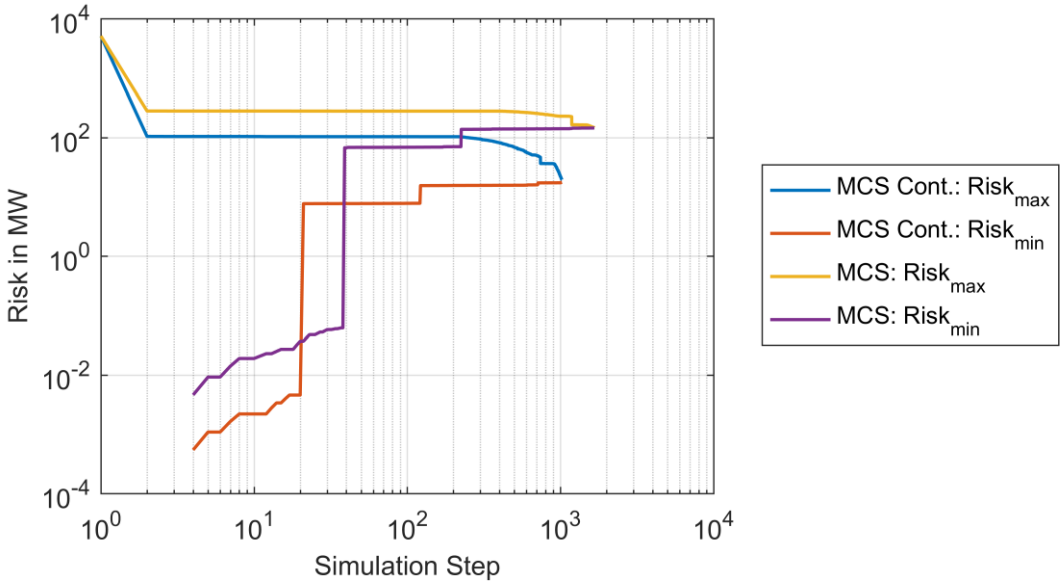

Figure 6-2. Overall system risk evolution during the simulation for the DC-MCS approach with different implementations of the tripping heuristic.

In Figure 6-2 the overall system risk evolution of one exemplary system use case is given for different method implementations. For this comparison the more detailed implementation, namely the DC-MCS approach, were the tripping heuristic is implemented in a continuous way, serves as benchmark. In contrary to the benchmark the tripping heuristic is implemented in the form of a stepwise approximation, for the scenario referred to in the figure as "MCS". The evaluation leads to the statement, that the approach implemented on the basis of the approximated heuristic overestimates the system risk compared to the benchmark, what is due to the way the heuristic was approximated. The numerical values for each implementation are given in Table 6-1 in terms of the maximum and minimum bound of the overall system risk and in terms of the maximum risk value a system state showed during the particular simulation.

Table 6-1. Risk measures.

	$R_{sys,min}$	$R_{sys,max}$	$R_{state,max}$
MCS Cont.	17.54	19.48	7.67
MCS	147.34	145.25	67.25

6.2 Comparison Based on Non-Gaussian Uncertainty Data

The evaluation presented in this subchapter compares the parametric load flow to a DC-MCS. In both cases the heuristic is implemented in an approximated way. Non-Gaussian Uncertainty Data was used for generation units active power. The results are visualized in Figure 6-3 in terms of the overall system risk evolution. The DC-PLF solution leads to an overestimation of the overall system risk compared to the DC-MCS.

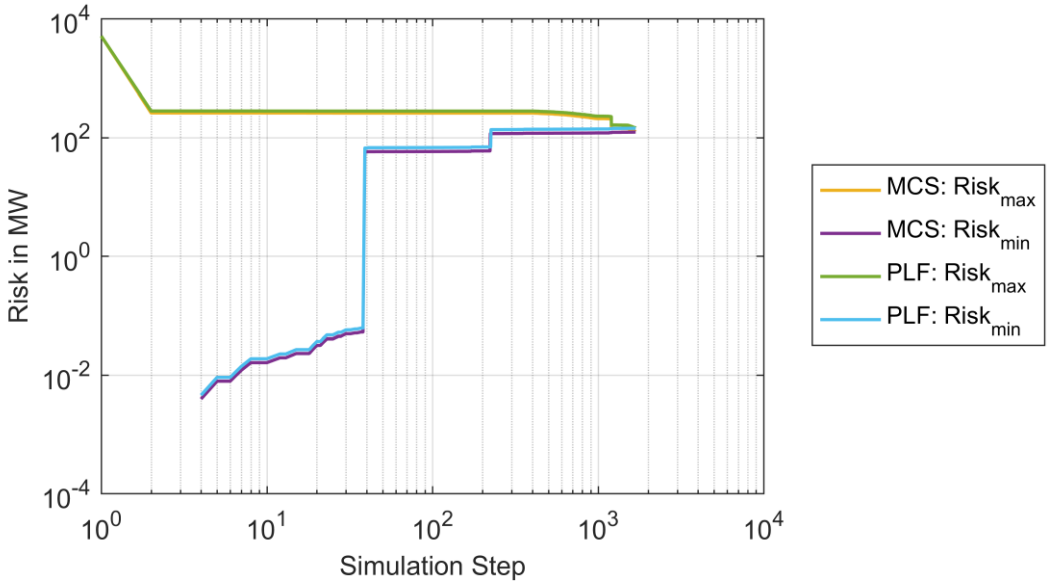

Figure 6-3. Overall system risk evolution during the simulation for the DC-PLF and DC-MCS approaches with different implementations of tripping heuristic for non-Gaussian uncertainty data.

However, the overall system risk is not the only measure of interest of a risk based security assessment. Also the maximum in state risk is of interest when comparing system states. In Table 6-2 the results are given in the form of aggregated measures in terms of maximum and minimum boundaries of the overall system risk and the maximum state risk. The results show, that the maximum state risk is the same, for both of the approaches. These results are in line with the results of the analysis regarding the use of DC-based load flow methods for the proposed approach given in chapter 5.2.3, where the statement was, that the results of the DC-PLF method are very close to the results of the DC-MCS even for non-Gaussian uncertainty data.

Table 6-2. Risk measures.

	$R_{sys,min}$	$R_{sys,max}$	$R_{state,max}$
MCS	123.65	125.72	57.12
DC-PLF	143.82	145.9179	57.12

6.3 Comparison of Different Utilization Cases

This subchapter holds a comparison of different N-0 secure utilization cases of the same test system as already used in the previous chapter. The upper and lower boundaries of the evaluated overall system risk are visualized in Figure 6-4 for utilization scenarios reaching from an active load scaling factor of 1.2 to 1.6. The results show, that the system risk increases with increasing utilization of the power system, what is due to the tripping heuristic which leads to higher tripping probabilities of highly loaded branches, which again directly influence a state's probability, which again is part of the overall system risk.

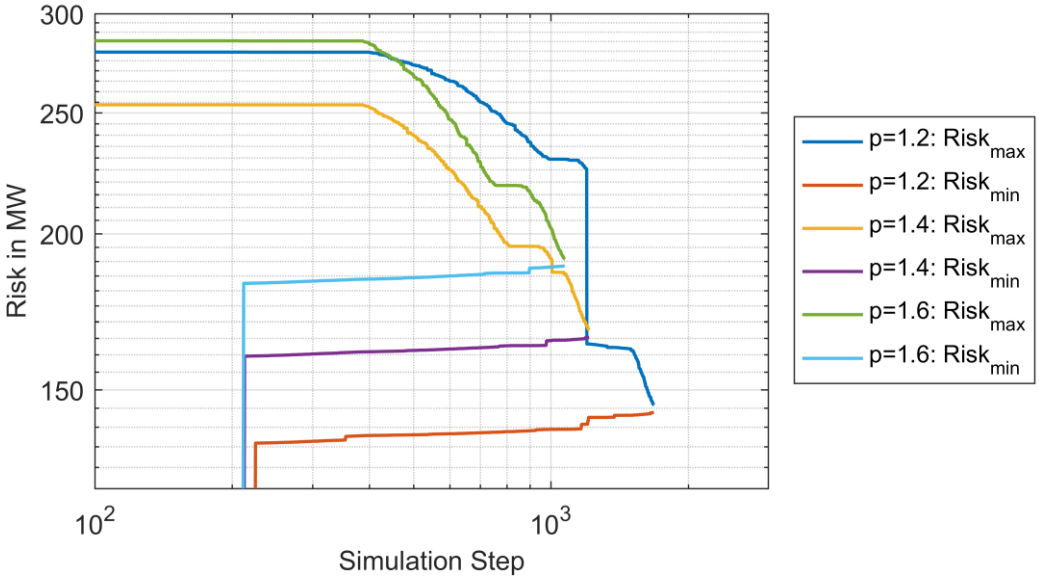

Figure 6-4. Overall system risk evolution during the simulation for the DC-PLF with a step wise tripping heuristic for non-Gaussian uncertainty data for different dispatches.

In Table 6-3 the results are presented numerically in the form of the upper and lower boundary of the evaluated system risk and the maximum state risk.

Table 6-3. Power system risk measures.

	$R_{sys,min}$	$R_{sys,max}$	$R_{state,max}$
p=1.2	143.82	145.91	66.5
p=1.4	165.22	167.46	78.59
p=1.6	188.41	190.85	89.88

This evaluation leads to the fact, that higher utilized power systems hold higher risks in terms of energy not supplied. In this case also the maximum state risk is rising for higher utilization cases, but this statement can not be generalized due to the fact, that it is topology and dispatch dependent.

In Figure 6-5 the evaluated upper and lower overall system boundaries are presented. The conclusions previously drawn for the DC-PLF approach are also valid for the DC-MCS approach with a continuous tripping heuristic.

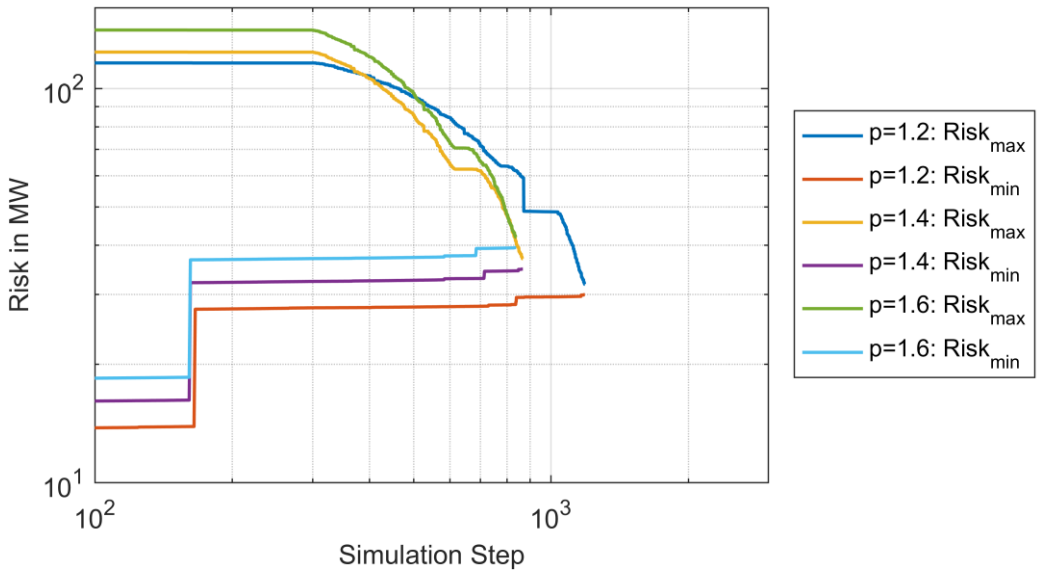

Figure 6-5. Overall system risk evolution during the simulation for the DC-MCS approach with a continuous implementation of the tripping heuristic for non-Gaussian uncertainty data and different dispatches.

The particular results are given numerically for the upper and lower boundary of the system risk and the maximum state risk in Table 6-4 for each analyzed utilization case. Both, the maximum state risk and the overall system risk are increasing with increasing utilization.

Table 6-4. Risk measures.

	$R_{sys,min}$	$R_{sys,max}$	$R_{state,max}$
p=1.2	29.92	31.82	13.62
p=1.4	34.76	36.94	15.92
p=1.6	39.42	41.88	18.20

The conclusion of the comparison is, that for both methods, the DC-MCS including continuous branch outage heuristics and a DC-PLF approach with an approximated implementation of the same function, the evaluation leads to the findings that the risk a power system holds increases with the utilization. The two methods show different risk measures in a quantitative view, but in a qualitative view both approaches lead to the same ranking of system states.

6.4 Comparison of Different Uncertainty Margins

This comparison consists of a set of simulations with the focus on different load and generation uncertainty margin. The uncertainty is expressed by the standard deviation of the power systems loads based on the set value from a dispatch. The power system under investigation is the modified IEEE 118-bus network with an active load scaling factor of $p = 1.2$.

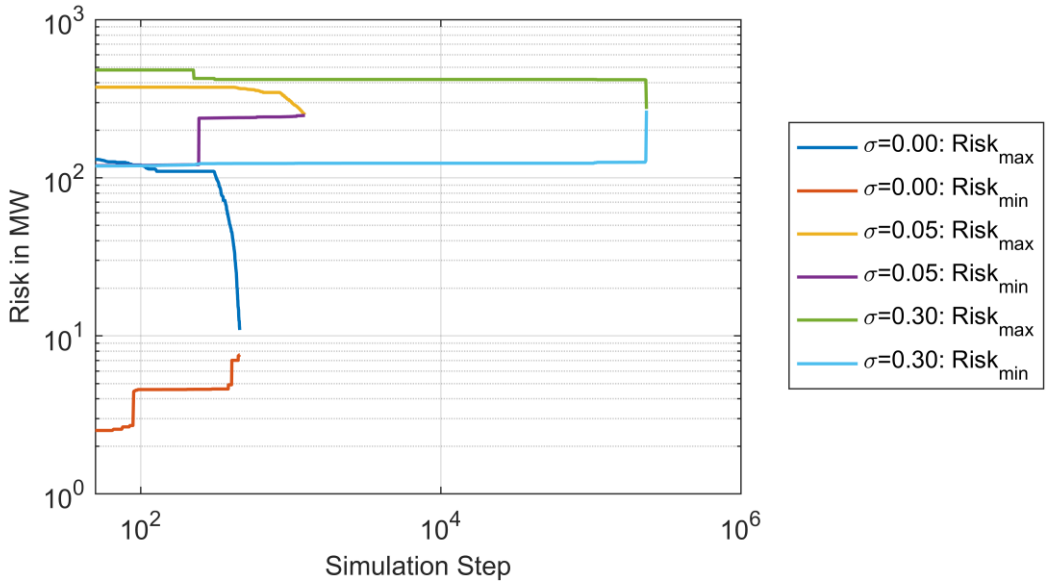

Figure 6-6. Overall system risk evolution during the simulation for the DC-PLF approach with step wise approximated implementation of the tripping heuristic for Gaussian uncertainty data and different uncertainty margins.

In Figure 6-6 the risk evolution during a risk based security assessment of one dispatch with different uncertainty margins are given for the DC-PLF approach and in Figure 6-7 for the DC-MCS approach with a continuous implementation of the tripping heuristic.

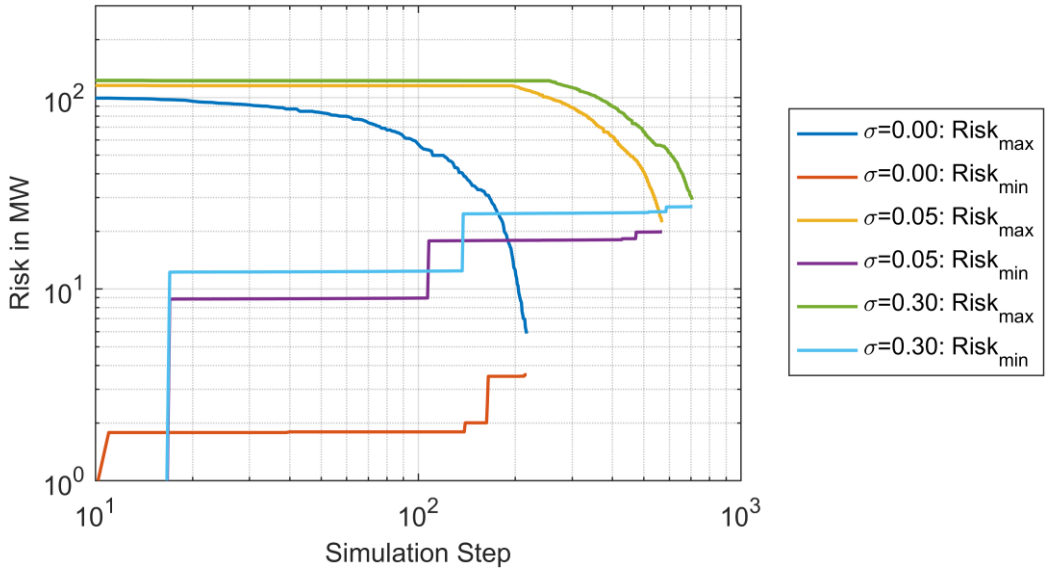

Figure 6-7. Overall system risk evolution during the simulation for the DC-MCS approach with a continuous implementation of the tripping heuristic for Gaussian uncertainty data and different uncertainty margins

Comparing the two different evaluations leads to the statement, that both the two methods differ in a quantitate way in terms of the overall system risk, but give the same ranking in terms of system

utilization cases. The results are presented in Table 6-5 in a numerical form for both approaches in terms of the system risk boundaries and the maximum state risk.

Table 6-5. Risk measures.

	DC-PLF			DC-MCS (cont.)		
	$R_{sys,min}$	$R_{sys,max}$	$R_{state,max}$	$R_{sys,min}$	$R_{sys,max}$	$R_{state,max}$
σ=0.00	7.57	10.84	1.72	3.57	5.86	0.94
σ=0.05	248.32	251.59	117.41	19.88	22.24	8.85
σ=0.30	266.53	272.81	115.95	26.89	29.23	12.22

Concluding this subchapter leads to the finding, that the uncertainty margin of power system loads and infeeds is highly connected to the risk a particular dispatch holds.

6.5 Correlation of Uncertainties

The effect of correlation of forecast uncertainties in a power system of interest on the system and maximum state risk is evaluated in this subsection. For these studies, one utilization case showing perfect correlation of all loads and also perfect correlation of all infeeds was compared to a utilization case showing neither a correlation for infeeds nor for loads. Only the overall load uncertainty was set to be fully negatively correlated to the overall load uncertainty, accounting for the power balance in terms of uncertainties. In Figure 6-8 the system risk evolutions during the simulations are given for two system utilization cases showing different uncertainty margins. For both of the cases one simulation accounting for and one neglecting the correlation of uncertainties was performed.

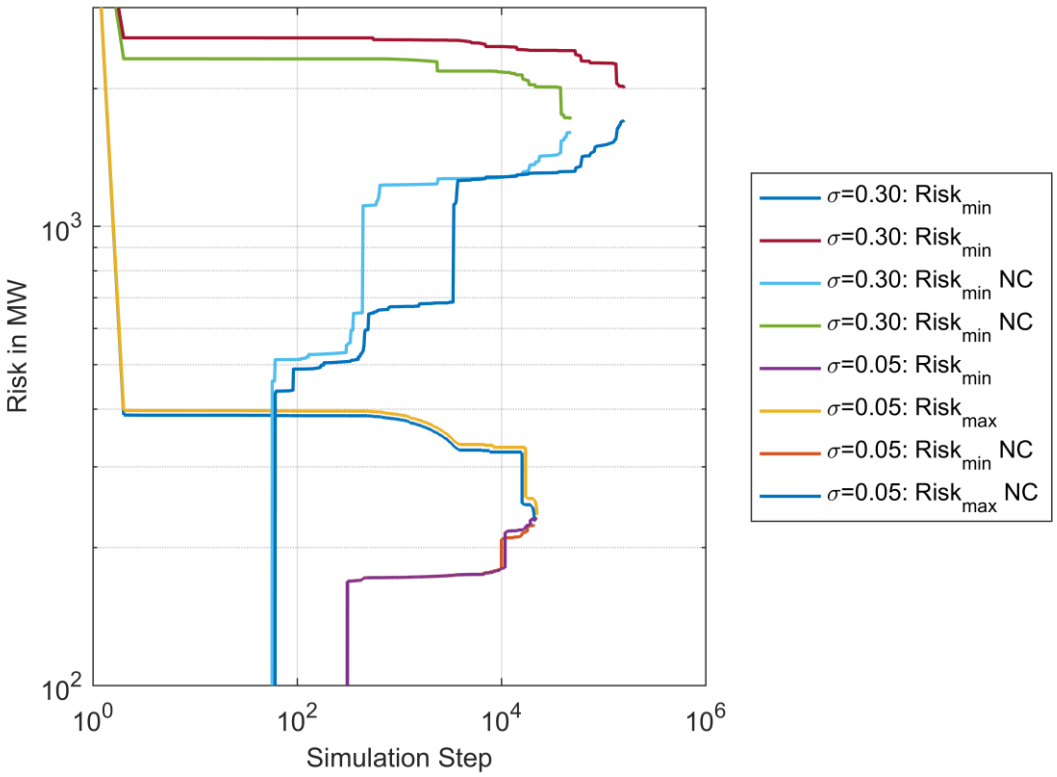

Figure 6-8. Overall system risk evolution during the simulation for the DC-PLF approach with correlated as well as uncorrelated (suffix NC) Gaussian uncertainty data for different uncertainty margins.

Studies were performed for multiple utilization cases of the IEEE 118-bus test system with different uncertainty margins for both scenarios – accounting or neglecting the correlation of uncertainties – leading to the statement, that a correlation of loads respectively infeeds leads to slightly higher overall system risk measures compared to uncorrelated uncertainty data. Compared to the outcomes of the previously presented studies analyzing the sensitivity of the risk subject to the utilization of a power system, or also the sensitivity analysis regarding the uncertainty margin the effect the correlation has on the power system risk is comparably low.

6.6 Large Scale System Simulation

To verify the applicability of the proposed method on real world transmission system simulations were performed for a real-world-alike test system consisting of 1354 busses, 1991 branches and 260 generation. The test system reflects the complexity of the European extra high voltage grid [65]. The evolution of the upper and lower risk boundaries are visualized in Figure 6-9.

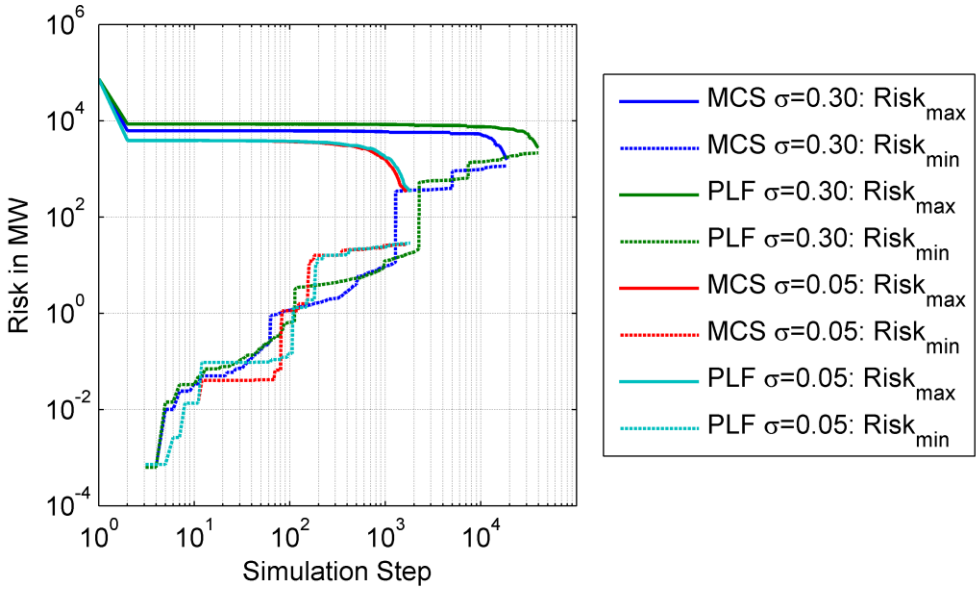

Figure 6-9. Overall system risk evolution during the simulation for the DC-PLF and DC-MCS approach with Gaussian uncertainty data for different uncertainty margins and a large scale test system.

In Table 6-6 the results of the four simulations are presented numerically in terms of the upper and lower boundary of the system risk, the maximum state risk. Additionally simulation related data as they are computation time and the number of system states scanned are given.

Table 6-6. Method measures and simulation results

	Computation time in h	System States	$R_{sys,min}$	$R_{sys,max}$	$R_{state,max}$
PLF σ=0.05	0.13	1816	28.99	332.16	3.13
MCS σ=0.05	0.27	1643	28.68	334.50	3.31
PLF σ=0.30	2.30	39606	2143.00	2763.34	678.94
MCS σ=0.30	2.74	18625	1145.95	1557.68	497.71

Comparing the DC-PLF and the DC-MCS solution leads to the statement, that the DC-PLF outperforms the DC-MCS computation in the case of the 1354-bus test system with artificial historical data of 1000 time steps in terms of computation time. Due to the fact, that the implementation of the branch loading to tripping probability is implemented in a stepwise approximation for the DC-PLF it

tends, referring to the findings of the foregone evaluations, to overestimate tripping probabilities and so there are more system states to scan for the DC-PLF implementation for both uncertainty scenarios. Simulations were performed for multiple scenarios in terms of uncertainty affliction leading an identical ranking in scenarios for both, the DC-PLF and the MCS approach.

6.6.1 Detailed State Risk Analysis

Facing the fact, that the simulation is an incomplete one, due to feasibility reasons in terms of computational time, the result is uncertainty afflicted as previously described in chapter 4.5. The following section gives a detailed analysis of the uncertainty affliction and the distribution of the remaining uncertainty over all the branches of the power system. In Figure 6-10 the risk measure and the chance measure as well as the remaining uncertainty are given for the dispatch under investigation for every single element first order contingency. The remaining multi-element first order contingencies are added as line number 1992 in an aggregated way. Summing up all the risks, chances and uncertainties leads to the overall system load.

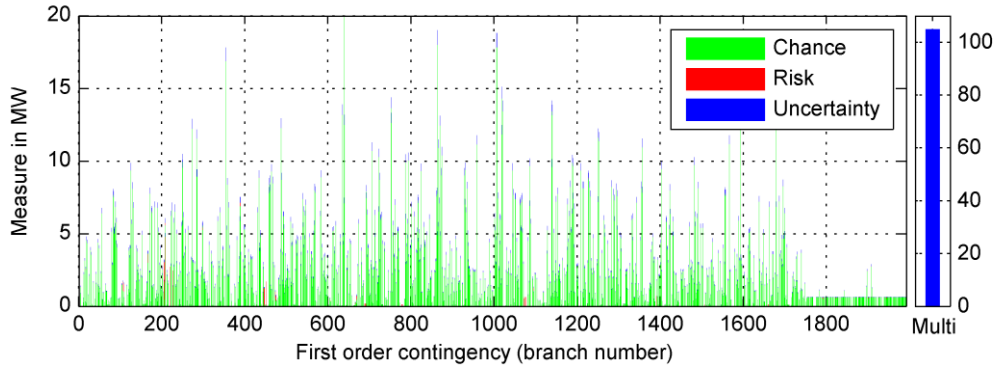

Figure 6-10. Detailed single-element first order contingency risk measures and aggregated multi-element first order contingency risk, chance and uncertainty measures for a given dispatch (σ=0.05) evaluated using the DC-PLF approach.

Focusing on the actual risk measure leads to Figure 6-11 in which the risk measure per first order contingency and the remaining uncertainty in risk is visualized.

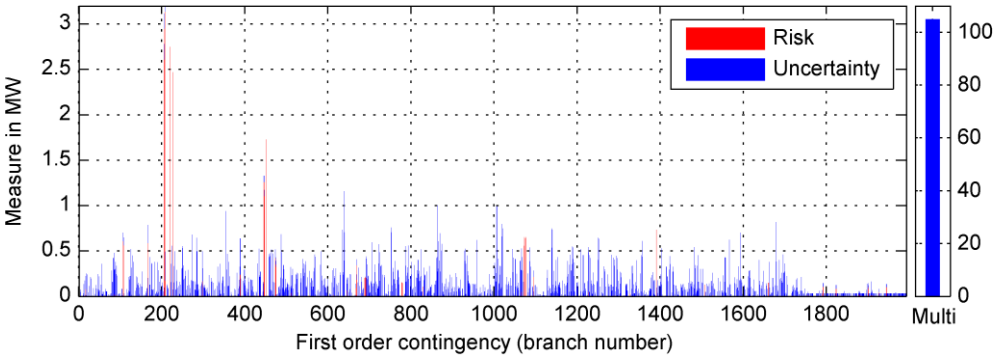

Figure 6-11. Detailed single-element first order contingency risk measures and aggregated multi-element first order contingency risk and uncertainty measures for a given dispatch (σ=0.05) evaluated using the DC-PLF approach.

In Figure 6-11 risks and uncertainties per first order contingencies are given in terms of overall measures summing up the risk measures hidden after a given contingency. For a risk assessment usually the worst case sets the actual risk value of the given dispatch, which is equal to the system

state showing the highest value in risk. In Figure 6-12 the maximum system state risks after a first order contingency are given.

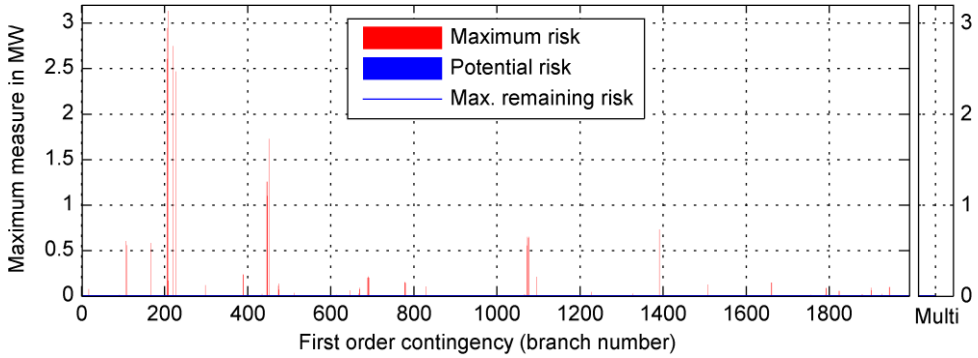

Figure 6-12. Detailed single-element first order contingency maximum risk measures for a given dispatch (σ=0.05) evaluated using the DC-PLF approach.

A detail view of Figure 6-12 is presented in Figure 6-13 with the scope on the remaining uncertainty in maximum state risk. As mentioned on a theoretically basis in chapter 4.7.2 the remaining is risk is related to the lower limit in system state probability available as an simulation input. In this example the limit was set to $p_{lim} = 10^{-7}$ and the system load is 73,060 MW leading to a uncertainty of approximately 7.3 kW in terms of risk. So in a worst case a system state not scanned during the simulation could hold at most 7.3 kW risk.

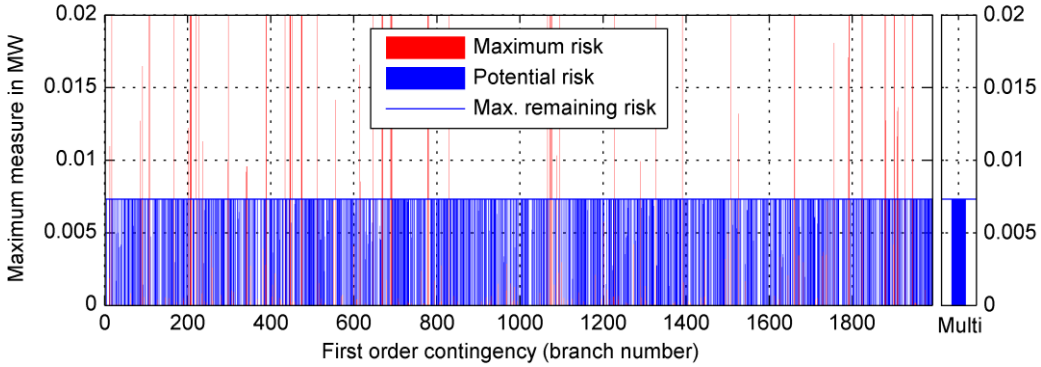

Figure 6-13. Detailed single-element first order contingency maximum risk measures for a given dispatch (σ=0.05) evaluated using the DC-PLF approach in the scope of remaining risk.

The maximum risk value is clearly set for the given power system and dispatch by branch 208 with 3.13 MW. Based on these results the classical N-1 cases can be ranked according to the risk they hold.

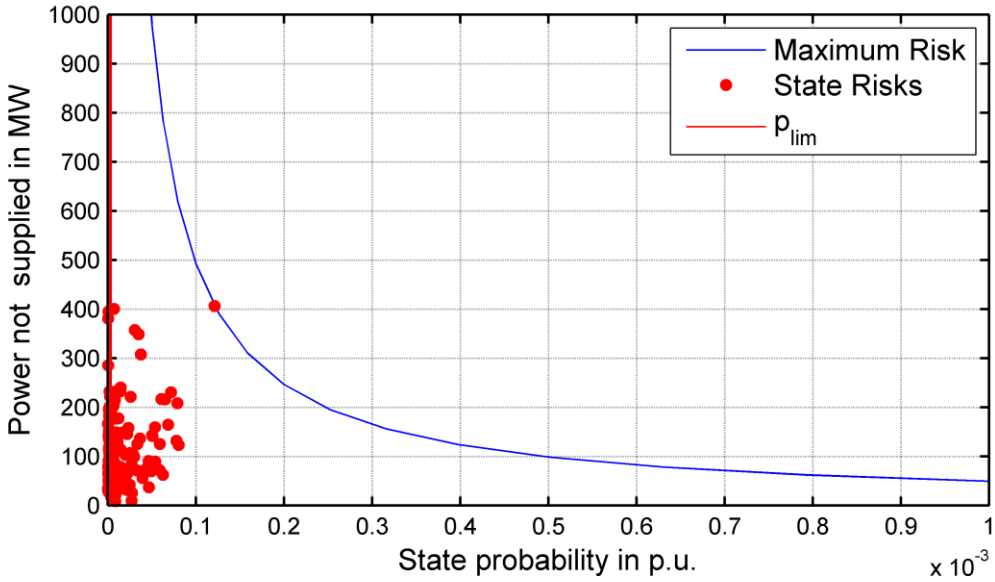

Figure 6-14. Iso-risk curve with evaluated system state risk and the lower limit in system state probability for a given dispatch (σ=0.05) evaluated using the DC-PLF approach.

This subchapter can be concluded by the statements, that the proposed method can be applied to real world problems in the scale of the central European interconnected network giving results in a reasonable time. A second finding is, that the results valid for the IEEE 118-bus network are also valid for the 1354-bus system. The ranking of system states is identical for both implementations, the DC-PLF and the DC-MCS approach, but the absolute risk values differ significantly. So a qualitative evaluation and comparison of power system utilization cases is possible, but not a quantitative one. The detailed analysis of first order contingencies allows a ranking of N-1 cases based on the risk they hold.

7 Conclusions

The risk based security assessment method presented in this thesis is able to assess the outage risk of a given power system of interest with uncertainty afflicted nodal power forecasts.

It is based on a recursive system state based approach leading to numerous possible states to be scanned during the simulation. Due to the computational effort the simulation of numerous system states holds, a filter criterion was introduced, to reduce the number of system states and so directly the computational burden. This filter leads to the fact, that the simulation is incomplete leading to an uncertainty afflicted result.

The main results the method provides are a lower and a n upper boundary for the overall system risk. By adjusting the filter criterion the number of scanned system states is effected and so directly the uncertainty affliction of the result. More scanned system states lead to a longer simulation time, but enhance the quality of the result.

An additional output of the method is a risk measure per first order contingency allowing a risk based ranking of the same, which could be used in the day-ahead processes of TSOs.

The method accounts for the loading dependency of branch tripping probability as well as for random outages. Therefore a tripping heuristic was developed.

A criterion was introduced based on available literature linking lost power as a significant system parameter to a direct blackout of the system.

The method was tested on a large scale power system and was proven to deliver results in a very limited time span.

Multiple sensitivity analyses regarding the proposed method show, that the results are not in the same range as the results of a DC-MCS based benchmark in a quantity, but the ranking of system states is identical, for the proposed method as well as the benchmark. The quantitative deviation of the results is manly due to the approximated implementation of the tripping heuristic in the proposed method.

8 References

[1] Directorate-General for Energy - European Commission, “Energy Community – Workshop on the 3rd Package – Vienna 15th April 2010.” 15-Apr-2010.

[2] D. Watts, “Security and vulnerability in electric power systems,” in *35th North American power symposium*, 2003, vol. 2, pp. 559–566.

[3] M. T. O. Amanullah, A. Kalam, and A. Zayegh, “Network Security Vulnerabilities in SCADA and EMS,” in *2005 IEEE/PES Transmission Distribution Conference Exposition: Asia and Pacific*, 2005, pp. 1–6.

[4] M. Elsberg, *BLACKOUT - Morgen ist es zu spät: Roman*. München: Blanvalet Taschenbuch Verlag, 2013.

[5] F. Vandenberghe, E. Grebe, D. Klaar, K. Kleinekorte, J. Rodriguez, H. Erven, H. Laffaye, C. Sabelli, F. Kropec, T. Tillwicks, and others, *FINAL REPORT of the Investigation Committee on the 28 September 2003 Blackout in Italy*. UCTE, 2004.

[6] G. Maas, M. Bial, and J. Fijalkowski, “Final report-system disturbance on 4 november 2006,” *Union Coord. Transm. Electr. Eur. Tech Rep*, 2007.

[7] B. Liscouski and W. Elliot, “Final report on the August 14, 2003 blackout in the United States and Canada: Causes and recommendations,” *Rep. US Dep. Energy*, vol. 40, no. 4, 2004.

[8] T. Hong, P. Wang, and H. L. Willis, “A Naive multiple linear regression benchmark for short term load forecasting,” in *2011 IEEE Power and Energy Society General Meeting*, 2011, pp. 1–6.

[9] J. W. Taylor and R. Buizza, “Neural network load forecasting with weather ensemble predictions,” *IEEE Trans. Power Syst.*, vol. 17, no. 3, pp. 626–632, Aug. 2002.

[10] S. Trento, B. Delenne, and C. Crocombette, “Residuals modeling with wind data to improve short-term load forecast,” in *PowerTech, 2011 IEEE Trondheim*, 2011, pp. 1–6.

[11] E. A. Feinberg and D. Genethliou, “Load Forecasting,” in *Applied Mathematics for Restructured Electric Power Systems*, J. H. Chow, F. F. Wu, and J. Momoh, Eds. Springer US, 2005, pp. 269–285.

[12] S. Ahmadi, H. Bevrani, and H. Jannaty, “A fuzzy inference model for short-term load forecasting,” in *2012 Second Iranian Conference on Renewable Energy and Distributed Generation*, 2012, pp. 39–44.

[13] D. Chen and M. York, “Neural network based very short term load prediction,” in *2008 IEEE/PES Transmission and Distribution Conference and Exposition*, 2008, pp. 1–9.

[14] Z. Yuan, S. Liu, L. Xue, and X. Yuan, “Short-term load forecasting based on chaos theory and RBF neural network,” in *2011 Seventh International Conference on Natural Computation (ICNC)*, 2011, vol. 1, pp. 526–529.

[15] J. W. Taylor and P. E. McSharry, “Short-Term Load Forecasting Methods: An Evaluation Based on European Data,” *IEEE Trans. Power Syst.*, vol. 22, no. 4, pp. 2213–2219, Nov. 2007.

[16] R. Bindiu, M. Chindris, and G. Pop, “Day-ahead load forecasting using exponential smoothing,” *Sci. Bull. Petru Maior Univ. Targu Mures*, vol. 6, p. 89, 2009.

[17] Y. Chakhchoukh, P. Panciatici, and L. Mili, “Electric Load Forecasting Based on Statistical Robust Methods,” *IEEE Trans. Power Syst.*, vol. 26, no. 3, pp. 982–991, Aug. 2011.

[18] J. W. Taylor, “Short-Term Load Forecasting With Exponentially Weighted Methods,” *IEEE Trans. Power Syst.*, vol. 27, no. 1, pp. 458–464, Feb. 2012.

[19] J. W. Taylor, L. M. de Menezes, and P. E. McSharry, “A comparison of univariate methods for forecasting electricity demand up to a day ahead,” *Int. J. Forecast.*, vol. 22, no. 1, pp. 1–16, Jan. 2006.

[20] C.-M. Lee and C.-N. Ko, “Short-term load forecasting using lifting scheme and ARIMA models,” *Expert Syst. Appl.*, vol. 38, no. 5, pp. 5902–5911, May 2011.

[21] Z.-X. Liu, “Short-term load forecasting method based on wavelet and reconstructed phase space,” in *2005 International Conference on Machine Learning and Cybernetics*, 2005, vol. 8, p. 4813–4817 Vol. 8.

[22] J. Kim, K. R. Wierzbicki, I. Dobson, and R. C. Hardiman, “Estimating Propagation and Distribution of Load Shed in Simulations of Cascading Blackouts,” *IEEE Syst. J.*, vol. 6, no. 3, pp. 548–557, Sep. 2012.

[23] H. Ren, I. Dobson, and B. A. Carreras, “Long-Term Effect of the n-1 Criterion on Cascading Line Outages in an Evolving Power Transmission Grid,” *IEEE Trans. Power Syst.*, vol. 23, no. 3, pp. 1217–1225, Aug. 2008.

[24] M. Papic, K. Bell, Y. Chen, I. Dobson, L. Fonte, E. Haq, P. Hines, D. Kirschen, X. Luo, S. Miller, N. Samaan, M. Vaiman, M. Varghese, and P. Zhang, “Survey of tools for risk assessment of cascading outages,” in *2011 IEEE Power and Energy Society General Meeting*, 2011, pp. 1–9.

[25] entsoe, “Network Code on Operational Security.” 24-Sep-2013.

[26] M. Zima and G. Andersson, “On security criteria in power systems operation,” in *IEEE Power Engineering Society General Meeting, 2005*, 2005, p. 3089–3093 Vol. 3.

[27] R. Baldick, B. Chowdhury, I. Dobson, Z. Dong, B. Gou, D. Hawkins, H. Huang, M. Joung, D. Kirschen, F. Li, J. Li, Z. Li, C.-C. Liu, L. Mili, S. Miller, R. Podmore, K. Schneider, K. Sun, D. Wang, Z. Wu, P. Zhang, W. Zhang, and X. Zhang, “Initial review of methods for cascading failure analysis in electric power transmission systems IEEE PES CAMS task force on understanding, prediction, mitigation and restoration of cascading failures,” in *2008 IEEE Power and Energy Society General Meeting - Conversion and Delivery of Electrical Energy in the 21st Century*, 2008, pp. 1–8.

[28] X. Zou, L. Cheng, and Y. Sun, “Evaluation of cascading failure in power system based on the operational reliability theory,” in *2010 IEEE 11th International Conference on Probabilistic Methods Applied to Power Systems (PMAPS)*, 2010, pp. 184–189.

[29] Q. Chen, C. Jiang, W. Qiu, and J. D. McCalley, “Probability models for estimating the probabilities of cascading outages in high-voltage transmission network,” *IEEE Trans. Power Syst.*, vol. 21, no. 3, pp. 1423–1431, Aug. 2006.

[30] D. S. Kirschen and D. Jayaweera, “Comparison of risk-based and deterministic security assessments,” *IET Gener. Transm. Distrib.*, vol. 1, no. 4, pp. 527–533, Jul. 2007.

[31] D. E. Newman, B. A. Carreras, V. E. Lynch, and I. Dobson, “Exploring Complex Systems Aspects of Blackout Risk and Mitigation,” *IEEE Trans. Reliab.*, vol. 60, no. 1, pp. 134–143, Mar. 2011.

[32] M. Vaiman, K. Bell, Y. Chen, B. Chowdhury, I. Dobson, P. Hines, M. Papic, S. Miller, and P. Zhang, “Risk Assessment of Cascading Outages: Methodologies and Challenges,” *IEEE Trans. Power Syst.*, vol. 27, no. 2, pp. 631–641, May 2012.

[33] S. T. Lee, “Probabilistic Reliability Assessment for transmission planning and operation including cascading outages,” in *Power Systems Conference and Exposition, 2009. PSCE ’09. IEEE/PES*, 2009, pp. 1–8.

[34] J. Zhang and F. L. Alvarado, “A heuristic model of cascading line trips,” in *2004 International Conference on Probabilistic Methods Applied to Power Systems*, 2004, pp. 647–650.

[35] O. Alizadeh Mousavi, R. Cherkaoui, and M. Bozorg, “Blackouts risk evaluation by Monte Carlo Simulation regarding cascading outages and system frequency deviation,” *Electr. Power Syst. Res.*, vol. 89, pp. 157–164, Aug. 2012.

[36] J. Chen, J. S. Thorp, and I. Dobson, “Cascading dynamics and mitigation assessment in power system disturbances via a hidden failure model,” *Int. J. Electr. Power Energy Syst.*, vol. 27, no. 4, pp. 318–326, May 2005.

[37] I. Dobson and B. A. Carreras, “Number and propagation of line outages in cascading events in electric power transmission systems,” in *2010 48th Annual Allerton Conference on Communication, Control, and Computing (Allerton)*, 2010, pp. 1645–1650.

[38] J. Kim and I. Dobson, “Propagation of Load Shed in Cascading Line Outages Simulated by OPA,” in *Complexity in Engineering, 2010. COMPENG ’10.*, 2010, pp. 1–6.

[39] M. de Jong, G. Papaeffhymiou, D. Lahaye, K. Vuik, and L. van der Sluis, “Impact of correlated infeeds on risk-based power system security assessment,” in *Power Systems Computation Conference (PSCC), 2014*, 2014, pp. 1–7.

[40] F. Xiao and J. D. McCalley, “Power System Risk Assessment and Control in a Multiobjective Framework,” *IEEE Trans. Power Syst.*, vol. 24, no. 1, pp. 78–85, Feb. 2009.

[41] L. Roald, M. Vrakopoulou, F. Oldewurtel, and G. Andersson, “Risk-constrained optimal power flow with probabilistic guarantees,” in *Power Systems Computation Conference (PSCC), 2014*, 2014, pp. 1–7.

[42] UCTE - union for the co-ordination of transmission of electricity, “Continental Europe Operation Handbook P3 – Policy 3: Operational Security.” 2009.

[43] NERC, “Standard TPL-002-0b — System Performance Following Loss of a Single BES Element.” .

[44] NERC, “Standard TOP-002-2b — Normal Operations Planning.” 2011.

[45] “HOME,” *TSC / TSCNET Services*. [Online]. Available: http://www.tscnet.eu/. [Accessed: 08-Jun-2016].

[46] “Coreso | Leading coordination for enhanced reliability of supply.” [Online]. Available: http://www.coreso.eu/. [Accessed: 08-Jun-2016].

[47] Becker, Raik, Köck, Klaus, Scheufeld, Oliver, Weber, Christoph, and UMBRELLA Project, “UMBRELLA Deliverable D 2.1: ‘Report on uncertainty modeling,’” 2013.

[48] D. Shi, “Power system network reduction for engineering and economic analysis,” Arizona State University, 2012.

[49] R. D. Zimmerman, C. E. Murillo-Sánchez, and R. J. Thomas, “MATPOWER: Steady-state operations, planning, and analysis tools for power systems research and education,” *Power Syst. IEEE Trans. On*, vol. 26, no. 1, pp. 12–19, 2011.

[50] UCTE Subgroup “Network models and forecast tools,” “UCTE data exchange format for load flow and three phase short circuit studies.” Mai-2007.

[51] T. Dietrichsteiner, “Lastflussregelung im vermaschten Netz.” TU Graz, Dec-2012.

[52] “Wiley-IEEE Press: Understanding FACTS: Concepts and Technology of Flexible AC Transmission Systems - Narain G. Hingorani, Laszlo Gyugyi.” [Online]. Available: http://eu.wiley.com/WileyCDA/WileyTitle/productCd-0780334558,miniSiteCd-IEEE2.html. [Accessed: 06-Jun-2016].

[53] G. Fujita, P. K. Goswami, R. Yokoyama, and G. Shirai, “Local power flow based decentralized TCSC controller,” in *1998 International Conference on Power System Technology, 1998. Proceedings. POWERCON ’98*, 1998, vol. 1, pp. 353–356 vol.1.

[54] B. Stott and O. Alsac, “Fast Decoupled Load Flow,” *IEEE Trans. Power Appar. Syst.*, vol. PAS-93, no. 3, pp. 859–869, May 1974.

[55] G. Valverde, A. T. Saric, and V. Terzija, “Probabilistic load flow with non-Gaussian correlated random variables using Gaussian mixture models,” *IET Gener. Transm. Distrib.*, vol. 6, no. 7, p. 701, 2012.

[56] M. B. De Kock, “Gaussian and non-Gaussian-based Gram-Charlier and Edgeworth expansions for correlations of identical particles in HBT interferometry,” University of Stellenbosch, 2009.

[57] J. Thorp, A. Phadke, S. Horowitz, and S. Tamronglak, “Anatomy of power system disturbances: importance sampling,” *Int. J. Electr. Power Energy Syst.*, vol. 20, no. 2, pp. 147–152, Feb. 1998.

[58] M. Obergünner, M. Schwan, C. Krane, K. von Sengbusch, C. Bock, K. Pietsch, and D. Quadflieg, “Ermittlung von Eingangsdaten für Zuverlässigkeitsberechnungen aus der VDN-Störungsstatistik.” 2001.

[59] J. Guo, Y. Fu, Z. Li, and M. Shahidehpour, “Direct Calculation of Line Outage Distribution Factors,” *IEEE Trans. Power Syst.*, vol. 24, no. 3, pp. 1633–1634, Aug. 2009.

[60] UCTE - union for the co-ordination of transmission of electricity, “Continental Europe Operation Handbook P1 – Policy 1: Load-Frequency Control and Performance.” 2009.

[61] Muckenhuber Richard, “Gutachten über dynamische Ausgleichsvorgänge bei Inselnetzbetrieb.” TU Graz Institut für Elektrische Anlagen, 1987.

[62] 50Hertz Transmission GmbH, Amprion GmbH, Tennet TSO GmbH, and TransnetBW GmbH, Eds., “Grundsätze für die Planung des deutschen Übertragungsnetzes.” Apr-2015.

[63] NERC - Reactive Support and Control Subteam, “Reactive Support and Control Whitepaper.” 18-May-2009.

[64] E. Kreyszig, *Statistische Methoden und ihre Anwendungen*, 7. Aufl., 5., Unveränd. Nachdr. Göttingen: Vandenhoeck & Ruprecht, 1998.

[65] S. Fliscounakis, P. Panciatici, F. Capitanescu, and L. Wehenkel, “Contingency Ranking With Respect to Overloads in Very Large Power Systems Taking Into Account Uncertainty, Preventive, and Corrective Actions,” *IEEE Trans. Power Syst.*, vol. 28, no. 4, pp. 4909–4917, Nov. 2013.

Appendix A Modified IEEE 118-Bus Test System

Table 8-1: Bus data of the modified 118-bus test system.

Bus Number	Bus Type	Active Power Demand	Reactive Power Demand	Nominal Voltage	Bus Number	Bus Type	Active Power Demand	Reactive Power Demand	Nominal Voltage
		MW	MVAr	kV			MW	MVAr	kV
1	PV	76,5	27	220	60	PQ	117	3	220
2	PQ	30	9	220	61	PV	0	0	220
3	PQ	58,5	10	220	62	PV	115,5	14	220
4	PV	58,5	12	220	63	PQ	0	0	380
5	PQ	0	0	220	64	PQ	0	0	380
6	PV	78	22	220	65	PV	0	0	380
7	PQ	28,5	2	220	66	PV	58,5	18	220
8	PV	42	0	380	67	PQ	42	7	220
9	PQ	0	0	380	68	PQ	0	0	380
10	PV	0	0	380	69	SL	0	0	220
11	PQ	105	23	220	70	PV	99	20	220
12	PV	70,5	10	220	71	PQ	0	0	220
13	PQ	51	16	220	72	PV	18	0	220
14	PQ	21	1	220	73	PV	9	0	220
15	PV	135	30	220	74	PV	102	27	220
16	PQ	37,5	10	220	75	PQ	70,5	11	220
17	PQ	16,5	3	220	76	PV	102	36	220
18	PV	90	34	220	77	PV	91,5	28	220
19	PV	67,5	25	220	78	PQ	106,5	26	220
20	PQ	27	3	220	79	PQ	58,5	32	220
21	PQ	21	8	220	80	PV	195	26	220
22	PQ	15	5	220	81	PQ	0	0	380
23	PQ	10,5	3	220	82	PQ	81	27	220
24	PV	19,5	0	220	83	PQ	30	10	220
25	PV	0	0	220	84	PQ	16,5	7	220
26	PV	0	0	380	85	PV	36	15	220
27	PV	106,5	13	220	86	PQ	31,5	10	220
28	PQ	25,5	7	220	87	PV	0	0	220
29	PQ	36	4	220	88	PQ	72	10	220
30	PQ	0	0	380	89	PV	0	0	220
31	PV	64,5	27	220	90	PV	244,5	42	220
32	PV	88,5	23	220	91	PV	15	0	220
33	PQ	34,5	9	220	92	PV	97,5	10	220
34	PV	88,5	26	220	93	PQ	18	7	220
35	PQ	49,5	9	220	94	PQ	45	16	220
36	PV	46,5	17	220	95	PQ	63	31	220
37	PQ	0	0	220	96	PQ	57	15	220
38	PQ	0	0	380	97	PQ	22,5	9	220
39	PQ	40,5	11	220	98	PQ	51	8	220
40	PV	99	23	220	99	PV	63	0	220
41	PQ	55,5	10	220	100	PV	55,5	18	220
42	PV	144	23	220	101	PQ	33	15	220
43	PQ	27	7	220	102	PQ	7,5	3	220
44	PQ	24	8	220	103	PV	34,5	16	220
45	PQ	79,5	22	220	104	PV	57	25	220
46	PV	42	10	220	105	PV	46,5	26	220
47	PQ	51	0	220	106	PQ	64,5	16	220
48	PQ	30	11	220	107	PV	75	12	220
49	PV	130,5	30	220	108	PQ	3	1	220
50	PQ	25,5	4	220	109	PQ	12	3	220
51	PQ	25,5	8	220	110	PV	58,5	30	220
52	PQ	27	5	220	111	PV	0	0	220
53	PQ	34,5	11	220	112	PV	102	13	220
54	PV	169,5	32	220	113	PV	9	0	220
55	PV	94,5	22	220	114	PQ	12	3	220
56	PV	126	18	220	115	PQ	33	7	220
57	PQ	18	3	220	116	PV	276	0	220
58	PQ	18	3	220	117	PQ	30	8	220
59	PV	415,5	113	220	118	PQ	49,5	15	220

Table 8-2: Generation unit data of the modified 118-bus test system.

Bus Number	Maximum Reactive Power	Minimum Reactive Power	Maximum Active Power	Minimum Active Power	Bus Number	Maximum Reactive Power	Minimum Reactive Power	Maximum Active Power	Minimum Active Power
	MVAr	MVAr	MW	MW		MVAr	MVAr	MW	MW
1	15	-5	100	0	65	200	-67	491	0
4	300	-300	100	0	66	200	-67	492	0
6	50	-13	100	0	69	300	-300	805,2	0
8	300	-300	100	0	70	32	-10	100	0
10	200	-147	550	0	72	100	-100	100	0
12	120	-35	185	0	73	100	-100	100	0
15	30	-10	100	0	74	9	-6	100	0
18	50	-16	100	0	76	23	-8	100	0
19	24	-8	100	0	77	70	-20	100	0
24	300	-300	100	0	80	280	-165	577	0
25	140	-47	320	0	85	23	-8	100	0
26	1000	-1000	414	0	87	1000	-100	104	0
27	300	-300	100	0	89	300	-210	707	0
31	300	-300	107	0	90	300	-300	100	0
32	42	-14	100	0	91	100	-100	100	0
34	24	-8	100	0	92	9	-3	100	0
36	24	-8	100	0	99	100	-100	100	0
40	300	-300	100	0	100	155	-50	352	0
42	300	-300	100	0	103	40	-15	140	0
46	100	-100	119	0	104	23	-8	100	0
49	210	-85	304	0	105	23	-8	100	0
54	300	-300	148	0	107	200	-200	100	0
55	23	-8	100	0	110	23	-8	100	0
56	15	-8	100	0	111	1000	-100	136	0
59	180	-60	255	0	112	1000	-100	100	0
61	300	-100	260	0	113	200	-100	100	0
62	20	-20	100	0	116	1000	-1000	100	0

Table 8-3: Branch data of the modified 118-bus test system.

From Bus	To Bus	Resistance	Reactance	Suceptance	Power Flow Limit	Base Tripping Probability	From Bus	To Bus	Resistance	Reactance	Suceptance	Power Flow Limit	Base Tripping Probability
		10^{-3} p.u.	10^{-3} p.u.	p.u.	MVA	10^{-6}			10^{-3} p.u.	10^{-3} p.u.	p.u.	MVA	10^{-6}
1	2	3,93	39,31	0	228,63	72,47	39	40	2,38	23,81	0	228,63	43,89
1	3	1,67	16,68	0	228,63	30,76	40	41	1,92	19,16	0	228,63	35,33
4	5	0,31	3,14	0	228,63	5,79	40	42	7,20	72,01	0	228,63	132,75
3	5	4,25	42,49	0	228,63	78,35	41	42	5,31	53,12	0	228,63	97,93
5	6	2,12	21,25	0	228,63	39,17	43	44	9,66	96,56	0	228,63	178,02
6	7	0,82	8,18	0	228,63	15,09	34	43	6,61	66,14	0	228,63	121,94
8	9	2,51	25,14	0	394,91	138,28	44	45	3,55	35,45	0	228,63	65,36
8	5	2,20	22,01	0	394,91	9,71	45	46	5,34	53,35	0	228,63	98,37
9	10	2,65	26,54	0	394,91	145,99	46	47	5,00	49,97	0	228,63	92,13
4	11	2,71	27,07	0	228,63	49,91	46	48	7,44	74,37	0	228,63	137,10
5	11	2,68	26,83	0	228,63	49,47	47	49	2,46	24,59	0	228,63	45,34
11	12	0,77	7,71	0	228,63	14,22	42	49	12,71	127,09	0	228,63	234,31
2	12	2,42	24,24	0	228,63	44,69	42	49	12,71	127,09	0	228,63	234,31
3	12	6,30	62,96	0	228,63	116,07	45	49	7,32	73,19	0	228,63	134,93
7	12	1,34	13,38	0	228,63	24,66	48	49	1,99	19,87	0	228,63	36,63
11	13	2,88	28,76	0	228,63	53,03	49	50	2,96	29,59	0	228,63	54,55
12	14	2,78	27,82	0	228,63	51,29	49	51	5,39	53,91	0	228,63	99,38
13	15	9,62	96,16	0	228,63	177,29	51	52	2,31	23,14	0	228,63	42,65
14	15	7,67	76,73	0	228,63	141,46	52	53	6,43	64,33	0	228,63	118,61
12	16	3,28	32,82	0	228,63	60,50	53	54	4,80	48,00	0	228,63	88,50
15	17	1,72	17,19	0	228,63	31,70	49	54	11,37	113,71	0	228,63	209,65
16	17	7,09	70,86	0	228,63	130,65	49	54	11,45	114,50	0	228,63	211,10
17	18	1,99	19,87	0	228,63	36,63	54	55	2,78	27,82	0	228,63	51,29
18	19	1,94	19,40	0	228,63	35,76	54	56	0,38	3,76	0	228,63	6,93
19	20	4,60	46,04	0	228,63	84,87	55	56	0,59	5,94	0	228,63	10,95
15	19	1,55	15,50	0	228,63	28,58	56	57	3,80	38,01	0	228,63	70,08
20	21	3,34	33,41	0	228,63	61,59	50	57	5,27	52,73	0	228,63	97,21
21	22	3,82	38,17	0	228,63	70,37	56	58	3,80	38,01	0	228,63	70,08
22	23	6,26	62,56	0	228,63	115,34	51	58	2,83	28,29	0	228,63	52,16
23	24	1,94	19,36	0	228,63	35,69	54	59	9,02	90,22	0	228,63	166,34
23	25	3,15	31,48	0	228,63	58,03	56	59	9,88	98,76	0	228,63	182,08
26	25	3,15	31,49	0	394,91	9,71	56	59	9,40	94,04	0	228,63	173,38
25	27	6,41	64,14	0	228,63	118,24	55	59	8,49	84,91	0	228,63	156,55
27	28	3,36	33,64	0	228,63	62,02	59	60	5,71	57,05	0	228,63	105,19
28	29	3,71	37,10	0	228,63	68,41	59	61	5,90	59,02	0	228,63	108,81
30	17	3,20	31,98	0	394,91	9,71	60	61	0,53	5,31	0	228,63	9,79
8	30	4,15	41,54	0	394,91	228,51	60	62	2,21	22,07	0	228,63	40,70
26	30	7,09	70,89	0	394,91	389,91	61	62	1,48	14,79	0	228,63	27,28
17	31	6,15	61,50	0	228,63	113,38	63	59	3,18	31,82	0	394,91	9,71
29	31	1,30	13,02	0	228,63	24,01	63	64	1,65	16,49	0	394,91	90,68
23	32	4,54	45,37	0	228,63	83,64	64	61	2,21	22,09	0	394,91	9,71
31	32	3,88	38,76	0	228,63	71,45	38	65	8,13	81,27	0	394,91	447,04
27	32	2,97	29,71	0	228,63	54,77	64	65	2,49	24,89	0	394,91	136,92
15	33	4,89	48,95	0	228,63	90,24	49	66	3,62	36,16	0	228,63	66,67
19	34	9,72	97,19	0	228,63	179,18	49	66	3,62	36,16	0	228,63	66,67
35	36	0,40	4,01	0	228,63	7,40	62	66	8,58	85,78	0	228,63	158,14
35	37	1,96	19,56	0	228,63	36,05	62	67	4,60	46,04	0	228,63	84,87
33	37	5,59	55,87	0	228,63	103,01	65	66	3,05	30,50	0	394,91	9,71
34	36	1,05	10,55	0	228,63	19,44	66	67	3,99	39,94	0	228,63	73,63
34	37	0,37	3,70	0	228,63	6,82	65	68	1,32	13,19	0	394,91	72,54
38	37	3,09	30,91	0	394,91	9,71	47	69	10,93	109,31	0	228,63	201,52
37	39	4,17	41,71	0	228,63	76,89	49	69	12,75	127,48	0	228,63	235,04
37	40	6,61	66,10	0	228,63	121,87	68	69	3,05	30,50	0	394,91	9,71
30	38	4,45	44,51	0	394,91	244,83	69	70	5,00	49,97	0	228,63	92,13

From Bus	To Bus	Resistance	Reactance	Suceptance	Power Flow Limit	Base Tripping Probability	From Bus	To Bus	Resistance	Reactance	Suceptance	Power Flow Limit	Base Tripping Probability
		10^{-3} p.u.	10^{-3} p.u.	p.u.	MVA	10^{-6}			10^{-3} p.u.	10^{-3} p.u.	p.u.	MVA	10^{-6}
24	70	16,19	161,91	0	228,63	298,51	99	96	7,16	71,61	0	228,63	132,03
70	71	1,40	13,97	0	228,63	25,75	101	96	2,09	20,85	0	228,63	38,45
24	72	7,71	77,12	0	228,63	142,18	102	96	3,42	34,19	0	228,63	63,04
71	72	7,08	70,82	0	228,63	130,58	103	97	3,68	36,75	0	228,63	67,75
71	73	1,79	17,86	0	228,63	32,93	104	98	4,25	42,49	0	228,63	78,35
70	74	5,21	52,06	0	228,63	95,97	105	99	8,11	81,06	0	228,63	149,44
70	75	5,55	55,48	0	228,63	102,28	106	100	11,61	116,07	0	228,63	214,00
69	75	4,80	48,00	0	228,63	88,50	107	100	2,28	22,82	0	228,63	42,07
74	75	1,60	15,97	0	228,63	29,45	108	96	2,15	21,52	0	228,63	39,68
76	77	5,82	58,23	0	228,63	107,36	109	97	3,48	34,82	0	228,63	64,20
69	77	3,97	39,74	0	228,63	73,27	110	100	7,04	70,43	0	228,63	129,85
75	77	7,87	78,65	0	228,63	145,01	111	100	3,20	31,99	0	228,63	58,98
77	78	0,49	4,88	0	228,63	9,00	112	101	4,97	49,66	0	228,63	91,55
78	79	0,96	9,60	0	228,63	17,70	92	102	2,20	22,00	0	228,63	40,55
77	80	1,91	19,08	0	228,63	35,18	101	102	4,41	44,07	0	228,63	81,25
77	80	4,13	41,31	0	228,63	76,17	100	103	2,07	20,66	0	228,63	38,08
79	80	2,77	27,70	0	228,63	51,07	100	104	8,03	80,27	0	228,63	147,99
68	81	1,67	16,65	0	394,91	91,58	103	104	6,23	62,33	0	228,63	114,91
81	80	3,05	30,50	0	394,91	9,71	103	105	6,39	63,94	0	228,63	117,88
77	82	3,36	33,56	0	228,63	61,88	100	106	9,01	90,10	0	228,63	166,12
82	83	1,44	14,42	0	228,63	26,59	104	105	1,49	14,87	0	228,63	27,42
83	84	5,19	51,94	0	228,63	95,76	105	106	2,15	21,52	0	228,63	39,68
83	85	5,82	58,23	0	228,63	107,36	105	107	7,20	72,01	0	228,63	132,75
84	85	2,52	25,22	0	228,63	46,50	105	108	2,77	27,66	0	228,63	51,00
85	86	4,84	48,40	0	228,63	89,23	106	107	7,20	72,01	0	228,63	132,75
86	87	8,16	81,61	0	228,63	150,45	108	109	1,13	11,33	0	228,63	20,89
85	88	4,01	40,13	0	228,63	73,99	103	110	7,13	71,34	0	228,63	131,52
85	89	6,81	68,07	0	228,63	125,50	109	110	3,00	29,98	0	228,63	55,28
88	89	2,80	28,02	0	228,63	51,65	110	111	2,97	29,71	0	228,63	54,77
89	90	7,40	73,97	0	228,63	136,38	110	112	2,52	25,18	0	228,63	46,43
89	90	3,92	39,23	0	228,63	72,32	17	113	1,18	11,84	0	228,63	21,84
90	91	3,29	32,89	0	228,63	60,65	32	113	7,99	79,87	0	228,63	147,26
89	92	1,99	19,87	0	228,63	36,63	32	114	2,41	24,08	0	228,63	44,40
89	92	6,22	62,21	0	228,63	114,69	27	115	2,92	29,16	0	228,63	53,75
91	92	5,00	50,05	0	228,63	92,27	114	115	0,41	4,09	0	228,63	7,54
92	93	3,34	33,37	0	228,63	61,52	68	116	0,33	3,34	0	394,91	9,71
92	94	6,22	62,17	0	228,63	114,62	12	117	5,51	55,09	0	228,63	101,56
97	94	2,88	28,80	0	228,63	53,10	75	118	1,89	18,93	0	228,63	34,89
98	95	1,71	17,08	0	228,63	31,48	76	118	2,14	21,40	0	228,63	39,46

Appendix B Statistical Data Regarding the Analysis of Power System Load Nodes

Table 8-4: Normal distribution parameters of the active power DACF and forecast error (TSO1).

Node Number	DACF	Forecast Error			
	Iqps	μ_{FCE}	iqps	μ_{FCE}	iqps
	in MW	in MW	in MW	in MW	in MW
1	171	-25.31	65.26	-14.80	38.16
2	340	-54.71	66.97	-16.09	19.70
3	261	11.74	55.79	4.50	21.38
4	220	7.60	39.18	3.45	17.81
5	138	7.06	28.80	5.12	20.87
6	159	-22.48	68.29	-14.14	42.95

Table 8-5: Normal distribution parameters of the active power DACF and forecast error (TSO2).

Node Number	DACF	Forecast Error			
	iqps	μ_{FCE}	σ_{FCE}	μ_{FCE}/iqps	σ_{FCE}/iqps
	in MW	in MW	in MW	in %	in %
1	79	-0.86	13.95	-1.09	17.66
2	71	-1.21	10.30	-1.70	14.51
3	97	-1.45	13.73	-1.49	14.16
4	94	-3.18	25.26	-3.38	26.87
5	151	-3.20	19.76	-2.12	13.09
6	185	-4.83	27.07	-2.61	14.63
7	76	-1.71	12.15	-2.25	15.98
8	73	0.90	15.80	1.23	21.64
9	162	-2.58	27.35	-1.59	16.88
10	200	-3.03	28.71	-1.51	14.36
11	75	-1.63	8.54	-2.18	11.39
12	153	-1.02	26.83	-0.67	17.54
13	97	-1.53	18.15	-1.58	18.71
14	166	-1.66	29.25	-1.00	17.62
15	99	-1.12	22.33	-1.13	22.55
16	157	-7.91	38.62	-5.04	24.60
17	180	-4.20	24.44	-2.34	13.58
18	176	-2.91	24.47	-1.65	13.91
19	71	5.13	15.19	7.22	21.39
20	103	-4.89	17.12	-4.75	16.62
21	89	-0.55	19.31	-0.61	21.70
22	249	-4.01	73.94	-1.61	29.70